William Harvey Research Institute

Barts and The London School of Medicine and Dentistry

Queen Mary University of London

Functional characterization of solute carrier family 39 member 8 variant in relation to hypertension and coronary artery disease

by

Ruoxin Zhang

Thesis for the degree of Doctor of Philosophy

2015

I dedicate this thesis to my parents, particularly in memory of my mum who was and will always be my motivation for scientific research.

Acknowledgement

First and foremost I want to thank the Clinical Pharmacology Department of William Harvey Research Institute (WHRI) for giving me the opportunity to carry out this exciting work. I gratefully acknowledge the funding body of my PhD, which was co-funded by the Chinese Scholarship Council and William Harvey Research Institute for 4 years. My research work was also supported by the British Heart Foundation and Henry Lester Trust. I also want to acknowledge British Pharmacology Society, Queen Mary University and Professor Caulfield and Prof. Ye for generously sponsoring my international conferences.

I would like to express my deepest gratitude to my supervisors Professor Shu Ye and Professor Mark Caulfield. It has been an honour to be supervised by these two respectable scientists, who have taught me, in their own ways, how a good genetics study is done. I appreciate their generosity in knowledge sharing, patience and skepticism in teaching, persistence and rigorousness in scientific delivery; all of which are the key traits I will truly benefit in my future scientific career. This PhD is the ultimate outcome of a successful academic relationship of which I'm deeply grateful.

The members of the Clinical Pharmacology have contributed immensely to my personal and professional development during my PhD. The group has been a real source of friendship as well as good advice and collaboration. I am particularly grateful to my colleagues Dr. Fu Liang Ng, Dr. Kate Witkowska and Dr. Qingzhong Xiao for teaching me of essential research techniques and supporting me whenever I need help. I also enjoyed the stimulating scientific exchange with my other team members Xiangyuan Pu, Meixia Ren and Andrew Moore.

In regards to great friendship I built over my PhD, I want to express my profound gratitude to Dr. Ming Yuan, Dr. Ping Pui Wong and Dr. Claudio Mauro. They have been a tremendous support and companion during my PhD. I am thankful for their time and insightful opinions, which usually took place over vibrant lunch sessions that I enjoyed the most; all of which have contributed to a lasting friendship.

A lot of thanks to our collaborators in Biochemistry Pharmacology Department, Dr. Dianne Cooper, Patricia Souza and Hefin Jones, who have kindly helped us with collection and isolation of human umbilical cords samples; similarly appreciation towards Genome Centre, for letting me use their cell culture facilities.

My time at WHRI was made enjoyable in large part due to many friends and groups that become a part of my life. I am grateful for the time spent with friends from Clinical Pharmacology and Microvascular Department, for enriching my time with fun outings and activities such as football.

Lastly, I would like to thank my family and friends for all their love and encouragement; for my parents who raised me with love and supported me in all my pursuits; for Shan Hiu who kindly helped with the manuscript and thesis corrections; for those who supported me through this wild journey filled with laughter and tears, which has become a valuable part of my life. Thank you.

Abstract

Hypertension and coronary artery disease are complex diseases with both environmental and genetic contributions. Genome-wide association studies (GWASs) have revealed a number of common genetic variants with modest effects on the disease susceptibility. One of the novel genetic variants (SNP rs13107325, C → T, Ala391Thr) identified in GWASs has been associated with a number of CVD-related traits, including SBP, DBP, HDL-C, body mass index, and schizophrenia. This SNP is located at exon 8 of the solute carrier family 39 member 8 gene (*SLC39A8*), and results in an amino acid substitution from Alanine to Threonine at amino acid position 391. *SLC39A8* was first found to be highly induced by *Mycobacterium bovis* BCG cell wall and TNF-α. The encoded protein ZIP8 is a divalent cation/bicarbonate co-transporter with different affinities for a number of metal ions. Recent studies revealed the major role of ZIP8 in the uptake of cadmium and manganese. The objective of this project is to investigate whether the Ala391Thr polymorphism has an impact on the structure or function of ZIP8, and the underlying mechanisms responsible for the deleterious cell events associated with cadmium exposure, that over time, may contribute to the development of hypertension.

We showed that ZIP8 containing the Ala391 variant resulted in higher intracellular accumulation of Cd^{2+} at low dose and Zn^{2+} at physiological concentration. Lower cell proliferation and higher cell death were observed in transfected HEKs and HuVECs exposed to Cd^{2+}. This was accompanied by stronger ERK1/2 and NF-κB activation in HEK293 possibly induced by Cd^{2+} uptake. We also showed some evidence of ZIP8 participation in HDL_3-mediated cholesterol efflux, however this needs to be further validated in an improved experimental model.

Bioinformatics analysis suggested a possible structural impact of Ala391Thr on ZIP8 function, which was supported by conservation analysis of the alanine amino acid. Membrane protein structure analysis predicted a shift of an α-helical domain possibly caused by the change of the amino acid hydrophillicity. The secondary structure predicted by the Robetta algorithm based on a similar homologue supported that this structural change may be caused by the Ala391Thr variation.

Our data indicate that the amino acid substitution (Ala391Thr) caused by SNP rs13107325 alters the transport activity of ZIP8 on metal ions, leading to differential activation of ERK1/2 and NF-κB pathways, which subsequently results in different levels of cell death on human kidney and endothelial cells. This study sought to provide the preliminary mechanistic explanations for the association of rs1310725 with blood pressure and HDL-C following the GWAS. These observations have demonstrated a promising start for further investigation of *SLC39A8* in the context of hypertensive mice or human populations. This may enable further pharmacological studies for the development of a potential therapeutic candidate for hypertension treatment.

Table of Contents

1. Introduction

Cardiovascular diseases (CVDs) are a combination of diseases including coronary heart disease (heart attack), cerebrovascular disease (stroke), raised blood pressure (hypertension), peripheral artery disease, rheumatic heart disease, congenital heart disease and heart failure. CVDs are known to be the number one cause of death globally. An estimated 17.5 million people died from CVDs in 2012, representing 31% of all global deaths. Of these deaths, coronary heart disease is responsible for 7.4 million, while stroke accounts for 6.7 million.[1] CVDs are caused by disorders of the heart and blood vessels. The high incidence of CVDs has caused enormous health and socioeconomic burden to all countries. Most CVDs are results of complex interactions of lifestyle and genetic contributors. A large proportion of CVDs is preventable through the understanding of established risk factors, such as unhealthy diet, physical inactivity, excessive use of alcohol, obesity, etc. This study mainly focuses on essential hypertension and coronary heart disease.

1.1 Aetiology of essential hypertension (HTN)

Hypertension is one the earliest recorded medical conditions (Huangdi Neijing around 221 BC), and is known to be a complex disorder affecting more than a quarter of the world's adult population,[2] accounting for 9.4 million deaths worldwide.[3] It is a major modifiable risk factor that relates to a range of diseases including coronary heart disease, cerebrovascular disease, peripheral vascular disease, chronic kidney disease and atrial fibrillation.[4; 5] The relationship between HTN and increased cardiovascular risk and CVD mortality has been demonstrated in numerous studies including prospective cohort studies and meta-analysis,[6-8]. The association between blood

pressure (BP) and stroke mortality is strong and direct across different age groups, almost as strongly with ischaemic heart disease (IHD) and with those from other vascular causes.[6] Lowering blood pressure has been linked with dramatic reduction in stroke, and smaller reduction in myocardial infarction.[9] An individual's BP depends on the complex interplay of blood vessels, as is controlled by two variables according to analogy of Ohm's law (shown in Fig.1.1).[10] The peripheral vascular resistance (R) is modified mainly by arterial wall modifications due to ageing or medial hypertrophy; the blood flow (Q) is modified by increased fluid volume due to elevated salt intake:

$$\Delta P = Q \times R$$

(ΔP = pressure difference, Q = bulk flow, R= resistance)

This relation can be restated for the whole circulation, suggesting that an elevation of mean BP is a result of increase in cardiac output, total peripheral vascular resistance, or a combination of both.

$$MAP = CO \times PVR$$

MAP = mean arterial pressure, CO = cardiac output (= stroke volume x heart rate),

PVR = total peripheral vascular resistance

Tremendous efforts have been placed to investigate the relationship of heart and blood vessels, which are key to the understanding of the pathophysiology of HTN. Any small changes in arterial diameter will result in a profound effect on the blood flow (or resistance). In short term, the diameter of small arteries and arterioles are controlled by the contractile state of their smooth muscle, which in turn are regulated by a network of local and systemic factors (Fig. 1.1). [10]

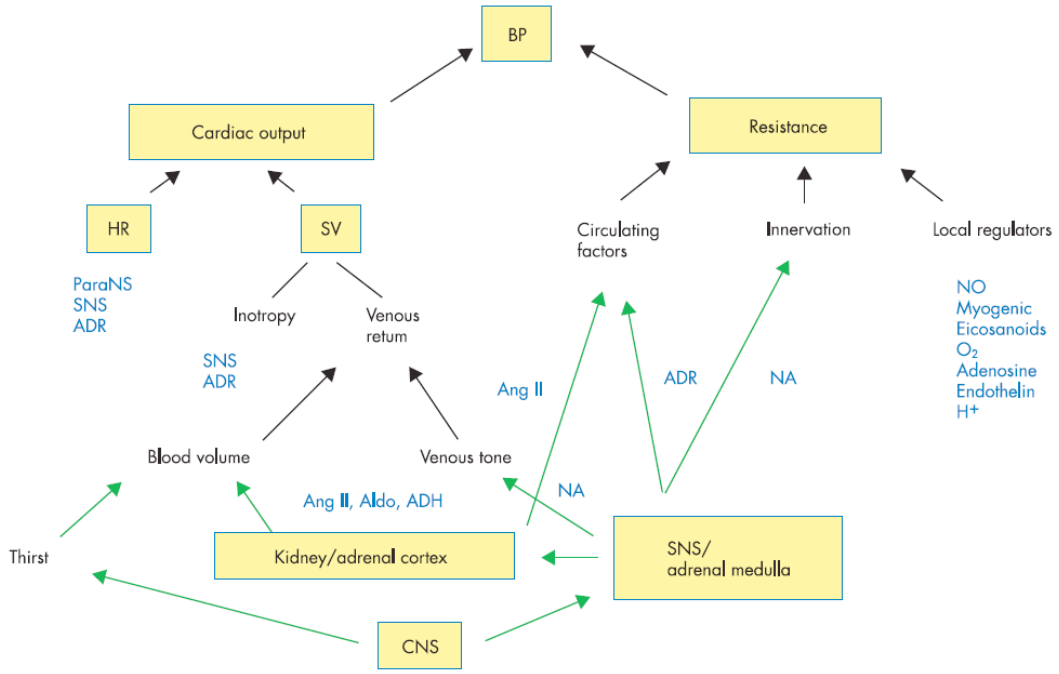

Figure 1.1. Mechanisms regulating mean arterial blood pressure. ADR= adrenaline, Aldo= aldosterone, Ang II= angiotensin II; ADH= antidiuretic hormone (arginine vasopressin); CNS= central nervous system; HR= heart rate; NO= nitric oxide; ParaNS= parasympathetic nervous system; SV= stroke volume; SNS= sympathetic nervous system. [10]

Several established constitutional and environmental factors that modify BP levels include: dietary salt intake, alcohol consumption, inactivity and body mass index. Despite its severe consequences (myocardial infarction, stroke and heart failure), the aetiology of HTN remains obscure; only approximately 5% of cases have an identifiable secondary cause.[11] Human essential or primary hypertension is defined as 'high blood pressure in which secondary causes such as renovascular disease, renal failure or other causes of secondary hypertension or Mendelian forms are not present.'[12] Essential or primary HTN accounts for approximately 95% of the HTN incidence.[13] Besides the high incidence, the rates of HTN control are generally poor, with an estimation of only 38% of the patients being treated to the target level across

Europe.[14]

1.2 Genetics of essential hypertension

Human essential hypertension is a complex (polygenic) trait, which arises from a combination of genetic and environmental factors. Data from the Framingham Heart Study suggest that heritability is 30-50% for long-term systolic or diastolic BP,[15] and is broadly related to a combination of pathophysiological conditions. The best example of genetic influence on BP is the presence of a HTN family history increases the risk of developing the disease by about four times compared to the general population.[16] Efforts to identify blood pressure related genes have been mainly relying on three approaches: linkage analysis, candidate genes, and genome-wide association studies.

1.2.1 Mendelian disorders of hypertension

Many successes have been achieved in the field of linkage study of Mendelian forms of hypertension and hypotension in which variations within single genes impart large effects on blood pressure. The methodology began with the identification of a chromosomal region that is transmitted within families, along with the disease phenotype of interest.[17] Between 1996 and 2004, 26 candidate genes had been identified by this method,[18] including genes encoding baroreceptors, natriuretic peptides and components of the renin-angiotensin-aldosterone system.[19-21] These systems have been extensively studied for their contributions to short-term blood pressure regulation through homeostatic response.[19] Most of the mutations in genes influencing renal salt handling pathways exhibit large effects on BP. All the mutations identified by this approach are rare variants, with minor allele frequency (MAF) <0.1%,

and additively explain only a small proportion of cases in the population. The vast majority of phenotype variance in the population is due to common genetic variations. The complex pathophysiology of HTN, as well as the pathways affecting long-term high blood pressure, remains largely elusive. The drawbacks of linkage studies are the lack of statistical power and low mapping resolution for variants of modest effects. As a consequence, the application of linkage analysis for complex disorders without an obvious Mendelian inheritance pattern has achieved limited success. The genes known to contribute to monogenic HTN is shown in Fig. 1.2.

Given the high heritability of high BP, more genetics approaches have been developed for the identification of BP related genes. They aims are to not only to reveal more primary physiological mechanisms of HTN but also provide insights into the architecture of this complex trait comprehensively.[22]

1.2.2 Identification of blood pressure related genes

Candidate gene study

Candidate gene studies are hypothesis driven, direct tests of common potentially functional variants in large samples combined with high-throughput strategies for genotyping and rigorous control of multiple tests. This approach has yielded a few consistently replicated candidates: two common variations at the *NPPA-NPPB* locus harbouring genes encoding atrial and B-type natriuretic peptides were associated with increased circulating natriuretic peptide concentrations and lower SBP (0.9-1.5 mmHg) and DBP (0.3-0.8 mmHg) (effect of two minor alleles rs5068 and rs198358), as well as reduced risk of hypertension.[23] The limitations for this method are the tested variants

are based on imperfect understanding of the biological pathway, therefore the associations observed are often inconsistent thus difficult to replicate.[24]

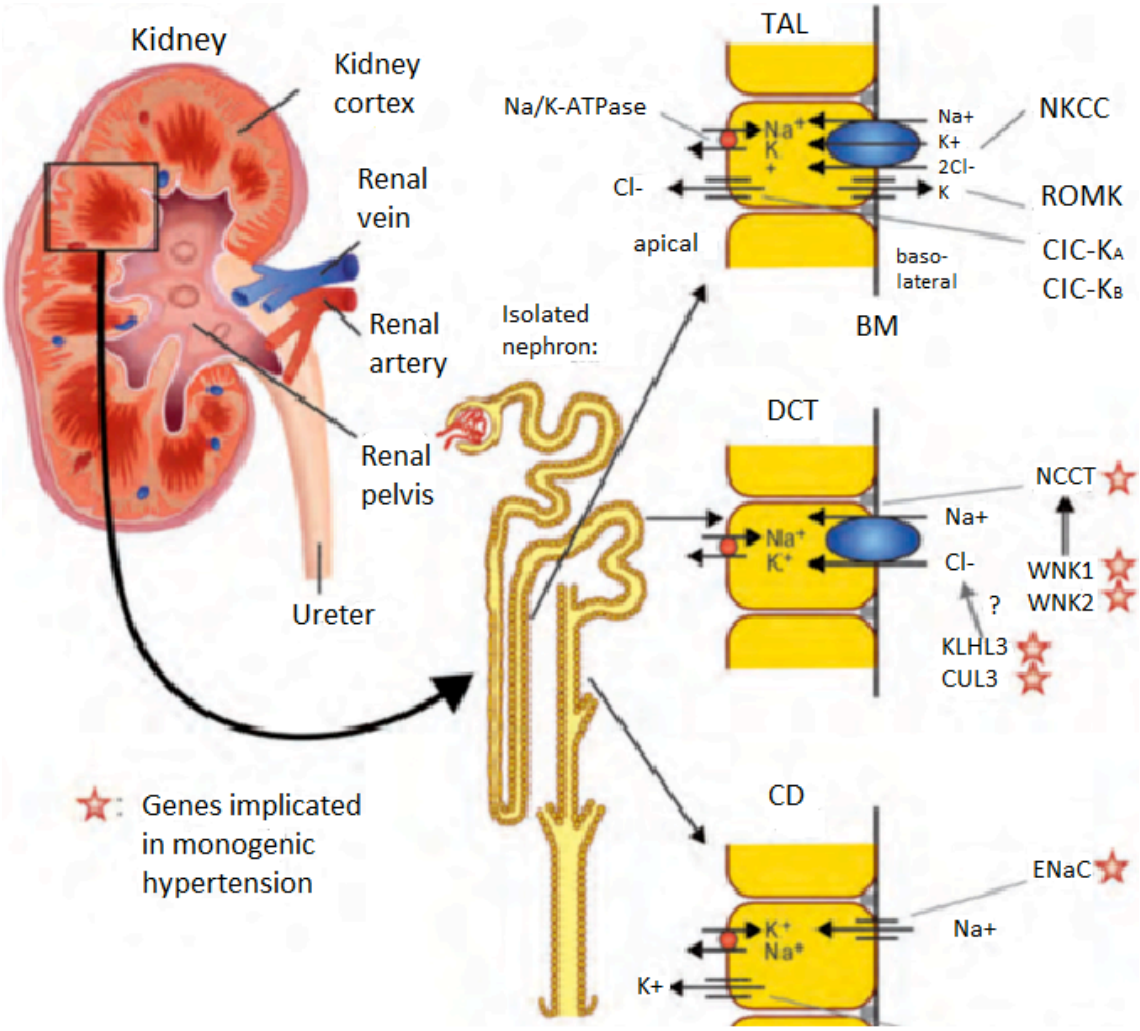

Figure 1.2. Pathways affected in monogenic hypertension in the kidney. The location of the mutated genes in monogenic hypertension are shown. Proteins mutated in monogenic HTN syndromes are marked by a red star. TAL, thick ascending limb of the loop of Henle; DCT, distal convoluted tubule; CD, collecting duct. (Adapted from Newton-Cheh et al., 2009, *Nat. Genet.*) [22]

Genome-wide association study (GWAS)

The HapMap and 1000 Genomes projects have identified millions of single nucleotide polymorphisms (SNPs) across the human genome.[25] GWAS represents a powerful tool to investigate the global genetic architecture of complex diseases. It has led to important achievements in identifying a considerable number of genetic variants associated with CVD phenotypes. HTN is one of the first diseases studied by GWAS. The first hypertension GWAS performed by the Wellcome Trust Case Control Consortium in 2007 revealed no SNP associated with BP at the genome-wide significance threshold of $p<10^{-7}$.[26] In the following eight GWAS papers published, some SNPs have begun to be associated with BP related traits with considerable statistical power, for instance SNPs within the serine threonine kinase 39 (*STK39*) at chromosome 2q24.3, which encodes a protein involved in cation transports within the nephron. A breakthrough from GWAS in BP was made in 2009 when two large meta-analysis from the Global BP Genetics (Global BPgen) and Cohorts for Heart and Aging Research in Genome Epidemiology [27] consortia identified a total of 13 loci associated with BP, in which two loci overlapped genes related to hypertension identified previously.

GWAS offers advantages in studying complex diseases because of its unbiasedness in interrogation of common genetic variants against the disease of interest. DNA samples from large size of cases and controls populations are genotyped using micro-array chips covering up to a million of SNPs. Specific GWAS algorithms can identify variants with statistically different frequencies in cases and controls. Testing a large number of SNP markers leads to a large number of multiple comparisons and thus increases false positive rates. Bonferroni corrections or the false discovery rate is generally applied to avoid false positive rates. Typically, the Bonferroni-corrected *p* value is set to 0.05 divided by the total number of SNPs

analyzed (e.g., p=1 x 10^{-7} for 500K SNPs, p=1 x 10^{-8} for 1 million SNPs).[28] A stringent genome-wide thresholds (nominal p values < 5x10^{-8}) is usually used for a conventional GWAS, although a possible relaxation of variants at boarderline association (p < 1x10^{-7}) may also be considered in the replication process. Top 'hits' are taken forward for replication in independent case-control sets using genotyping approach. These disease loci are then subjected to further functional studies to identify causal variants and the disease-causing mechanisms.[29] Any associations reported in GWAS study will ne need to be verified in several well established studies across populations. This is particularly suited for discovering common variants with small to moderate effects. To date, 15 GWAS have reported associations of 159 common genetic variants (SNPs) with BP. [22; 27; 30; 31] The recent GWAS study led by the International Consortium of Blood Pressure has identified 10 new loci in or near genes that were not previously known to be associated with BP or HTN.[30] Each of these reported variants may individually have small effect sizes, but they open up new horizons for potentially unknown mechanisms that alter the phenotype.[32] One of the major limitations of GWAS is the lack of direct information provided on the causal SNP. Therefore in order to translate GWAS findings into discovery of novel biological functions and future drug targets, it is of great importance to prioritize these reported variants for functional follow-up studies, and to investigate the molecular effects in the context of CVD pathogenesis.

Missing heritability

The collective effect of BP loci identified through GWAS explains only a small proportion of BP heritability (<1%). Taken all types of genetic studies together, a large proportion of heritability is still unexplained by the current knowledge. The potential sources contributing to this missing heritability may be: rarer variants (less than 5% in

the population); structural variants that are not covered by the existing genotyping arrays; copy number variants (CNVs) or smaller (<1kb) insertion-deletion mutations; gene-gene interactions; and inadequate accounting for shared environmental factors in families.[33] Therefore, besides continuous efforts in uncovering additional common variants of small effect, other strategies to identify more types of genetic variants need to be sought to fill in our knowledge gap.[34]

1.3 Coronary heart disease (CHD)

Every year, 3.8 million men and 3.4 million women worldwide die from coronary heart disease,[35] which represents the leading cause of mortality worldwide. The main underlying pathology of CHD is atherosclerosis, which is the process of cumulative plaques formation inside the arteries supplying oxygen-rich blood to the heart and brain that eventually leads to impaired or absent blood supply and myocardial infarction or stroke.[36] Over the past decades, atherosclerosis has been considered to be a cholesterol storage disease, but now it is been acceped that inflammation also plays an important role.[37] Vascular injury and thrombus formation are the key events in the initiation and progression of atherosclerosis and in the pathogenesis of the acute coronary syndromes.[38] The mechanism of coronary thrombosis has been addressed mainly on plaque rupture, which is the most common cause of fatal acute myocardial infarction. The fibrous cap of the plaque typically overlies the necrotic core (lipid-rich center) and stands between the blood compartments. Ruptured plaques tend to have large lipid cores, and abundant inflammatory cells, as well as punctate or spotty calcification,[39] which indicate the critical role of lipid composition in the pathogenesis of atherosclerosis.

1.3.1 Lipoprotein concentrations and CHD

There are four major clinically used blood lipid indexes: total cholesterol, low-density lipoprotein cholesterol (LDL-C), high-density lipoprotein cholesterol (HDL-C), and triglycerides. Consistent and ample evidence from large clinical trials have demonstrated the association between lipoprotein-related lipid levels and CVD incidence.[40; 41] High concentrations of LDL-C are associated with increased risk of CHD, whereas high concentrations of HDL-C are inversely associated with the risk. Epidemiological studies have estimated that a 10% decrease in LDL-C can reduce the cardiovascular death by 10% and cardiovascular events by 25%,[37] whereas each 1% increase in HDL-C concentrations reduces the CHD risk by 2%.[42] While therapies including statins have proven the efficacy of lowering LDL in reducing CVD risk across the populations,[43] other therapies targeting alternative aspects of the lipid profiles have so far been disappointing in clinical trials. Despite the association between low plasma HDL-C level and increased CVD risk, this has not been translated into proven evidence that raising HDL-C prevents CVD, as clinical trials of HDL-C raising interventions have shown no benefit.[44; 45] More attention has now shifted to specific HDL sub-fractions as potential therapeutic targets or biomarkers for cardiovascular protection. [46]

1.3.2 Cholesterol efflux and HDL functions

Cholesterol plays an indispensable role for cell structure and function, but excess cholesterol may lead to abnormal proliferation, migration, inflammatory responses and/or death of cells.[47] Intracellular cholesterol may be eliminated through two different mechanisms: one is the esterification of cholesterol into cholesteryl esters, an option with limited capacity as overloading cells with cholesteryl esters is also toxic; the other is cholesterol efflux, an option with potentially unlimited capacity. After being proposed

by Glomset in 1968,[48] reverse cholesterol transport (RCT) now represents the most widely accepted mechanism underlying the HDL-C metabolic pathways.[46] RCT is the process by which cells transport excessive cholesterol back to the liver for bile acid synthesis and excretion, thus lowering the peripheral lipid burden.[49] However, more recent studies have also shown that the cholesterol efflux from liver cells is also an important mechanism that determines HDL-C levels. Cholesterol efflux is regulated by a number of intracellular transporters, such as ATP-binding cassette subfamily A, member 1 (ABCA1) and subfamily G, member 1 (ABCG1) and scavenger receptor class B1 (SR-B1).[50] ABCA1 and ABCG1 are responsible for the majority (~70%) of the total cholesterol efflux to serum or HDL in macrophage foam cells.[51] ABCA1-mediated RCT can lead to the simultaneous efflux of phospholipids and free cholesterol to lipid-free apoA-I (plasma pre-β1-HDL), which contributed to the assembly of nascent HDL particles.[52] The concept of using HDL cholesterol (HDL-C) as a biomarker for cholesterol efflux transport, which further associates with CVD risk, has shown certain limitations in clinical studies.[53] Recent studies have indicated cholesterol efflux capacity from macrophages, a metric of HDL function as an independent predictor of CVD risk.[54]

1.3.3 Identification of CHD related genes

Similar to HTN, CHD is also a polygenic disorder in most cases. Although the clinical heterogeneous nature of CHD hinders the phenotypic characterization of cases and controls for genetic studies,[55] GWASs have so far identified a total of ~46 loci associated with CHD. Most of these loci are in regions previous unknown to be associated with CHD, which altogether explain approximately a total of 10% of the CHD phenotypic variance.[56] The functions of many of these loci relating to CHD pathogenesis remain unknown. Therefore study of the underlying biology mechanisms

will broaden our understanding of the disease hence facilitates the translation and development of new therapeutic targets.

1.4 Association of SNP rs13107325 in *SLC39A8* with hypertension and other cardiovascular traits

1.4.1 GWAS report of SNP rs13107325 (Ala391Thr)

In a GWAS paper published by the International Consortium of Blood Pressure (ICBP), an index SNP (rs13107325, C>T) located in the solute family 39 member 8 gene (*SLC39A8*) on chromosome 4q22 was reported to be associated with systolic blood pressure (SBP) and diastolic blood pressure (DBP).[30] The rare allele T was associated with reduction of SBP (β = -0.981, p=3.3 x 10^{-14}, 0.98 mmHg), DBP (β = -0.684, p = 2.3 x 10^{-17}, 0.69 mmHg) and high expression of this gene in liver tissues.[22; 57] This SNP is also independently associated with circulating high-density lipoprotein cholesterol (HDL-C) concentrations [allele T, β = -0.023 (0.004), p=1.6 x 10^{-8}], but not with CHD [allele T, OR=0.89 (0.79-0.99), p = 0.04].[57] In a seperate meta-analysis of GWAS in >200,000 individuals the same SNP was significantly associated with SBP and DBP, and this was the only significant SNP in the *SLC39A8* region (P. Munroe, personal communication). This SNP is a nonsynonymous polymorphism located in exon 8 of *SLC39A8,* causing an amino acid change from alanine to threonine (Ala391Thr). Its minor allele frequency (MAF) is ~9.7% in individuals of European ancestry (CEU), but is much lower in other populations. According to HapMap statistics, this SNP is approximately 1% in Southwest USA African (ASW), 1.2% in Han Chinese Beijing (CHB), 10.5% in Toscans in Italy (TSI), and absent in Japanese (JPT) and Yoruba African (YRI).

Apart from the association with BP and HDL-C, this SNP has also been associated with two additional phenotypes, which are body mass index [allele T, β = 0.19 (± 0.04) kg/m^2, p = 1.93 x 10^{-7}] and schizophrenia [allele T, OR=3.30 (1.76-6.17, 95% CI), p=0.027x10^{-8}, homozygous genotype].[57-59] The associations with different phenotypes indicate pleiotropy of this allele, which may be caused by different underlying molecular mechanisms. The variant allele T seems protective for BP, but risk-increasing for all other phenotypes reported (debatable on HDL-C). Therefore caution is required when interpretating functional result, as the mechanism affecting one phenotype may not be applicable to others. Given all these associations are true, when characterizing the underlying biological mechanism of pleiotropic effects, several alternative models can be proposed to fit the observed data. If the variant decreases the risk of HTN but increases the risk of obesity, schizophrenia, questions need to be addressed on whether the opposite effects correspond to functional changes in different cell lines. It is important to test the following hypothesis: the effects of the same allele in different cell populations underlying associations with different diseases, a single molecular effect on multiple morphological or physiological consequences, or tagging of other potential causal variants within the same gene that result in different functions and phenotypes.[60]

Bioinformatics prediction

Bioinformatics tools are commonly used in prioritizing genes and variants based on their potential functionality. First of all, the linkage disequilibrium (LD) structure in the genomic region is examined. LD indicates the non-random association of alleles at different loci. The principle behind this method is that the index SNP can presumably display the association signal through its LD with causal variants.[61] Once the variants within the target region in LD with the index SNP are identified, a series of

bioinformatics tools can be used to evaluate the possible properties of these variants. Evaluation criteria include prioritization of functional SNPs and mutations, annotation of known functional sites, predicted impact on splicing, transcription factor binding and gene expression, the effect of amino acid substitution on protein function.

This SNP is located in a highly conserved genomic region with only one SNP in high LD across 100 kb of genomic sequence spanning the *SLC39A8* gene in the CEU population according to HapMap release 21 (r^2>0.8) by SNAP proxy research, and is not in high LD with any other SNP based on results from the 1000 Genome database, which implies a high possibility of this index SNP being functional (Fig. 1.3 A). The predicted topology of the ZIP8 protein consists of 7 putative transmembrane (TM) domains. The alanine-to-threonine substitution resulting from SNP rs13107325 is predicted to be located on the TM domain 6. Based on the fact that alanine at this position is found to be well conserved among mammals and birds,[62; 63] the change of hydrophilicity from alanine to threonine can possibly have an effect on the protein function (Fig. 1.3 B).

SNP rs13107325 is in LD (r^2 = 0.841) with SNP rs1813006 located at the intergenic region near the gene *BANK1*, which encodes a B-cell-specific scaffold protein that functions in B-cell receptor-induced calcium mobilization from intracellular stores. Polymorphisms in this gene are associated with susceptibility to systemic lupus erythematosus.[64] Being predominantly a complex disorder of perturbations in vasculature, kidney and central nervous system, some links have been established between inflammatory cells and end-organ damage which may contribute to HTN.[65] The role of B-lymphocyte in the pathophysiology of HTN has been reported to be through activation and agonistic autoantibodies to the angiotensin II type I receptors.[66] However, the MAF of ~2% for rs1813006 makes it difficult to perform genetic study on this SNP with our existing sample pool.

Conservation analysis revealed that the common allele C at rs13107325 site is well conserved in 22 out of the 23 amniote vertebrates in the alignment (Fig. 1.3 C), which suggests that the C allele may be important in preservation of protein function. The output of ConSurf analysis also indicates the alanine residue is highly conserved and buried (normalized conservation score 9, structural residual) when compared with 142 reference sequences (Fig. 1.3 D). The degree to which an amino acid position is evolutionarily conserved is strongly dependent on its structural and functional importance. The substitution from a hydrophobic amino acid (Ala) to a hydrophilic polar amino acid (Thr) may change the position of the amino acid across the lipid bilayer of the cell membrane.

A

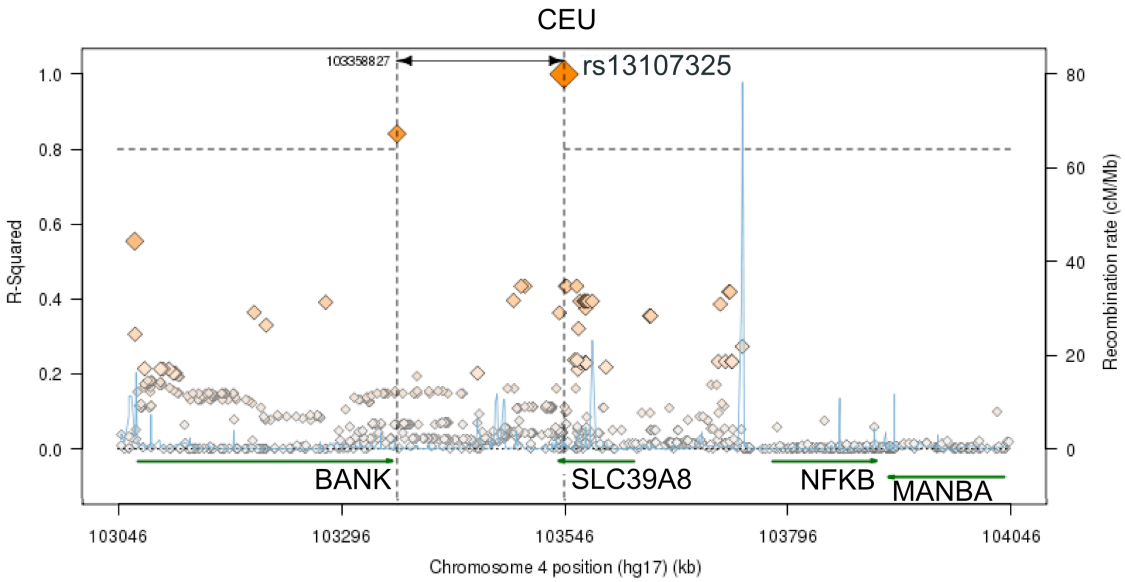

B

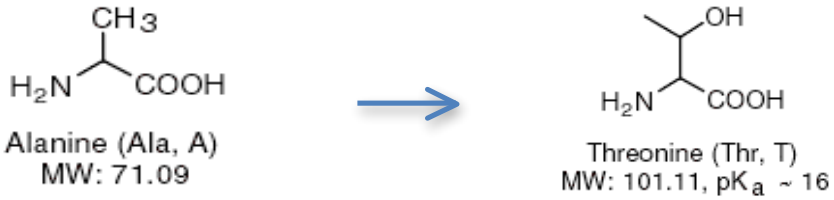

C

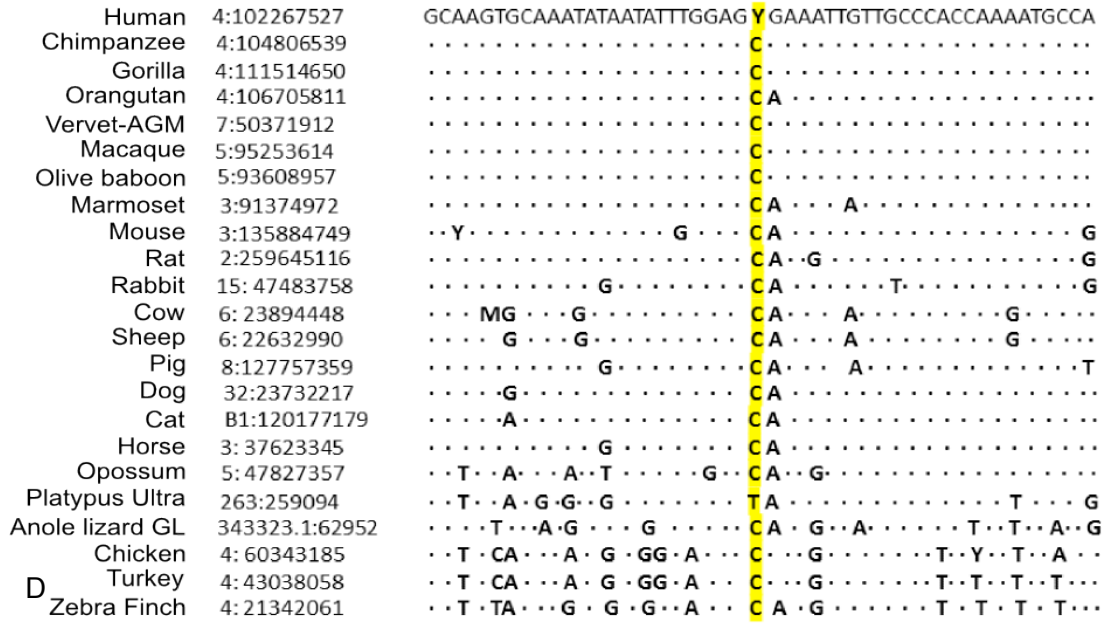

D

D

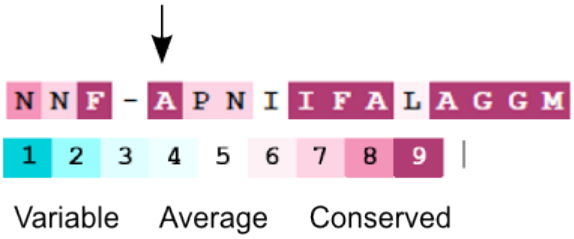

Figure 1.3. Bioinformatics prediction of rs13107325. (A) LD block of rs13107325 by SNAP proxy search (https://www.broadinstitute.org/mpg/snap/ldsearch.php), under HapMap release 21 database (B) Amino acid change arising from the SNP rs13107325 (C) Comparative genomics from 23 mammals from Ensembl version 78 (D) The output of ConSurf Server analysis based on 142 reference sequences, the arrow points the major amino acid alanine at position 391 on the protein sequence of ZIP8.

1.4.2 Transmembrane protein and Solute Carrier (SLC) gene family

Transmembrane protein

Membrane proteins can selectively transport molecules to allow the cell to control and maintain its intracellular composition. There are three main ways for molecules to pass through cell membranes.[67] Passive transport allows small uncharged solute particles diffuse across the membrane by the concentration gradient, until both sides of the membrane reaches an equilibrium. Facilitated diffusion, mediated by transporter proteins, also passes molecules from high to low concentrations in an attempt to achieve equilibrium, for instance glucose transport. However, charged molecules are unable to diffuse through a phospholipid bilayer, hence active transport is required by transmembrane proteins. These transport proteins determine the selective permeability of cell membranes and play a critical role in membrane function. Two classes of membrane transport proteins are reported, which are channel proteins and carrier proteins.

Solute carrier family 39

The solute carrier gene (SLC) superfamily comprises at least 374 putative protein-coding genes spanning across 58 families. SLC39 family proteins are members of the zinc- and iron-related protein (ZIP) family of metal ion transporters, which transport a wide range of substrates including essential metals, amino acids and various ions.[68] The human SLC39 family contains 14 members of the ZIP members, which transport divalent metal ions from cell exterior or lumen of intracellular organelles into the cytoplasm.[69] These proteins are highly conserved in human and mouse.[70] ZIP proteins

appear to play crucial roles in metal homeostasis and perhaps unrevealed signalling pathways.[71]

SLC39A8 encodes a zinc (Zn^{2+}) transporter protein ZIP8, which also exhibits high affinity for other divalent metals such as cadmium (Cd^{2+}), manganese (Mn^{2+}) and iron (Fe^{2+}).[33] Residing primarily on the plasma membrane of cells,[72] ZIP8 functions as a divalent cation/HCO_3^- symporter, bringing metal ions from blood into tissues and organs such as lung, pancreas, placenta, kidney tubules and testis.[73; 74] It has been shown in Madin-Darby canine kidney cells that ZIP8 is largely internalized during Zn^{2+} homeostasis, but moves predominantly to the cell surface membrane during Zn^{2+} depleted conditions.[75] Down-regulation of ZIP8 reduces cellular Zn^{2+} content in lung epithelia and correlates with reduced rates of Cd^{2+} uptake in small cell lung cancer derived cell lines transfected with glutamate-cysteine ligase catalytic subunit (GCLC). [76; 77]

ZIP8 was first identified in 2002 in a screen of monocyte cDNAs induced by *Mycobacterium bovis* bacteria cell wall components.[78] ZIP8 closely relates to ZIP14 in structure and function, both encompassing nine exons and three alternatively spliced noncoding exons 1.[70] They are distinguished by a signature sequence (HEXPHEXGD) in TM-V that is not found in other ZIP transporters. HEXXH is a Zn binding motif found in most Zn metalloproteases.[79] In ZIP8, the first histidine in this motif is replaced by a glutamic acid (E), which is suggested to confer the ability to bind/transport other metal ions such as Cd^{2+}, Mn^{2+} and Hg^{2+}.[80] ZIP8 has been reported to transport Cd^{2+}, Zn^{2+}, Mn^{2+}, Fe^{2+} and Co^{2+} in cRNA-injected oocytes, with a v_{max} value of Cd^{2+} >Zn^{2+} > Fe^{2+},[81; 82] There is not enough evidence yet in whether other divalent metals can also be transported by ZIP8.[82]

1.4.3 Distribution and functional characterization of ZIP8

ZIP8 functions as a divalent cation/bicarbonate symporter,[83] moving both metal ions (Zn^{2+}, Mn^{2+}, Fe^{2+}, Hg^{2+}) and HCO_3^- into the cell in an electroneutral manner.[84; 85] ZIP8 has been found to be ubiquitously expressed in various tissues and is localized predominantly on the apical side of the plasma membrane, which is a key feature for metal uptake and disposition.[86] The presence of ZIP8 on the intracellular membranes of endoplasmic reticulum, Golgi apparatus, lysosomes and mitochondria were also reported.[76; 87; 88] The distribution of ZIP8 in other cellular domains suggests the possibility of trafficking between the intracellular compartments and membrane during physiological and pathophysiological conditions.[84]

ZIP8 is expressed at medium to high levels in 32 organ systems, most abundant in kidney, testis, breast, placenta, lung, duodenum, etc.[89; 90] Gene expression can be induced in primary human lung epithelia, monocytes and macrophages in response to tumour necrosis factor alpha (TNFα) or lipopolysaccharide (LPS).[91; 92] This up-regulation can be significantly inhibited by NF-κB suppression using an inhibitor (Bay11-7082) or RELA-specific siRNA. This transporter has been reported to be a NF-κB negative feedback regulator and is known to participate in the immune balance regulation through zinc-mediated suppression of IKK activity in monocytes, macrophages, and lung epithelia.[93] In fact, *SLC39A8* transcription is directly regulated by NF-κB; binding of NF-κB to the *SLC39A8* promoter region has been demonstrated by chromatin immunoprecipitation [59] and electrophoretic mobility shift assay (EMSA).[93]

Glycosylation is a common post-translational modification in ZIP proteins. In fact the predicted N-linked glycosylation sites have been proposed to modulate metal ion transport activity.[94] Glycosylation of ZIP8 has been reported by many research

groups.[86] There are three predicted N-linked glycosylation sites in the N-terminal region of ZIP8. The fact of heavy glycosylation following stimulation indicates the occurrence of additional post-translational regulatory events in controlling protein function.[93]

A considerable body of evidence identified ZIP8 as a regulator of intracellular Cd^{2+}: down-regulation of ZIP8 and ZIP14 were found in the metallothionein-null Cd-resistant cells,[95] whereas ZIP8 shRNA resulted in a decrease in Cd^{2+} accumulation; ZIP8-expressing mouse fetal fibroblasts have demonstrated a 10-fold increase in the rate of intracellular Cd^{2+} uptake and accumulation;[96] ZIP8 was responsible for the genetic difference in damage to the testicular vasculature endothelium in mouse;[97] *He et al*. reported that ZIP8-mediated Cd^{2+} transport acts in an active transporter manner in MFF cells by moving metal ions against concentration gradient in an energy-dependent manner.[84] As a cotransporter, ZIP8 has its maximal activity at an extra-cellular pH of 7.5, which is the physiological pH of a lot of tissue fluids. Electrogenicity studies showed an influx of two HCO_3^- anions per one Cd^{2+} (or one Zn^{2+}) cations, suggesting the transport occurred in electroneutral complexes. In organ with different HCO_3^- gradient such as kidney, HCO_3^- might act as the driving force for Cd^{2+} uptake, which is ~24mM at the proximal tubule then decreases as the glomerular filtrate passes through S2 and S3 through to the ascending loop of Henle. Abundant expression of ZIP8 on the apical side of the renal epithelial tubule cells may be responsible for the reported accumulation of Cd^{2+} in kidney proximal tubule.[98] This altogether might explains the accumulation of Cd^{2+} in kidney proximal tubule and the ultimate nephrotoxicity. Studies have revealed that ZIP8 is responsible for causing Cd-induced testicular necrosis and acute renal failure -- the symptoms seen in BTZIP8-3 mice (harbouring 3 additional times copies of *SLC39A8*), implying its function as an important metal transporter involved in renal metabolic acidosis and kidney damage in human.[99]

The global *SLC39A8(-/-)* knockout was prone to be early embryo-lethal, resulting in hypomorphic *SLC39A8*(neo/neo) mice with a marked reduction in ZIP8 expression in the embryo, yolk sac, fetus and placenta. Additionally, there was the presence of severe congenital defects, including hypoplasia of multiple organs, followed by death between gestational day 18.5 and 48 hours postnatally.[100] Histologically, *SLC39A8* (neo/neo) mice had diminished levels of plasma iron, zinc, total iron-binding capacity (TIBC), serum alanine aminotransferase (ALT), aspartate aminotransferase (AST) and triglycerides (TGs) comparing to *SLC39A8* (+/+) and *SLC39A8* (+/neo) at postnatal day 1. This suggests ZIP8-mediated metal ion transport plays a critical role *in utero*, promoting neonatal growth, organ morphogenesis, and haematopoiesis. Other improved models such as *SLC39A8* (neo/neo) BTZIP8-3 line and hypomorphic *SLC39A8 (neo)* allele mouse with downregulation of ZIP8 have circumvented the mentioned congenital defects.[100; 101] BTZIP8-3 line has 3 additional copies of the *SLC39A8* gene comparing to its diploid pair found in WT mice, therefore expresses ~ 2.5 times greater amounts of ZIP8 comparing to WT mice on the cDNA level. A single dose subcutaneous administration of Cd^{2+} (30μmol/kg) caused acute renal failure and histological evidence of proximal tubular damage in the BTZIP8-3 mice but not their non-transgenic littermates.[70] Supplementation of $CdCl_2$ in drinking water (100mg/L-8,800 mg/L for 20 weeks) of the BTZIP8-3 mice resulted in increase in tissue-specific increase in Cd^{2+} (kidney, liver and lung but not testis), Zn^{2+} (liver > kidney, lung or testis) and Mn^{2+} content (liver and lung > lung or testis) and decrease in Ca^{2+} content when compared with the WT. No difference was seen in both WT and BTZIP8-3 mice in terms of levels of AST, ALT, iron and copper in liver, kidney, lung and testis.[102]

1.4.4 Structural analysis

Transmembrane protein is a type of membrane protein that spans across the entire biological membrane. It is been classified into the integral and peripheral membrane proteins. Integral membrane proteins are polypeptide chains embedded into biological membranes, whereas peripheral membrane proteins adhere only temporarily to the biological membrane by attaching to integral membrane proteins or penetrating the peripheral regions of the lipid bilayer. Membrane proteins are typically associated with lipid bilayers by extending through the lipid bilayer in an α-helical conformation. Most of these transmembrane proteins are amphipathic by consisting of both hydrophobic and hydrophilic regions. The hydrophobic regions pass through the membrane and interact with the hydrophobic tails of the lipid molecules in the interior of the bilayer and are composed largely of amino acid residues with nonpolar side chains, whereas the hydrophilic regions are exposed to water on either side of the membrane and composed mainly of amino acids with polar side chains. A representative interpretation of membrane-spanning segments of polypeptide chains is illustrated in Fig. 1.4.

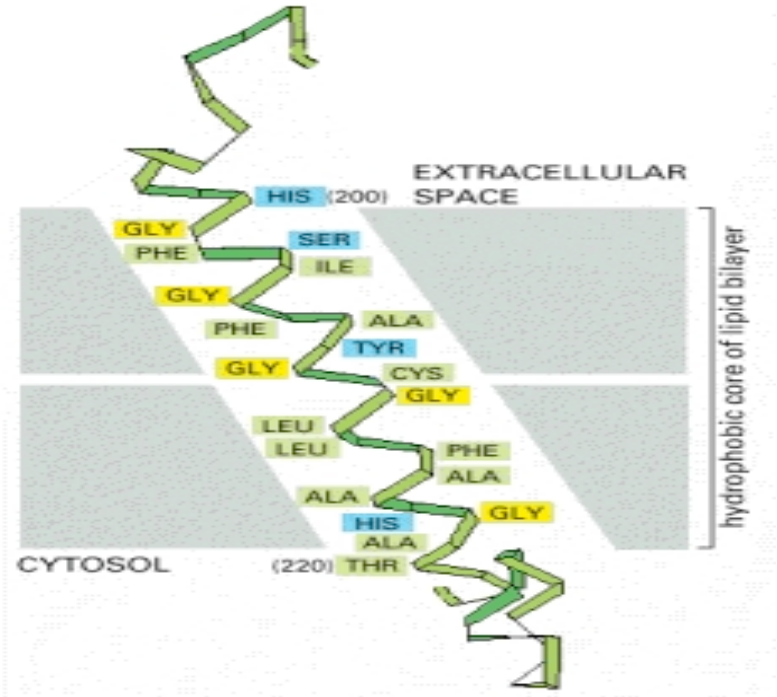

Figure 1.4. Segment of transmembrane polypeptide chain crossing the lipid bilayer as an α-helix. Hydrophobic amino acids are labelled in green and yellow. Usually an α-helical region consists of 20-25 hydrophobic amino acids. (from Molecular biology of the Cell, 4th edition) [103]

1.5 Biological effects of trace metals and their relationship with CVD

1.5.1 Zinc

Zinc (Zn) is an essential metal element serving as catalytic or structural components of enzymes and proteins that are indispensable in our body. It is estimated that ten percent of genes encode zinc-binding proteins.[104] Zn^{2+} maintains the normal structure and physiology of cells by participating in a variety of biological events including intracellular signal transduction,[105] cell cycle and proliferation,[86] and maintenance of

numerous transcription factor functions.[106] Zn^{2+} homeostasis is particularly important during anti-inflammatory response, for example Zn^{2+} deficiency increases systemic inflammation, tissue injury in response to sepsis.[107] Zn^{2+} plays a critical role in the redox signalling pathway, whereby deficiency of Zn^{2+} under oxidative stress leads to the degradation of critical proteins, i.e. protein kinase C (PKC).[108] Zn^{2+} deficiency may also result in an increased risk of infections including pneumonia and diarrhoea.[109] Lower serum Zn^{2+} level has been assoiciated with coronary heart events in patients with Type II diabetes.

1.5.2 Cadmium

Cadmium (Cd) is a highly toxic metal and one of the concerned pollutants that is distributed widely in air, soil, sediment and water.[110] It is commonly considered as a 'guest' metal generated in the lead : zinc mining, smelting and use of fertilizers.[111] It is one of the hazardous pollutants widely distributed in soil, sediment, and water, particularly in areas with high levels of particulate matter under diameter of 2.5 μM (PM2.5).[110] Non-occupational exposure mainly comes from diet and smoking, and it accumulates in the human body with a long biological half-life of 15-30 years.[86] It has been classified as a group I carcinogen by International Agency for Research in Cancer (IARC) and group B1 human carcinogen by Environmental Protection Agency (EPA).[112] It is also been classified as the Class D element, together with mercury, lead, for which is highly toxic even at low levels, with no clear biological function established to date.[113] The critical cadmium concentration in the kidney cortex defined by the World Health Organization is 200mg/kg, which corresponds to approximately 1mM.[114] The direct exposure to Cd^{2+} may cause harm to a variety of organs including lung, liver, kidney and bone.[115; 116] Long-term exposure to low doses of Cd^{2+} can result in severe diseases such as nephropathy and osteomalacia.[84] The main mechanism of Cd^{2+}

toxicity is through oxidative stress, and damage of enzymes and proteins by forming disulphide bonds.[99] The main target organs in humans are kidney and liver.[117]

The damage that Cd^{2+} causes to a target cell becomes effective only after influx (Cd^{2+} uptake) by that cell. Following its primary absorption from the intestinal or lung (portals of entry), the main means of transportation is through binding with various polypeptides such as metallothionein (MT), reduced glutathione and other thiol-proteins in the blood. The complex accumulates in liver and especially kidney cells, and ultimately deposited predominantly in these two organs. Because Cd^{2+} is not essential to living organisms, its transport mechanisms can be related to channels developed for other essential metals. Several ion channels and transporters have been described to transport Cd^{2+} across the plasma membrane, such as DMT1 (encoded by *SLC11A2)*,[118] and voltage-gated calcium channels.[119] By sharing the same transporters, other divalent cations (i.e. Zn^{2+}, Cu^{2+}, Mg^{2+}, Mn^{2+}) can compete with Cd^{2+} for cell entry.[75] Among all the transporters, it is reported that ZIP8 has higher Cd^{2+} transport affinity (K_m=0.48μM) than that of DMT1 and Ca^{2+} channels. It is therefore speculated that under low Cd^{2+} exposure, ZIP8 may be favoured over other transporting systems in transporting Cd^{2+}.[99] The cellular Cd^{2+} detoxification/efflux pathway is mostly dependent on the up-regulation of MT proteins. MT consists of multiple cysteine residues by which heavy metal ions can be immobilized and becomes less toxic.[120] Cd^{2+} efflux system is also mediated by the multidrug resistance protein (MRP) family. Human MRP1 is induced by Cd^{2+} exposure and its expression levels are associated with Cd^{2+} resistance.[121]

The renal cortex is one of the major target sites for acute or chronic Cd^{2+} exposure. Absorbed Cd^{2+} in the blood circulation in the MT-binding complex is filtered by the glomeruli, followed by reabsorption at the proximal tubule.[113; 122] Several studies have suggested that endothelial cells of the kidney can be damaged by low level of

Cd^{2+}. The endothelial nitric oxide synthase (eNOS) has been shown to be up-regulated by 10 to 20 fold in rats after 9-week sub-chronic exposure to Cd^{2+}.[123] Cd can also stimulate the release of a number of pro-inflammatory components from endothelial cells that would facilitate the progression of atherosclerosis.[124; 125]

1.6 Relationship between metal exposure and CVD

1.6.1 Effects of Cd^{2+} exposure and hypertension

Chronic Cd^{2+} exposure is associated with hypertension in animal models.[126] A large number of epidemiological studies have suggested a possible link between exposure of Cd^{2+} and the development of hypertension.[127; 128] However, the exact influence of Cd^{2+} on human BP has been inconsistent in the literature.[129] Tellez-Plaza *et al.* analysed data from the 1999-2004 US National Nutrition Examination Survey (NHANES) consisting of 10,991 participants (hypertensive and non-hypertensive) and they reported a modest association of blood Cd^{2+} (BCd) levels with elevated BP (SBP: 1.36 mmHg, CI=-0.28-3; DBP: 1.68 mmHg, CI=0.57-2.78),[130] followed by a similar association reported in a high Cd^{2+} exposure Korean population.[131] A recent meta-analysis in 2010 based on 12 studies demonstrated a positive association between BCd level and BP among women (including premenopausal and antihypertensive women), the BCd showed a larger estimated effect in the smoking-adjusted anaysis (SBP: β =1.85 mmHg; 95% CI, 0.52-3.19; DBP: β = 2.01 mmHg; 95% CI, 0.86-3.15).[129] This finding was supported by three recent studies on the positive association between BCd and BP in women.[132-134] On the contrary, a prospective study led by Staessen *et al.* including 692 subjects failed to establish any significant link between BCd or urinary Cd^{2+} (UCd) with increased HTN risk, albeit the positive association between BCd and BP in premenopausal women (n=179).[135] Based on available

literature, the positive relationship seems to be more evident in females. The discrepancies across studies might be due to outcome misclassification bias (inconsistently defined across studies), limited small sample size, lack of adjustment for potential confounders (presence of other metals), or lack of standardization on BP measurements.[130] This line of research would benefit from both physiological studies of cadmium mode of action, and longitudinal epidemiological studies of never-smoking, general populations to evaluate the relationships among BCd and UCd, and SBP, DBP, and sustained HTN. Most review papers highlighted the possible effect on cardiovascular systems at low Cd^{2+} exposure levels.[125 136-138]

1.6.2 Effects of Cd^{2+} exposure and other CVD

The types of Cd^{2+} exposure are through intake of contaminated food, drinking water, or by inhalation of polluted air or industrial occupation. Increased cardiovasculcar mortality was documented in areas with increased potential for cadmium exposure [geometric mean levels: 0.28 and 0.40 μg/g (urinary cadmium per gram of urinary creatinine) for men and women] based on 13,958 adults from The Third National Health and Nutrition Examination Survey.[139] Cadmium exposure has been associated with numerous CVDs including atherosclerosis, peripheral arterial disease, myocardial infarction. In the Atherosclerosis Risk Factor in Female Youngsters (ARFY) study from 195 healthy individuals, Cd^{2+} level was independently associated with early atherosclerotic vessel wall thickening.[140] Houtman *et al.* also observed a higher incidence of atherosclerosis in a Cd-contaminated area in the Netherlands.[141] Numerous studies reported the adverse cardiovascular effects Cd^{2+} exerts by promoting atherosclerosis and causing abnormal cardiac function.[125; 138] Urinary Cd^{2+} level was independently associated with myocardial infarction [142] and serum Cd^{2+} level was associated with high intima media thickness as a sign of early atherosclerotic

vessel wall thickening.[140] The National Health and Nutrition Examination Survey (NHANES) in 1999-2000 reported the blood Cd^{2+} (BCd) and Pb^{2+} levels were associated with peripheral arterial disease，which is defined as a blood pressure ankle brachial index <0.9 in at least one leg. [31;143] UCd levels were reported to be 36% higher in subjects with PAD than in those without, BCd was 16% higher in PAD cases than in noncases.[143] Circulating Cd^{2+} level has also been reported to be increased in patients with coronary artery disease. However, epidemiological data has not yet firmly established a link between Cd^{2+} levels and CVD, with possible confounding effects such as smoking status and other confounding metals.[144] Evidence of endothelial cell death induction is thought to be fundamental in the atherosclerosis-promoting properties of cadmium. [136]

1.6.3 Mechanism of actions of Cd^{2+} poisoning

The established hypothesis is that Cd^{2+} exerts its toxicity to the vascular endothelium through several mechanisms, typically through direct vasoconstriction and inhibition of the vasodilator substance nitric oxide.[145] A separate mechanism is the increase of oxidative stress caused by lipid peroxidation leading to injury of cellular components due to the interaction of metal ions with the cell organelles.[146] Cd^{2+} can display its detrimental effect to the vascular cells by increasing monocyte/macrophage transdifferentiation into foam cells, by causing endothelial dysfunction and subsequent cell death, and by stimulating smooth muscle cell proliferation at low Cd^{2+} concentrations.[136] These actions can lead to the initiation and promotion of atherosclerosis. It is noteworthy that different effects have been observed with high and low doses of Cd^{2+} exposure.[147] Cadmium is toxic to the vascular system as well as the kidney, but it remains to be determined how these various effects of Cd summate to influence the net regulation of BP. [148]

1.6.4 Effect of Zn^{2+} exposure and CVD

Low serum Zn^{2+} levels are correlated with hypertension, CHD, type II diabetes and hyperlipidemia.[149; 150] Zinc deficiency may lead to increased oxidative stress, mitochondrial dysfunction, cardiomyocyte dysfunction, which can lead to abnormal cardiac remodelling, heart failure, or hypertension.[151] An inverse correlation of BP and serum Zn^{2+} was observed in 35 hypertensives compared to 50 normotensives (75.34 ± 13.33 μg/dL in hypertensives, and 89.62 ± 23.79 μg/dL in normotensives, p<0.001).[152; 153] Increased gastrointestinal absorption and urinary excretion of Zn^{2+} was confirmed in primary arterial HTN from experimental models and clinical studies.[154] Loss of Zn^{2+} homeostasis may either considered to be the primary (cause) or the secondary (effect) of increased arterial blood pressure.[155] Zinc can inhibit gene expression including NF-κB and is an important cofactor for superoxide dismutase (SOD), therefore is served as an antioxidant.[149] Low serum Zn^{2+} levels were found in elderly hypertensives with low plasma renin activity.[156] These effects altogether may account for the antihypertensive effects of Zn^{2+}.[149; 157]

Zinc has shown to have protective effects in coronary artery disease and cardiomypathy.[104] On the molecular level, its mediation of adhesion molecule expression through inhibiting NF-κB transcription in endothelial cells may act as a critical step in development of atherosclerosis.[158] According to the “response to injury” hypothesis proposed by Ross and Glomset that atherosclerosis commences with endothelial cell injury,[159] Zn^{2+} may have a protective role in maintaining the integrity of endothelial cells and thus decrease vessel susceptibility to atherosclerosis.[160] Myocardium dysfunction is intimately involved in the aetiology of many forms of CVDs and the possible relationship of Zn^{2+} homeostasis and heart failure has been investigated by a number of studies. In humans, it has been demonstrated that plasma

Zn^{2+} levels decreased after acute myocardial infarction.[161-163] The involvement of Zn in insulin signalling and pathogenesis of diabetes has further indicated its potential role in diabetic cardiomyopathy.[164; 165] A graphic summary of the effects of Zn^{2+} deficiency on CVD pathogenesis is shown in Fig. 1.5.

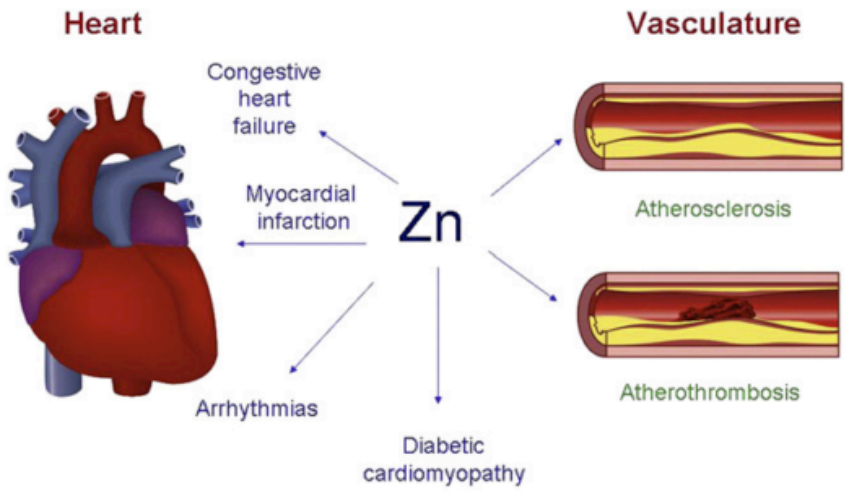

Figure 1.5. Role of Zn^{2+} deficiency in cardiovascular pathologies

(cited from *P.J.Little et al*, *Nutrition,* 2010) [104]

1.7 Proposed mechanisms of metal ions contributing to the pathogenesis of vascular disease

1.7.1 NF- κB pathway

NF-κB is a transcription factor that regulates a broad spectrum of physiological processes including innate- and adaptive-immune response, cell adhesion and proliferation, embryonic development and tissue remodelling.[166] Most mammalian cells comprise of five NF-κB family members, RelA (p65), RelB, c-Rel, p50/p105 (NF-κB1) and p52/p100 (NF-κB2), which form different NF-κB complexes in homo- and heterodimers.[167] The predominant complex in many cell types is the p65:p50 heterodimer. NF-κB complexes are normally retained in the cytoplasm by a family of inhibitory proteins IκBα, which is phosphorylated by IκB kinase (IKK) and degraded by the 20S proteasome. This process results in IκBα degradation and release of NF-κB, allowing it to translocate into the nucleus to transactivate target genes.[168] These pathways are classified as canonical (classical) and non-canonical (alternative). In the canonical pathway, the IKK dimer is activated by signalling through TNFR1 and IL-1R, TLRs (Toll-like receptors) in response to cognate ligands, leading to the modification of TRAF6 with Lys^{63}-linked polyubiquitin chains (Ub). A schematic representation of TNF-R1-induced NF-κB activation is shown in Fig. 1.6.

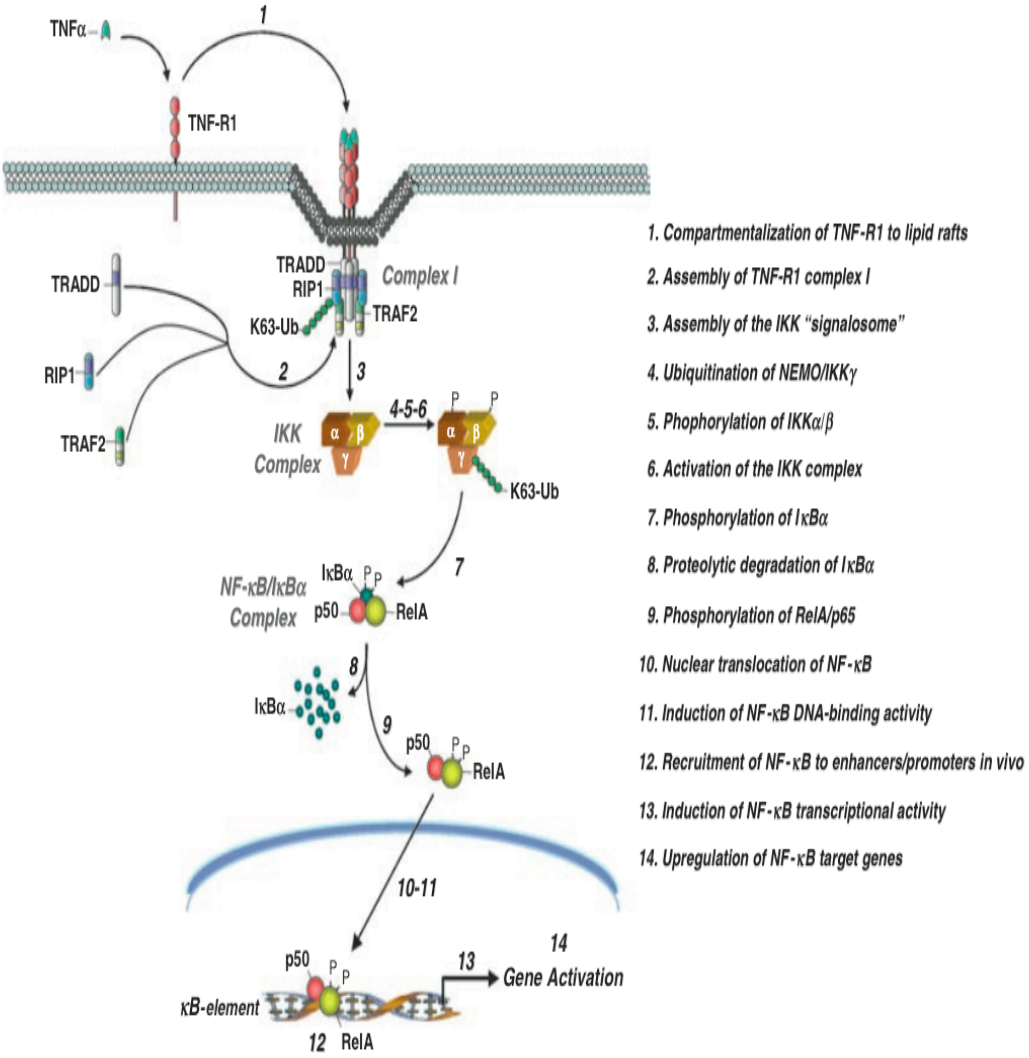

Figure 1.6. Schematic representation of the TNF-R1-induced pathway of NF-κB activation.[169]

Various techniques can be used to assess the activation triggered by extracellular stimuli based on essential steps in this pathway. These include activation of IKK complex (western blotting, ubiquitination and kinase assay), the phosphorylation and proteolysis of IκBs (western blotting), phosphorylation of RelA/p65 (western blotting), induction of NF-κB transcriptional activity (luciferase reporter assay), etc.

Effect of Zn^{2+} influx on NF-κB activation and cholesterol efflux

Studies in humans and animals suggest that Zn^{2+} can potentially affect lipoprotein metabolism and hence impact on CVD risk.[170] Zn^{2+} metabolism is primarily coordinated by ZnT (exporters) and ZIP (importers) transporters which maintain its normal cellular homeostasis. ZIP8 is a major Zn^{2+} importer, supported by the fact that *SLC39A8* hypomorphic mice exhibited reduced Zn^{2+} uptake and increased NF-kB activation.[93] Overexpression of ZIP8 results in enhanced Zn^{2+} uptake in Chinese hamster ovary cells, which highlights its important role in Zn^{2+} transport in the cells devoid of efficient Zn^{2+} transporters.[171] Zn^{2+} can inhibit NF-kB activation through binding of IKKβ kinase, it is therefore proposed that ZIP8 acts as a negative feedback regulator of NF-kB and innate immune activator through coordination of Zn metabolism (Fig. 1.7).[93] The association between HDL-C and rs13107325 in *SLC39A8* brings forward the possible involvement of ZIP8 in cholesterol efflux which participates in the pathogenesis of coronary artery disease. HDL is a complex molecule containing apolipoproteins such as ApoA-I which is an acceptor for cholesterol. As discussed earlier, the transporter ABCA1 plays an important role in cholesterol efflux from cells. The ABCA1 expression is positively regulated by NF-kB in macrophages.[172] It is possible that ZIP8 could partially influence cholesterol efflux through its effect on Zn^{2+} metabolism and consequently on NF-kB activity. Zn^{2+} influx can negatively regulate NF- kB activation, leading to downregulation of *ABCA1*, which will result in reduced cholesterol efflux activity and lower levles of extracellular HDL-C. However formation of HDL-C is a complex process whereas some steps are ABCA1 independent.

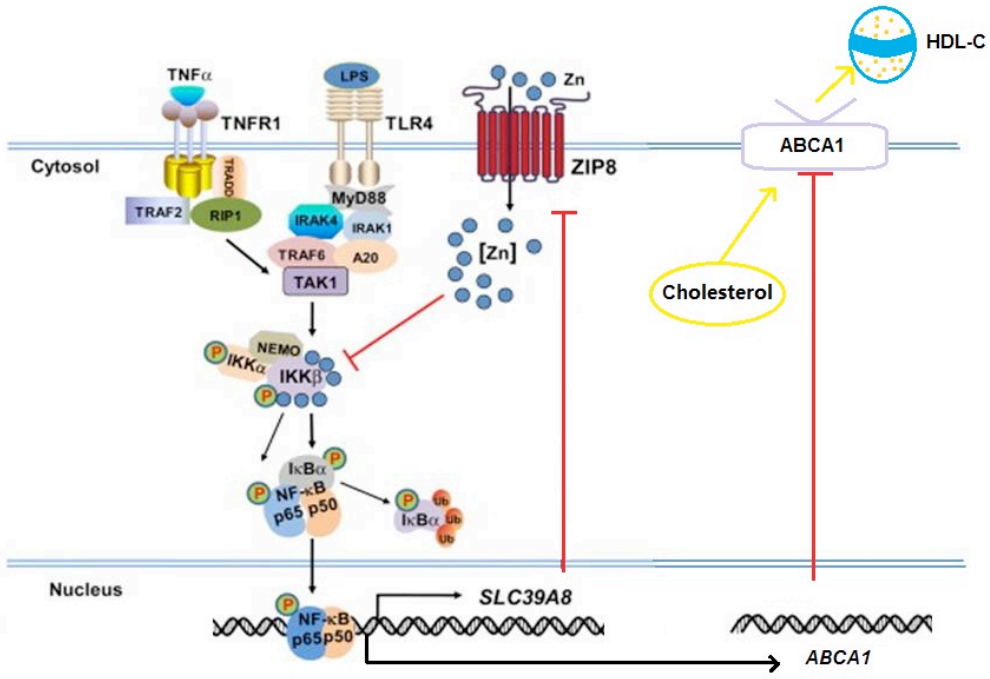

Figure 1.7. Schematic representation of regulation of Zn^{2+}, NF- kB signalling and cholesterol transport pathway (diagram adapted from *M.Liu et al. Cell Reports*, 2013)[93]

NF- kB signalling in CVD

NF-kB has been linked to both cardiovascular health and disease. In the adult, NF- kB can have both beneficial and detrimental effects in the cardiovascular system, with the pathway being either over- or under-stimulated in certain disease settings.[173] It is shown that NF-kB is cardioprotective during acute hypoxia and reperfusion injury, whereas prolonged activation appears to be detrimental and promotes heart failure by inducing chronic inflammation and through enhanced elaboration of cytokines including TNF- α , interleukin-1 and 6.[174] The NF-kB signalling controls many processes including inflammation, cell survival, differentiation and proliferation, in particular its effect on cell survival/apoptosis may have larger impact on CVDs. The canonical pathway is

implicated in atheroslerosis, myocardial infarction, ischaemic preconditioning, hypertrophy and heart failure. NF- kB is considered to play a pathophysiological role in the development of pulmonary arterial hypertension, however its role in arterial hypertension is not well documented.[175]

1.7.2 Extracellular-signal-regulated kinases (ERK1/2) pathway

Extracellular-signal-regulated kinases (ERKs) are members of the larger family of mitogen-activated protein kinases (MAPKs). ERK1/ERK2 (also known as p44/p42 MAPK, respectively) are two isoforms of ERKs which are 84% identical and similar in functions.[176] Activation of ERK involves diverse sequential phosphorylation cascades. One route is through stimulation of G protein-coupled receptors (GPCRs) and release of Gβγ subunits, the other is through activation of growth factor-stimulated tyrosine kinase receptors such as the epidermal growth factor (EGF) (Fig. 1.8). The ligation of EGF and cell adhesion receptors lead to GTP loading and activation of Ras, a small GTPase which recruits the MEK kinase Raf to the membrane where it is activated, which in turn activates MEK. ERK1/2 are activated through the Ras/Raf/MEK cascade, where activated MEK will then phosphorylate threonine 202 and tyrosine 204 residues on the dual-specificity motif (T-E-Y) to activate ERK1/2.[177]

The proposed ERK response to Cd^{2+} poisoning can be via multiple pathways, as shown in Fig. 1.8. In the calcium-mitochondria-caspase apoptosis pathway, Cd^{2+} enters cells through the ZIP8 transporter, the accumulation of the ions may act on the endoplasmic reticulum to increase the cytosolic Ca^{2+} concentration and subsequently the production of ROS.[178] ROS participates in both the activation of ERK and in the inhibition of dual-specificity phosphatases including MKP3, which may further participate in the constitutive and long-term activation of ERK.[179] This activation will

ultimately result in the activation of caspase-3 and -8 and cell apoptosis.[180] In the ROS-GSK3β pathway, Cd^{2+} might act on the mitochondria to generate ROS, which in turn activates GSK-3β and leads to autophagic cell death. Other parallel pathways may be present such as protein kinase C (PKC) signalling, which is shown to play a prodeath role.[181] Cd^{2+}-induced cell death can cause nephrotoxicity which will have a further impact on the regulation of blood pressure. The ability of ZIP8 to transport Cd^{2+} is essential to the accumulative toxicity of Cd^{2+}. Therefore, genetic variation of *SLC39A8* which leads to less accumulation of Cd^{2+} will protect cells from the Cd^{2+}-induced cytotoxicity.

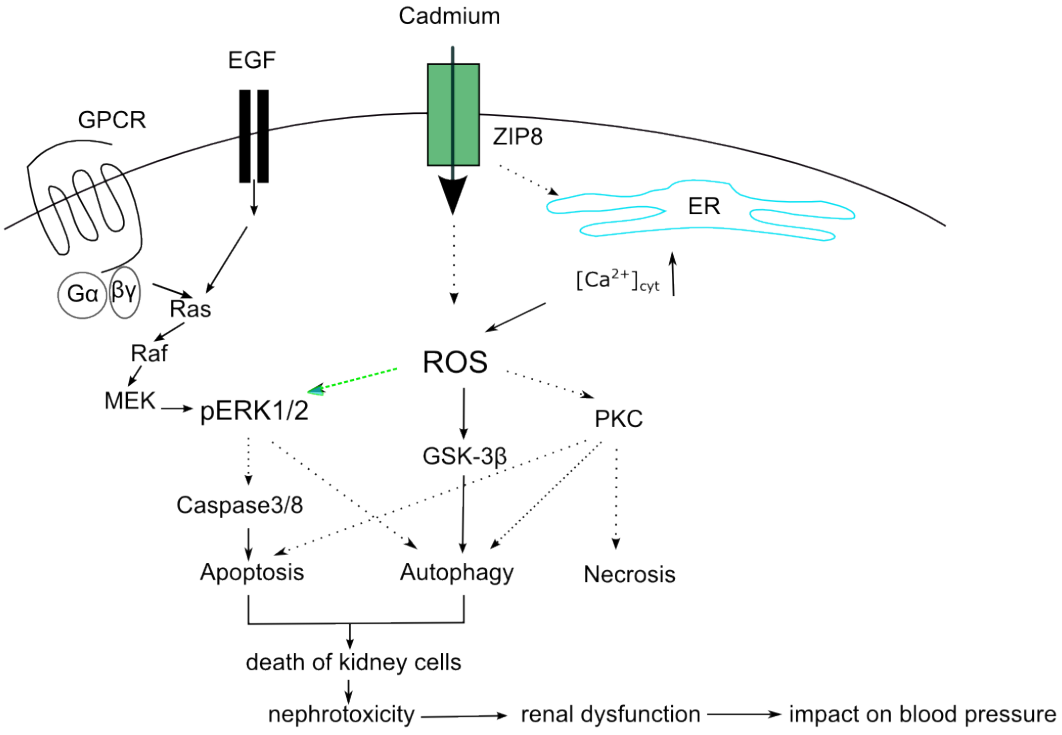

Figure 1.8. Schematic diagram of the potential mechanisms of Cd^{2+} induced ERK1/2 activation and cell death in kidney. EGF, epidermal growth factor; GPCR, G protein-coupled receptor; MEK, mitogen-activated protein kinase kinase; (Diagrams modified from P. Martin et al., FEBS, 2009 and L. Yang et al., Autophagy, 2009) [182; 183]

Phosphorylated ERK1/2 can enter the nucleus, and thereafter phosphorylate transcription factors involved in cell-cycle regulation. ERK is a promiscuous kinase which can phosphorylate more than 100 different substrates. It has been widely associated with every major aspect of cell physiology, including cell proliferation, survival, apoptosis, motility, transcription, metabolism and differentiation.[177] Activated ERK can control many cell responses depending on the kinetics of activation,[184] the subcellular localization and scaffolding proteins.[185] The biphasic kinetics of ERK activation is characterized by a rapid and transient burst of activation (phosphorylation of Tyr and Thr residues) upon first few minutes of stimulation, followed by a second stable activation that lasts for a few hours.[186]

The Ras/Raf/ERK pathway is found to be frequently deregulated in tumours. Many studies have associated its oncogenic properties to increased cell survival, by upregulating the pro-apoptotic proteins such as Bax,[187] or by promoting the activity of anti-apoptotic proteins such as Bcl-2 and Bcl-X1.[177; 187] ERK is also reported to promote the activity of the tumour suppressor gene p53, which is supported by its ability to bind to p53 and phosphorylating Ser15 *in vitro*.[188; 189]

Evidence for ERK activity in hypertension

Basal intracellular ERK activities are elevated in a number of animal models of hypertension, including aorta of the spontaneously hypertensive rats (SHRs).[190-192] In addition, inhibition of ERK activation attenuates the VSMC response to vasoconstrictors. ERK also plays a role in mediating vascular smooth muscle cell growth.

Role of ERK1/2 in cell death

A growing body of evidence suggests that aberrant ERK activation can promote cell death. Sustained cytoplasmic ERK activity might promote senescence or autophagy, whereas sustained nuclear sequestration of ERK activity triggers apoptosis.[193] The intrinsic apoptotic pathway is characterized by release of cytochrome c from mitochondria and activation of initiator caspase-9,[194; 195] whereas the extrinsic apoptotic pathway is linked to the activation of caspase-8/3, poly (ADP-ribose) polymerase (PARP) cleavage and DNA condensation.[184; 186; 196]

Role of ERK in vascular smooth muscle cell (VSMCs) growth regulation

Abnormal growth and proliferation of VSMC lead to thickening of the SMC layer and narrowing of the lumen which are key features of hypertension.[197] The association between ERK activation and cell proliferation suggests a potential role for ERK activation in the regulation of vascular smooth muscle cells proliferation: prolonged ERK activation is associated with the modulation of VSMCs from a contractile to a proliferating phenotype; transactivation of the EGF receptor leading to activation of ERK has been shown to be involved in the induction of VSMC growth after treatment of α1-adrenoceptors;[198] therapeutic inhibition of ERK activation *in vitro* has been shown to improve smooth muscle hyperplasia and contributed to the restoration of the contractile response of SMC at tissue level.[199]

Cd^{2+} uptake and ERK activation

An unconventional activation pattern has been observed in cells exposed to micromolar concentrations of cadmium. A sustained ERK activation, which lasts up to

6 days post cadmium stimulation (1.25μM) was reported in HEK293 cells.[196] Similar observations have been made in other cell types (primary mouse and rat fibroblasts, kidney-derived epithelium cell lines, bone marrow derived macrophages, primary calvaria cells, HeLa cells, mouse myoblast cells, human T cells, mouse macrophages, rat lung cells).[181; 200-203] However, the classical anti-apoptotic function of ERK following cadmium exposure has been reported in other cell types, for example ERK1/2 activities were decreased in human non-small cell lung carcinoma CL3 cell line (<80 μM Cd^{2+}) and moderately activated at higher doses.[179] Others have reported a MAPKs-independent cell apoptosis induced by Cd^{2+} in human lymphoblastoid Boleth cells. These apparent discrepancies indicate that the relationship between ERK activation and cell death may be cell type specific, in which different regulation mechanisms may be in place contributing to Cd-induced cell death. In conclusion, the sustained activation of ERK in a number of cells can associates with, or at least partially contribute to cell death signalling.

The entry of cadmium into cells is necessary for the sustained ERK activation, which is tightly associated with cell death,[183] however the cadmium-induced sustained activation of ERK may be a result of survival mechanism following cadmium poisoning. Cadmium has been reported to induce two types of cell death in mesangial cells, including both autophagy and apoptosis,[194] which suggests that activation of ERK also occurs through a caspase-independent pathway. Cd^{2+} induces an increase of cytosolic Ca^{2+}, followed by ERK activation and mitochondrial depolarization, which then triggers autophagy and apoptosis.[194] Similar observations were also seen in NIH3T3 cells, rat astrocytes and tumour-derived Saos-2 cells.[204;178; 188] The increase of Ca^{2+} in turn leads to an increase in reactive oxygen species (ROS) and mitochondrial impairment. Taken together, these correlations suggest that Ca^{2+} might play a role in the cadmium response upstream of ROS production.

In addition, the entry of Cd^{2+} in cells can also result in a time- and dose-dependent oxidative response by production of ROS.[205] Several studies demonstrated the role of ROS in ERK activation, supported by a strong activation of ERK leading to apoptosis which can be alleviated by antioxidants *in vitro*.[205] However, the mechanisms by which ROS activate MAPK are still inconclusive. Some groups reported ROS could stimulate the Ras/Raf/ERK pathway by promoting the activation of tyrosine kinase receptors or increasing activation of Raf signalling;[184; 186] whereas others demonstrated a correlation between MKP3 degradation and a strong activation of ERK.[206] It is likely that ROS production in response to Cd^{2+} results in the activation of the MAPK cascade and inactivation of MKP3 that contribute to the initiation and stabilization of ERK activation, respectively.[183]

The occurrence of cell death following cadmium poisoning including apoptosis, necrosis and autophagy. The type of cell death induced depends on factors such as the cadmium concentration, and the inducing pathway (i.e. lipid peroxidation, ROS production, intracellular calcium concentration).[194; 207] Although ERK alone is sufficient to induce cellular response leading to cell death in certain systems, cadmium can trigger a panel of pathways other than caspase activation that also culminate in cell death.[208]

1.8 Summary

These molecular pathways identified a potential link between ZIP8 and CVD events possibly via transportation of Cd^{2+}. The entry of Cd^{2+} into the cells causes sustained activation of the extracellular signal-regulated kinases signal transduction pathway.[123] Cd^{2+} exposure results in a complex response including increased oxidative stress,[209] kinase activation, protein degradation, and sustained activation of ERK,[183] which has been directly linked to cell death signaling.[196] ZIP8 might be involved in the activation of some of these pathway by transporting Cd^{2+} into the cells, which leads to the development of various cardiovascular events.

Further studies are required in order to understand the roles of ZIP8 and the molecular functional effects of the *SLC39A8* variant that has been found to be associated with BP and HDL-C levels. Knowledge gained from such studies may facilitate development of novel therapeutic interventions.

1.9 Aims and objectives

1. To investigate whether the Ala391Thr substitution resulting from SNP rs13107325 affects *SLC39A8* gene expression in human umbilical vein endothelial cells and human umbilical artery smooth muscle cells at mRNA and protein levels

2. To perform a functional study of the Ala391Thr substitution resulting from SNP rs13107325 in relation to ZIP8 function in transporting metal ions *in vitro*, i.e. Cd^{2+} and Zn^{2+}

3. To perform pathway analysis on whether *SLC39A8* overexpression or the Ala391Thr substitution triggers different signalling pathway activations (i.e. ERK1/2 and NF-κB) under Cd^{2+} treatment

4. To investigate a possible effect of *SLC39A8* overexpression and Ala391Thr substitution on cholesterol efflux *in vitro*, a potential underlying mechanism for the reported association of rs13107325 with circulating HDL-C level

5. To investigate whether the Ala391Thr substitution has an effect on Cd^{2+} toxicity shown by phenotypic change (i.e. proliferation and apoptosis) in transfected HEK293 and HUVECs *in vitro*

6. To conduct bioinformatics study on the impact of Ala391Thr substitution on ZIP8 function and secondary structure of the protein

2. Materials and Methods

2.1 Subjects and samples

2.1.1 Collection of human umbilical cords for isolation and primary culture of vascular cells

Fresh human umbilical cords of about 10cm in length were collected from healthy newborn babies from the Royal London Hospital. Cords from miscarriages, stillbirths, HIV positive, group B Streptococcus positive or hepatitis B infected mothers were excluded, however pre-eclamptic or diabetic individuals were not included in the exclusion criteria. The sections were stored for less than 48h at 4°C in sterile physiological saline solution (PSS, components of PSS are listed in **A2**) (Ethical approval number: 08/H0704/140, AM05 Minor Amendment, 01 Jan 2013).

Human umbilical artery smooth muscle cells (HUASMCs)

The dissection of the umbilical arteries was performed under sterile conditions containing PSS at 37 C°. The Wharthon's jelly adventitia surrounding the arteries was removed. The thick wall of the arteries was stripped off. Once the arteries were separated from all the connective tissues, they were then transferred to a clean Petri dish and cut into small fragments of about 2mm long using a scalpel. They were washed twice with PSS, and once with serum-free DMEM. After washing, the pieces of artery were evenly distributed onto a gelatin coated (0.2%, Sigma, G1393) T-25 flask (Nunc). The medium was removed and the flask was placed inside the incubator in a vertical position for 1-2 hours to allow the attachment of the pieces to the culturing surface. After the incubation, 5ml of Dulbecco's modified Eagle's medium (DMEM, Sigma, D5796) (additional supplements listed in **A2.5**) was added to the flask, which

was then placed flat inside the incubator for one week without disturbance to allow for explant of smooth muscle cells from the tissue to the dish surface. Subsequently, the medium was changed and the detached tissues were removed from culture until cells reached 90% confluence. For passaging, the cells were rinsed with 0.5ml of pre-warmed trypsin (Sigma, T4049) and then incubated with the same solution for no longer than 10 min, until all the cells were detached. The trypsin was neutralised by addition of FBS containing medium, and the cells were then transferred into a newly coated T-25 flask and cultured as required.

Human umbilical vein endothelial cells (HUVECs)

The isolation of HUVECs was carried out following a protocol established by Jaffe *et al*.[210] In summary, the veins of the umbilical cords were identified, then cannulated and clamped in position. Hank's Balanced Salt solution (HBSS, 50ml) was poured through the cannula to rinse off the intraluminal clots. Following the wash, type I collagenase (Sigma, C9891, 0.2% w/v) diluted in HBSS was infused into the vein *via* the cannula. Cords were clamped on both sides when the collagenase started to drip out from the distal end. Further collagenase was added until the vein was significantly distended. An average of 15 to 20 ml of collagenase solution was used for a section of 15 cm umbilical vein. The preparation was then incubated for 10 min at 37°C with gentle massaging of the cord at the start.

After incubation, the collagenase solution containing the endothelial cells was collected in a sterile falcon tube, and the vein was further flushed by perfusion with PBS to achieve a final volume of 50 ml. The solution was centrifuged at 1,000 x g for 10 min at room temperature. The supernatant was discarded and cell pellet was re-suspended in supplemented M199 (Sigma, M4530) medium. (Supplements listed in

Appendix 2.5) The cells were plated in T-75 flasks pre-coated with 0.2% w/v gelatin. The medium was changed the next day to remove non-adherent cells. Subsequently, the medium was changed every two or three days until appropriate confluency was reached for further subculture.

2.1.2 Cell culture

Cell culture and maintenance

HUASMCs and HUVECs were both isolated from human umbilical cords. HUASMCs were cultured in DMEM supplemented with 15% fetal bovine serum (FBS), 1% penicillin/streptomycin and supplements (listed in **A2.5**). HUVECs were cultured in supplemented M199 (supplements listed in **A2.5**). All the cells were incubated at 37°C with 5% CO_2. When passaging, cells were trypsinized and split in 1:3 ratio.

HepG2 is a human liver hepatocellular carcinoma cell line. HepG2 cells are adherent, epithelial-like cells growing as monolayers and in small aggregates. They were cultured in DMEM supplemented with 10% FBS and 1% antibiotics. The rest of the culture protocol was consistent with other cell types. Cells were passaged in 1:4 ratio or had culture medium changed every 3 days. MCF-7 is a breast cancer cell line given by Barts Cancer Institute. MCF-7 cells were cultured in DMEM supplemented with 15% FBS and 1% antibiotics. The cells were processed every three days by changing medium, passaging or freezing.

Human embryonic kidney 293 cells (also referred to as HEK293), are a specific cell line derived from human embryonic kidney cells, initiated by the transformation and culturing of normal HEK cells with sheared human adenovirus type 5 (Ad5) DNA. The transformation resulted in the incorporation of approximately 4.5kb from the viral

genome into human chromosome 19 of the HEK cells. HEK cell line has been extensively used as an expression tool for recombinant proteins over the last 35 years. The HEK293 cells used in this project were derived from commercial source, and maintained in DMEM supplemented with 10% FBS and 1% antibiotics. A summary of all the experimental cells lines are listed in **Table 2.1.**

Cell type	Rationale	Experiment type
HUASMC	Primary human embryonic smooth muscle cells; representative of human vasculature with endogenous genetic variation	*SLC39A8* expression study (AEI, immunoblotting)
HUVEC	Primary human embryonic endothelial cells;	*SLC39A8* expression study (AEI, immunoblotting) Cd^{2+} uptake, ERK1/2 and NF-κB signalling activation studies
HEK293	Embryonic kidney cells, good transfection model, representative of the human nephron	Cd^{2+} uptake, ERK1/2 and NF-κB dual luciferase reporter, cell death
HepG2	Encompass cholesterol efflux machinary (transporter) and efficient transfection model	Zn^{2+} uptake, cholesterol efflux and qRT-PCR
MCF-7	Breast cancer cell line, positive control for *SLC39A8* expression	*SLC39A8* expression positive control, ZIP8 transfection

Table 2.1. Summary of experimental cell lines

Cryopreservation

For long-term storage, cells were trypsinized, re-suspended in an appropriate freezing medium (components listed in **A2.5**) and transferred into cryovials. They were placed in a cryopreservation box and gradually frozen in a -80°C freezer and then transferred to liquid nitrogen tank for long term storage.

2.2 Genomic DNA and Polymerase chain reaction

2.2.1 Assessment of linkage disequilibrium

Before genotyping the index SNP of interest, the linkage disequilibrium (LD) block of the region containing the SNP of interest was determined using SNAP program (www.broadinstitute.org/mpg/snap/), under the category of HapMap release 21 dataset (contains all processed data from the HapMap project, including phase I+II, completed in year 2006).[211] The population panel was set at Northern Europeans from Utah (CEU), and the square of the correlation coefficient between two indicator variables (r^2 value) was set at threshold of greater than 0.8. The aim of this search was detect whether any other SNPs in the genomic region were in high LD with the index SNP in the available ancestries.

2.2.2 Preparation of samples for genotyping

DNA was extracted from cell pellets. Lysis buffer (components listed in **A2.2**) was added directly to the pellets, followed by addition of 275µl of 5M NaCl and 5 min incubation with gradient agitation. After centrifugation, the supernatant was mixed with 500 µl isopropanol. The precipitated protein in the supernatant was discarded and the

DNA pellet was washed with 70% ethanol. Supernatant was again removed and the DNA pellet was left to air dry. Finally, 40µl of nuclease free (NF) - H_2O was added, followed by mixing and incubation at 50°C for 10 min. The DNA concentration was determined by using NanoDrop Spectrophotometer ND-1000. A_{260}/A_{280} ratio and A_{260}/A_{230} ratio provide additional information on the purity of the DNA sample. An A_{260}/A_{280} ratio value of between 1.8 and 2 indicates that the DNA is of high purity. A lower value of this ratio indicates contamination of the sample with proteins which have the highest absorbance at 280nm. An A_{260}/A_{230} value of 2.0-2.2 indicates the sample is free from, or has minimal salt contamination, whereas a lower value will suggest that the sample is contaminated with salts or other impurities such as carbohydrates, or other precipitating agents such as phenol, guanidine or glycogen.

2.2.3 Polymerase chain reaction (PCR)

Polymerase chain reaction (PCR) is a technique used to amplify a piece of DNA fragments, generating thousands to millions of copies. Where not specified, PCR conditions and primers were designed according to the following protocol. All primers used (listed in **A1**) were designed using Primer3 program (http://bioinfo.ut.ee/primer3-0.4.0/). For SNP specific primers, the primers were designed to flank the region of interest with 100-200 bp on either side of the target DNA region. Default settings were used for all the other parameters. The PCR reaction components for genomic DNA and cDNA are listed in **A2.2**. The amplification program is listed in Table 2.2. A duration of 35 sec was chosen for the extension step, because Taq polymerase synthesizes about 1,000 bp per minute, and 35 sec would be sufficient for the extension step in a PCR to amplify a fragment of 200-300bp in size.

Temp (°C) gDNA/cDNA	Time (sec)	Cycles	Description
95	300	n/a	Initial denature
94	35	30-40	Denature
48/ 52 (dependent on primers)	35		Anneal
72	35		Extension
72	600	n/a	Elongation

Table 2.2. Thermal cycling conditions for PCR reaction of genomic DNA and cDNA

2.3 Genotyping

Genotyping is a method for determination of the genetic make-up (genotype) of individual human-derived sample. As described below, 3 genotyping methods were performed in this project. KASPar genotyping was primarily used on HUASMC DNAs. Due to the presence of false positive results generated by KASPar, TaqMan assay was applied to both HUASMCs and HUVEC DNAs, whereas aditional restriction enzyme digestion method was used to verify the genotyping results of the two methods above.

2.3.1 KASPar genotyping

KASPar is a genotyping system developed by KBioscience Ltd. It is a PCR-based technology that consists of two major components: the KASP primer mix and master mix. The primer mix contains two allele-specific forward primers (listed in **A1**, primer 1 and 2) each having a proprietary tail containing sequence complementary to the FAM or VIC dye in the master mix, and one common reverse primer (listed in **A1**, primer 3). Each oligo was resuspended in ddH_2O to a concentration of 100μM (Table 2.3 A). The

master mix was the same for every KASP assay, containing the FAM™ and VIC™ specific FRET (fluorescence resonance energy transfer) cassette reporter system, Taq polymerase, dNTPs, ROX passive reference dye and $MgCl_2$ (2.5mM) in an optimized buffer solution. The 2 x master mix was defrosted and diluted to 1 x by NF-H_2O and mixed well before use. The components for PCR reaction on one 384-well plate are listed in Table 2.3. The schematic workflow of the assay is shown in Fig. 2.1.

A

Components	**Volume (µl)**
Allele specific primer 1 (100µM)	12
Allele specific primer 2 (100µM)	12
Common primer (100µM)	30
NF-H_2O	46

B

Components	**Volume required for a 384-well plate (µl)**
DNA (5ng/ml, dried)	n/a
1 x Reaction mix	1060
Primer mix (100µl)	14.1
$MgCl_2$ (50mM)	6.7
Total volume for 1 well	2.5

Table 2.3. KASPar SNP genotyping. (A) Components of primer mix (B) Constituent reagent volumes for the 384-well plate genotyping

The 384-well plate was subjected to the cycling program detailed in Table 2.4. Some reactions may proceed faster hence the number of cycles can be reduced from 21 to 18 in the latter part of the program. Some reactions may proceed slower and additional cycles may be necessary to achieve a better separation of the clusters.

Temp (°C)	Time (sec)	Cycles	Description
94	900	n/a	Hot-start activation
94	10	20	Denature
57	5		Anneal
72	10		Extend
94	10	21	Denature
57	20		Anneal
72	40		Extend
Additional cycling conditions			
94	20	5	Denature
57	60		Anneal
72	40		extension

Table 2.4. Thermal cycling conditions for KASPar genotyping

After the PCR was completed, the end plate read was performed immediately using an ABI 7900HT sequence detection system using FAM or VIC detectors. The fluorescence data were analysed using SDS2.4 software (Applied Biosystems). Four separate sample clusters could be identified on the output plot, three corresponding to the different genotypes and one to the non-template controls. Fluorescence signals uniquely corresponding to either VIC or FAM represented major and minor homozygotes, whereas the presence of dual fluorescence signals indicated heterozygous populations (Fig. 2.1 B).

A

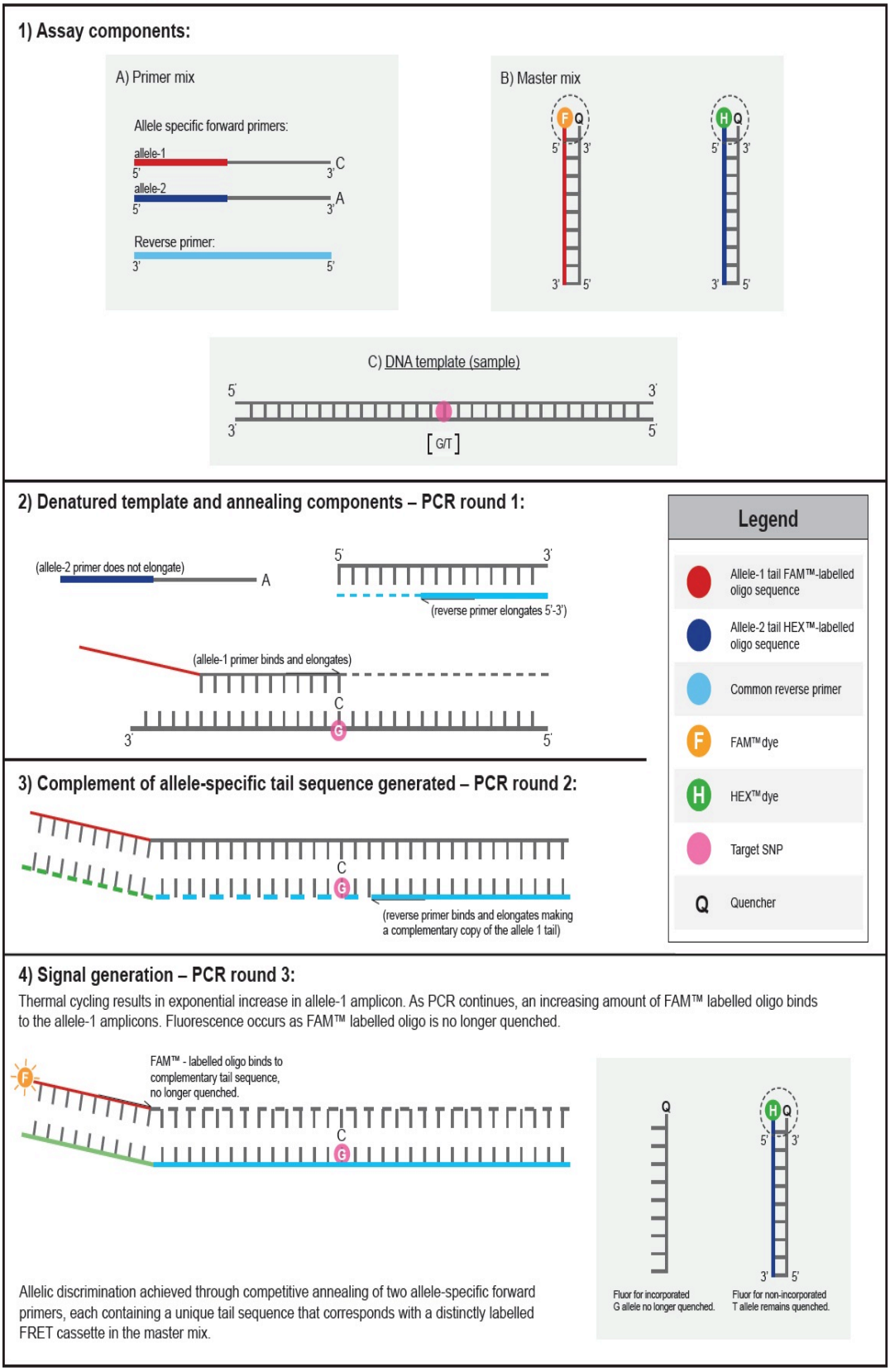
1) Assay components:
A) Primer mix
Allele specific forward primers:
allele-1
5'
3'
C
allele-2
5'
3'
A
Reverse primer:
3'
5'
B) Master mix
F
Q
5'
3'
3'
5'
H
Q
5'
3'
3'
5'
C) DNA template (sample)
5'
3'
3'
5'
[G/T]
2) Denatured template and annealing components – PCR round 1:
(allele-2 primer does not elongate)
A
5'
3'
(reverse primer elongates 5'-3')
(allele-1 primer binds and elongates)
C
G
3'
5'
3) Complement of allele-specific tail sequence generated – PCR round 2:
C
G
(reverse primer binds and elongates making a complementary copy of the allele 1 tail)
Legend
Allele-1 tail FAM™-labelled oligo sequence
Allele-2 tail HEX™-labelled oligo sequence
Common reverse primer
F
FAM™ dye
H
HEX™ dye
Target SNP
Q
Quencher
4) Signal generation – PCR round 3:
Thermal cycling results in exponential increase in allele-1 amplicon. As PCR continues, an increasing amount of FAM™ labelled oligo binds to the allele-1 amplicons. Fluorescence occurs as FAM™ labelled oligo is no longer quenched.
F
FAM™ - labelled oligo binds to complementary tail sequence, no longer quenched.
C
G
Allelic discrimination achieved through competitive annealing of two allele-specific forward primers, each containing a unique tail sequence that corresponds with a distinctly labelled FRET cassette in the master mix.
Q
H
Q
5'
3'
3'
5'
Fluor for incorporated G allele no longer quenched.
Fluor for non-incorporated T allele remains quenched.

B

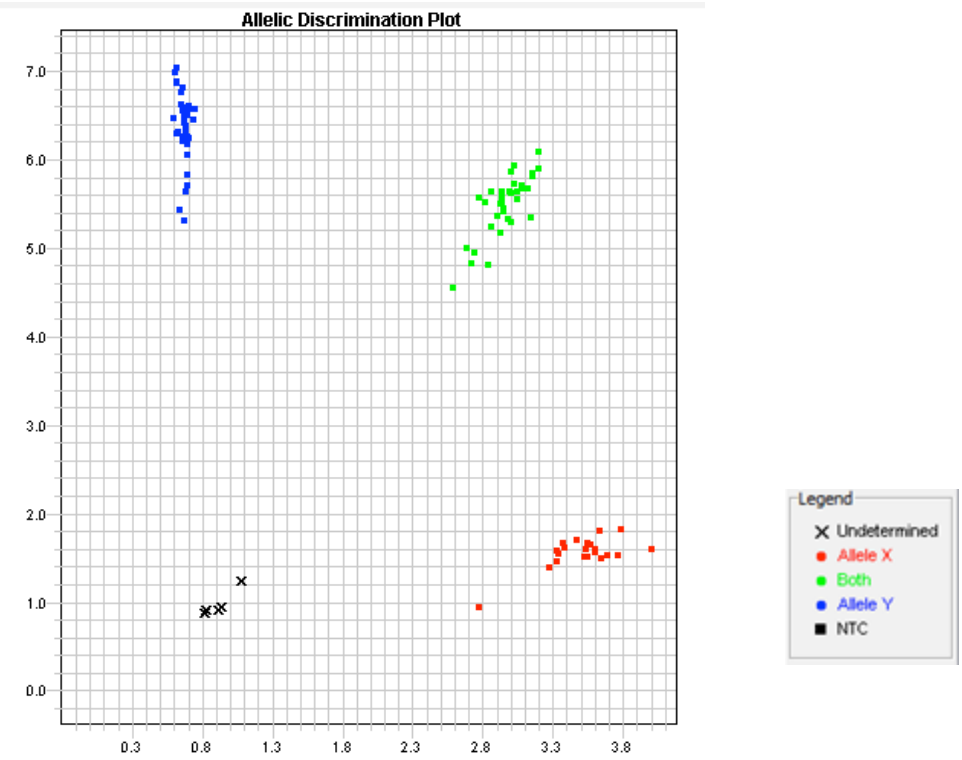

Figure 2.1. Workflow of KASPar genotyping. (A) Schematic workflow of KASPar genotyping (Diagram referenced from KASP genotyping chemistry user guide and manual) HEX™ dye was shown in the workflow diagram whereas VIC dye was used in our assay)[212] (B) Representative image of genotyping outcome

2.3.2 TaqMan® SNP genotyping assay

KASPar assays generated some inaccurate genotype clusters in a smaller sample pool i.e. HUVECs. Therefore a second assay was used to confirm genotyping results. TaqMan® SNP genotyping assay (5'-nuclease allelic discrimination assay) was also used to distinguish genotypes for DNA samples (Fig. 2.2). Relying on the FRET technology, the pre-designed TaqMan SNP genotyping assay consists of two allele-specific TaqMan® minor groove binder (MGB) probes labelled with a FAM or VIC

reporter fluorescent dye, and a sequence-specific forward and reverse PCR primers to amplify the DNA sequence containing the polymorphism of interest. FAM™ or VIC™ reporter dye is located at the 5' end of the probe and a non-fluorescent quencher lies in the 3' end of the probe. The reporter dye is quenched when the MGB probe is intact. During the PCR reaction, the 5'-nuclease activity of Taq DNA polymerase cleaves the reporter dye from the probe that is completely hybridized to the DNA strand, which then fluoresces upon separation from the quencher. When a single point mismatch is present in the DNA sequence due to a SNP, the binding of the probe to DNA is destabilized during strand displacement in PCR, which will in turn reduce the efficiency of the one of the probe cleavage and the fluorescence intensity from the corresponding reporter dye. Therefore an increase in either FAM or VIC fluorescence will indicate homozygosity for FAM- or VIC- specific alleles (X:X or Y:Y), an increase in the fluorescence for both dyes indicates heterozygosity (X:Y).[213]

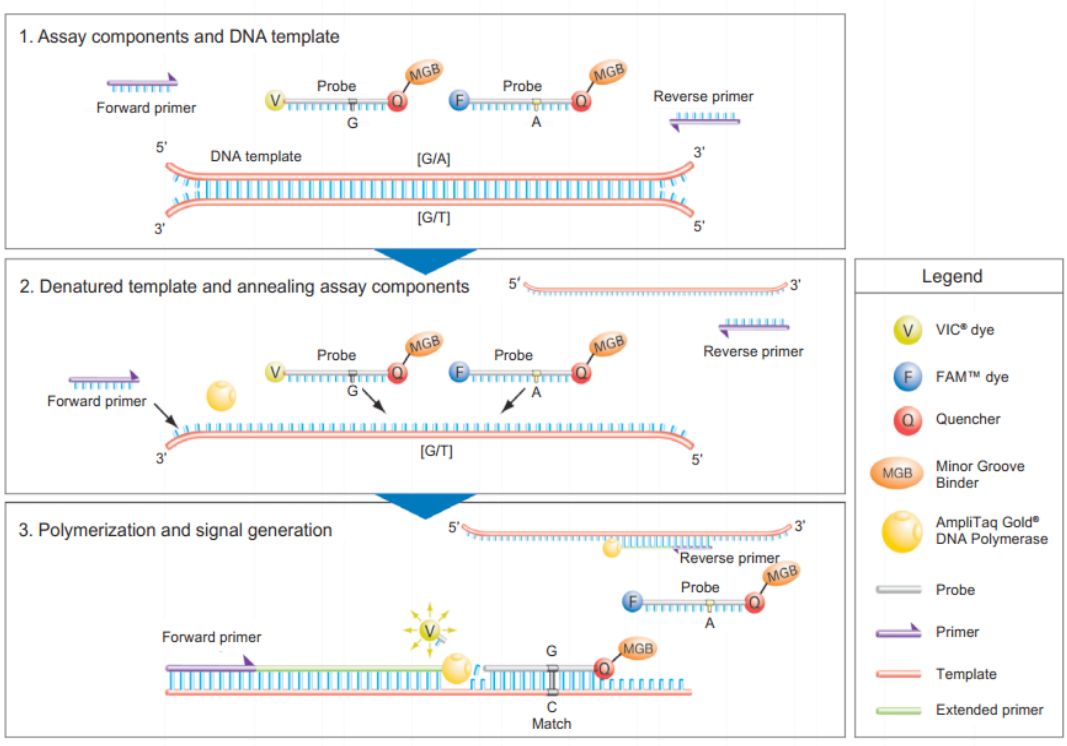

Figure 2.2. Mechanism of the allelic discrimination of the Taqman 5' nuclease assay (from Life Technologies TaqMan SNP genotyping assays product bulletin) [214]

The extraction of genomic DNA is described in Section 2.2.2. The procedure for performing the TaqMan SNP genotyping is described as follows: 10 ng genomic DNA was added to each well of the 384-well optical PCR plate (Thermo Scientific, AB-1384), and then been dried down in a 37°C oven overnight. A representation of TaqMan master mix setup is shown in Table 2.5. The loaded plate was then centrifuged at 2000 x g for 1 min to ensure the equal amount of the solution in each well. The PCR plate was then sealed with an optical adhesive cover and placed in an MJ-Tetrad PTC-225 PCR thermal cycler.

	Reagent volume per 384-well plate (µl)	Master mix volume with 10% excess (384x1.1) (µl)
20x SNP genotyping assay (Applied Biosystems, c_1827682_10)	0.125	52.8
2x TaqMan universal PCR master mix	1.25	528
NF H_2O	1.125	475.2
Genomic DNA (dried)	10 ng	n/a
Total volume	2.5	n/a

Table 2.5. TaqMan genotyping master mix setup

PCR was performed using the thermal cycling conditions described in Table 2.6. After the PCR was completed, the end plate read was performed immediately using an ABI 7900HT sequence detection system (Applied Biosystems, Foster City, CA, USA). This system can distinguish and quantify the two signals from FAM or VIC, which then form three clusters representing genotypes of the DNA samples, similar to the

description above in Section 2.3.1.

Temp (°C)	Time (sec)	Cycles	Description
95	600		AmpliTaq Gold, UP Enzyme activation
92	15	40	Denature
60	60		Anneal/extend

Table 2.6. Thermal cycling conditions for TaqMan SNP genotyping

2.3.3 Restriction enzyme digestion genotyping

The underlying principle of this technique is that the nucleotide substitution of a SNP may create or abolish a restriction endonuclease cutting site and therefore can be utilized for genotype determinations of DNA samples. If a SNP results in a C to T substitution and the DNA sequence including the SNP is a specific target of the restriction enzyme, a PCR reaction can be used to amplify the DNA sequence of interest, which, in turn, can be used as a template for restriction enzymatic restriction. In the case of SNP rs13107325, the site is targeted by BcgI enzyme. As such, DNA amplicons homozygous for the C allele are cleaved into two fragments, whereas DNA amplicons homozygous for the T allele will not be cleaved by BcgI. In the case of a DNA samples from a heterozygote, 50% of the PCR amplicons will be cleaved and the other 50% will not. The genotyping outcome can be visualized using a 2% agarose gel, where a single band represents uncleaved homozygotes (T/T), double bands represent cleaved homozygotes (C/C), and triplicate bands indicate heterozygotes (C/T). Therefore, analyzing the *Bcg*I digests of the PCR products by gel electrophoresis will allow one to determine the genotypes of the DNA samples (Fig. 2.3).

The relevant sequence flanking the SNP was obtained from dbSNP (http://www.ncbi.nlm.nih.gov/snp/). The NEBcutter V2.0 software was used to search for a restriction site that is affected by the polymorphism by selecting a particular enzyme which cuts only one allele. In this project, BcgI (NEB, R0545S) enzyme was used. The full length uncut PCR product was 274 bp in length. After cutting, the PCR amplicon will generate one fragment of 123 bp and the other of 151 bp (shown in Fig. 2.3, C/C genotype). All samples showing 3 clear bands (274 bp, 151 bp, and 123 bp in Fig. 2.3 C/T genotype) were subjected to DNA sequencing and confirmed to be heterozygotes. The reagent mix for post PCR restriction enzyme digestion reaction is listed in **A2.2**. The mixture was incubated at 37°C overnight on a heating block before subjecting to gel electrophoresis.

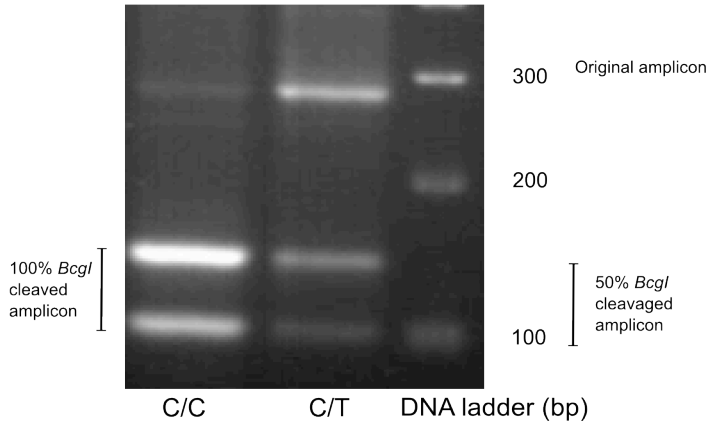

Figure 2.3. Gel electrophoresis of the genotyping executed by restriction enzyme digestion

2.4 cDNA synthesis and quantitative gene expression analysis

2.4.1 mRNA extraction

HUVECs and HUASMCs

Total messenger RNA (mRNA) was extracted from cell lysates and purified using the GenElute™ Mammalian Total RNA Miniprep Kit (Sigma, RTN350-1KT). In summary, isolated RNA preserved from degradation by addition of β-mercaptoethanol was first bound to the extraction column, followed by multiple washing steps and then eluted as described by the manufacturer's protocol.[215] Once the extraction was finished, the RNA concentration was determined by NanoDrop Spectrophotometer ND-1000 instrument, as described previously in Section 2.2.2, with an $A_{260/280}$ of ~ 2 is considered to be pure for RNA.

HepG2

HepG2 cells were cultured on 12-well plates, and transfected with pCDNA3.1(+/-)-SLC39A8-Ala/Thr391 and pCDNA3.1 vector control plasmids followed by cholesterol efflux assay. By the end of the assay, cells in each well were washed with PBS and pelleted, whereas half of the cell pellets were used for the assay and half were subjected to mRNA extraction. Additional mRNA was extracted from HepG2 cells 12h post transfection without performing cholesterol efflux. Total mRNA was extracted from cell lysates and purified using the GenElute™ mammalian total RNA miniprep kit.

2.4.2 Reverse transcription and cDNA synthesis

After determining the concentrations of the RNA samples, 0.5µg or 1µg of the RNA was mixed with random primers (RP, Promega, C118A) at a ratio of 1µg RNA/1µg (RP) and the required amount of NF-H_2O to make up to the final reaction volume of 25µl. The mixture was incubated at 70°C for 5 min to disrupt the secondary structures of the template. The reverse transcription (RT) reaction was performed using the cocktail described in **A2.3**. The PCR program for RT was 25°C for 5 min, 42°C for 1.5 h, and 70°C for 15 sec. After synthesis, cDNA was diluted to a stock concentration of 10ng/µl with NF-H_2O.

2.5 Allelic expression imbalance (AEI)

Allelic imbalance is a powerful method to identify *cis*-acting regulatory variation for gene expression. The rationale behind it is that *trans*-acting regulatory elements and environmental factors influence gene expression at both chromosomes while *cis*-acting regulatory elements affect gene expression in an allele-specific manner.[216] Expression levels from each of the two alleles can be directly compared within the same heterozygous individual and within the same experiment, therefore variations in *trans*-acting regulatory elements and environmental effects are not expected to affect the ratio between the two alleles. Departure of cDNA expression ratios from those observed in genomic DNA provide unequivocal evidence of *cis*-acting polymorphisms. The cDNA samples used in this assay were derived from the mRNA extraction and cDNA synthesis described in the Methods Sections 2.4.1-2.4.2. The gDNA used was derived from the same cell lines as described in methods Section 2.2.2. The cDNA and gDNA from the cell samples identified as heterozygous for SNP rs13107325 were used and amplified using primers specific for rs13107325 (primers 5 and 6 for gDNA,

primers 8 and 10 for cDNA, as listed in **A1)**. After gel electrophoresis, the corresponding PCR products were excised and purified using the Wizard® SV gel and PCR clean-up system (Promega, A9282). The purified PCR products were then subjected to Sanger sequencing. AEI quantifies the cDNA levels of the two alleles within the same cell, the higher the expression of an allele, the higher its relative peak height is on the sequencing chromatogram. If the ratio of the peak heights ratio of the two alleles from PCR products of the cDNA sample is significantly different than that in the gDNA sample, this indicates that the SNP, or other SNPs in LD, regulates the mRNA expression of this gene. However low transcript levels can affect measurement of gene expression and reproducibility. Intra-sample variation can also be increased with reduced copy number of the target and (or) increased length of the amplicon.[217] These limitations need to be taken into consideration of the experimental design.

2.5.1 Quantification of peak heights and statistical analysis

The sequencing results were aligned and analysed by BioEdit software (version 7.1.3). The relative fluorescent intensities for the two alleles at the SNP site were quantified and compared between cDNA and gDNA. PeakPicker software (http://genomequebec.mcgill.ca/EST-HapMap) was used to analyse the sequencing data to quantify the relative fluorescent intensities for the two alleles at the SNP site. The ratio of normalized peak heights, allele 1 versus allele 2, was calculated. By pooling the results from all heterozygote samples, the allelic expression would be considered imbalanced if mean ratio difference was deemed to be different as indicated by $p<0.05$ by Mann-Whitney t test.

2.6 Real-time quantitative reverse transcription PCR using SYBR Green I method (qRT-PCR)

2.6.1 SYBR Green I principle and reaction set up

Two of the most commonly used real-time qRT-PCR assays are TaqMan and SYBR Green I assays. First reported by Santhosh *et al*.,[218] SYBR Green I-based qRT-PCR is a sensitive method for rapid detection and quantification of target gene mRNA expression using primers specific to the gene of interest.[219] SYBR Green I chemistry is a sequence-independent cost effective method that relies on the intercalation of the SYBR Green I dye into double stranded DNA (PCR products). However if reaction conditions are not optimized, this technique is susceptible to low specificity of hybridization of the SYBR Green I dye to the PCR product of interest. The specificity of SYBR Green I may be compromised by the formation of primer dimers, lack of primer specificity, sub-optimal primer concentrations. All of these factors could lead to the creation of unexpected double stranded DNA products that result in false fluorescent signal from incorporation of SYBR Green I dye. Primer pairs were designed to amplify the gene of interest targeting a specific region of 100 to 150bp, which were shown to produce the most effective amplification. Primer concentration was used based on empirical data, which proved to be optimal when specific amplification relative to primer dimer was maximal in a positive versus negative control experiment. The components of PCR reaction are listed in Table 2.7.

Components	Volume (µl)
2 x Buffer	5
Forward and reverse primer mix (2µM)	1
DNA	4 (10ng)
Total volume	10

Table 2.7. Components of real-time qRT-PCR reaction

2.6.2 qRT-PCR primer design

The primers used were selected from an online primer database GETPrime (http://updepla1srv1.epfl.ch/getprime/). The primers in this database have been experimentally validated extensively demonstrating high transcript specificity in complex samples.[220] This enables users to design their primers with tailored criteria specific to their needs, for example, targeting all gene splice variants or specific gene product isoforms. In our study, we chose primer pairs that allowed detection of all gene splice variants predicted for genes of interest. The primer sequences for the genes under investigation are listed in **A1**. These were tested using end-point PCR and agarose gel to ensure single product detection before qRT-PCR application (Fig. 2.4). The target PCR amplicon size for all primers tested is expected to be around 100bp. Bands below 100bp would normally be considered primer dimers. If any primer pair generated more than one band (e.g. ABCG1 in Fig. 2.4 A), alternative primer set would be tested and used for the subsequent qRT-PCR assay (Fig. 2.4 B). From our primer test, *ABCG1* seems to minimumly/not expressed in HUASMC samples.

A B

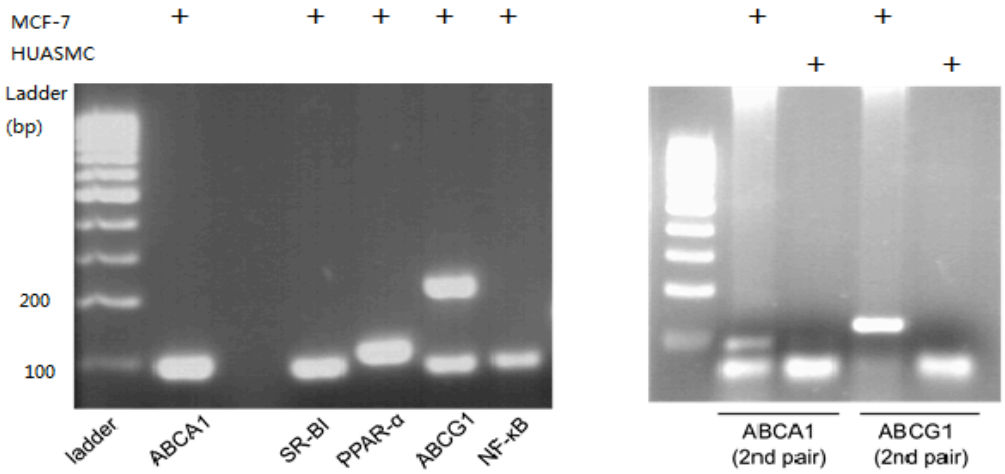

Figure 2.4. End-point PCR assessment of qRT-PCR primers. (A) Electrophoretic gel image of qRT-PCR primers testing. Bands at ~100bp are the specific PCR products corresponding to the target gene. DNA samples are labelled at the top (B) Electrophoretic gel image of PCR products from alternative primer pairs for *ABCA1* and *ABCG1*

2.6.3 Analysis and calculation of SYBR Green I results

The real-time qRT-PCR read-out is given as the fractional PCR cycle number at which the reporter fluorescence is greater than the threshold ('cycle threshold', C_T). The threshold is an arbitrary level of fluorescence chosen on the basis of the baseline variability. Threshold can be adjusted for each experiment to ensure it is in the region of exponential amplification across all plots. The PCR cycle can be divided into three stages. During the exponential phase of the PCR the fluorescent signal doubled at each cycle. After certain number of cycles, the intensity of fluorescent signal usually began to plateau, indicating that the PCR had reached a saturation status (Fig. 2.5). As C_T is proportional to the logarithm of initial amount of target in a sample, the relative

concentration of target gene to the reference gene is calculated by the difference in cycle number (ΔC_T) (ΔC_T = C_T of the target gene - C_T of the reference gene). In our experiment, the reference housekeeping gene 18S was used to normalize mRNA levels between different samples. The PCR program is listed in the Fig. 2.6 A&B. C_T values were generated automatically by the SDS 2.4 program (ABI) after the PCR cycles finished. The $\Delta\Delta C_T$ method was used to calculate the fold expression differences of the target gene in different samples compared to the control sample. The fold difference was calculated as $2^{-\Delta\Delta C}$, where $\Delta\Delta C_T = \Delta C_T^{(\text{sample of interest})} - \Delta C_T^{(\text{control sample})}$. In our experiment, two groups of samples (transfected with the pCDNA3.1-SLC39A8-Ala and pCDNA3.1-SLC39A8-Thr plasmids) were evaluated against the control sample (transfected with the pCDNA3.1 vector control). The fold difference was described as $2^{-\Delta\Delta C}$, whereas $\Delta\Delta C = \Delta C_T^{(\text{pCDNA3.1-SLC39A8-Ala391/Thr})} - \Delta C_T^{(\text{pCDNA3.1})}$

A dissociation/melting curve analysis is routinely performed for SYBR Green qRT-PCR following the PCR thermal cycling to verify the correct PCR product according to its specific melting temperature (Tm). It is important to perform this analysis to detect the presence of primer-dimers or nonspecific products, which also generate fluorescent signals that reflect in the final C_T values. A single peak in the amplification plot suggests the presence of a single size product, because the target sequence should have a specific T_m (indicated as peak B in Fig. 2.6 C). Melting curve analysis can identify the presence of primer-dimers because they exhibit a lower Tm than the amplicon (pointed as peak A in Fig. 2.6 C).

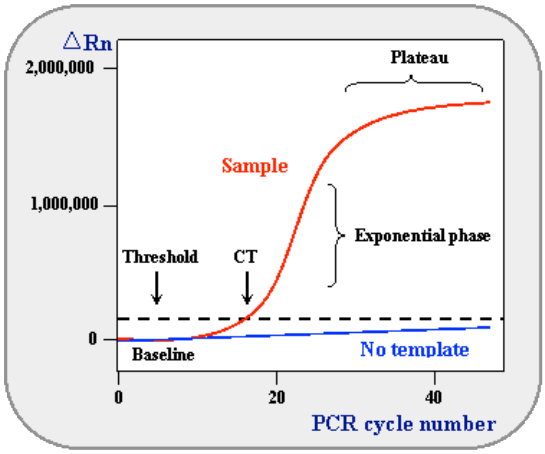

Figure 2.5. The annotation of a qRT-PCR amplification curve. The ΔRn values are plotted versus the cycle number. ΔRn is an increment of fluorescent signal for each time point. Baseline is defined as PCR cycles in which reporter fluorescent signal is accumulated beneath the detection limit of the instrument

A

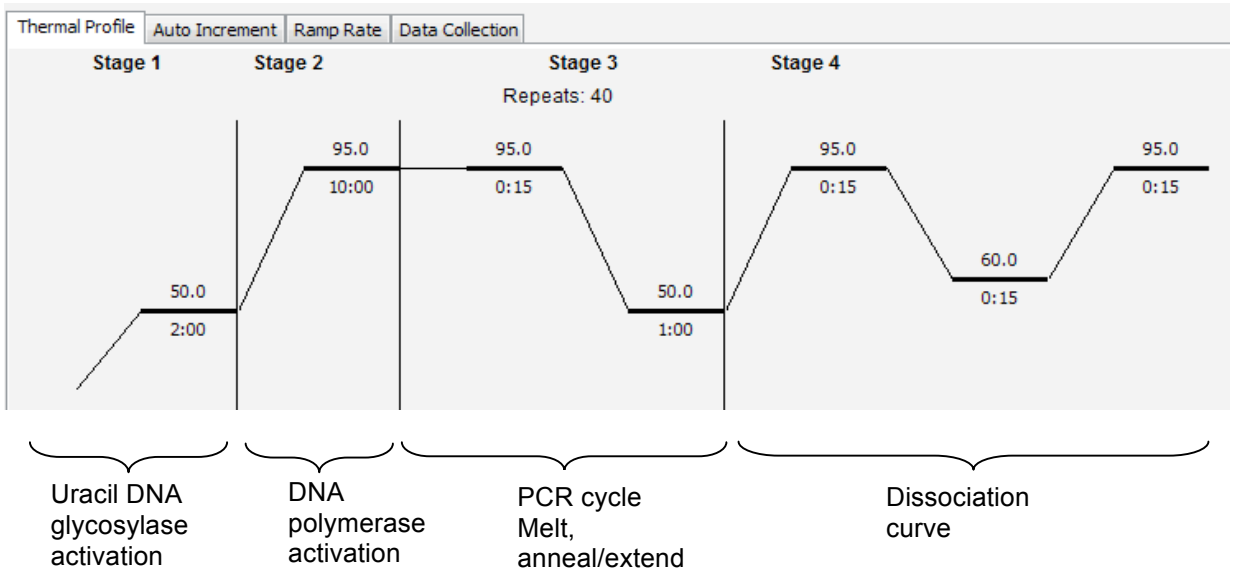

B

Step	Temp (°C)	Time (min)	cycles
Uracil DNA glycosylase activation	50	2	1
DNA polymerase activation	95	10	1
Melt	95	0.25	40
anneal and extend	50	1	
Dissociation/melting curve	95	0.25	1
	60	0.25	
	95	0.25	

C

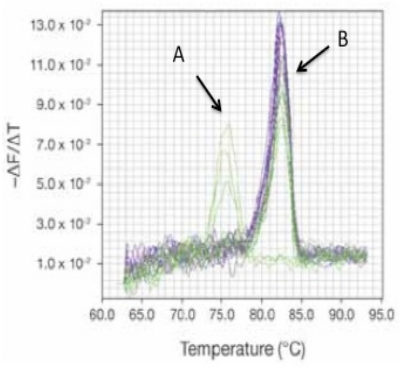

Figure 2.6. SYBR Green based real-time qRT-PCR. (A) and (B) Steps and thermal conditions of qRT-PCR (C) Representative of a melting curve graph generated by SDS software.

2.7 Protein study

2.7.1 Protein isolation

Total protein extraction

Total cell lysates were harvested from cultured cells from either 6 well plates or T-25 flasks. Each well or flask was first washed with ice cold PBS and drained completely before addition of radio-immunoprecipitation assay (RIPA) lysis buffer containing protease inhibitor (PI) (components listed in **A2.4**). Cells were detached using single-use cell lifters. The mixture was transferred to an ultracentrifuge tube, sonicated in a cold water bath for 1 min, and then incubated on ice for 30 min with further disruption by a vortex mixer at 10 min intervals. Subsequently, the tube was centrifuged for 10 min at 13000 rpm at 4°C to pellet the cell debris. The supernatant solution, containing the total cellular protein, was then transferred to a new tube and stored at -80°C.

Subcellular protein fractionation

Different subcellular protein fractions were extracted and separated according to weight differences. Confluent cells of HUASMC or HUVEC were lysed with 500µL homogenization buffer (components listed in **A2.4**), then scraped immediately and transferred to 1.5mL ultracentrifuge tubes. The lysates were then passed through 25G needle 10 times using a 1mL syringe. The lysates were centrifuged at 900 x g for 10 min at 4°C. The supernatants were transferred to a clean EP tube and the pellet (containing the nucleic fractionation and cell debris) was resuspended in 35µL RIPA lysis buffer (+P.I.), followed by sonication to further shear nuclear DNA. The supernatant from above procedure was centrifuged again at 10,000 x g at 4°C to generate pellet containing mitochondria fraction, which was resuspended in 35µL RIPA

lysis buffer (+ proteinase inhibitor). The supernatants from above procedure was then subjected to ultra-centrifugation at 100,000 x g for 1h at 4°C, generating a small pellet containing the membrane fractionation, which was also resuspended in 35μL RIPA lysis buffer (+P.I.). The supernatant from above procedure was treated as the cytosolic fraction. All the protein fractions were stored at -80°C.

2.7.2 Protein quantification

Protein concentrations were quantified using the bicinchoninic acid assay (BCA) protein assay reagent (Pierce, 23227). The BCA protein assay utilizes the reduction of cuprous cation Cu^{2+} to Cu^{1+} by protein in an alkaline medium and the selective colorimetric detection of Cu^{1+} by bicinchoninic acid. For each quantification, a standard curve was performed by using serial dilutions of bovine serum albumin (BSA) solutions. First a total of 10μl of either BSA or protein solution was added to each well on a 96 well plate, then 200μl of the reagent A and B (50:1) mixture was added into each well, followed by incubation at 37°C for 30 min. The plate was read by a spectrophotometer with the Revelation program (Dynex Tech. V. 4.22) at a wavelength of 570nm. A standard curve was first generated from known amounts of bovine serum albumin (BSA), then the concentration of each of the protein samples was determined using the standard curve.

2.7.3 Immunoblotting assay for detection of ZIP8 expression

Proteins were mixed with lysis buffer (+P.I) and 5 x loading buffer (components listed in A 2.4) containing 5% β-mercaptomethanol. Membrane proteins were denatured by heating at 70°C for 5 min and denaturation for other protein fractions was carried out at

95°C for 8 min. Proteins were then electrophoretically separated on a 10% polyacrylamide gel (or lower percentage, if bigger size proteins were to be detected), and transferred to a PVDF membrane (Amersham Hybond-P, GE Healthcare). The membrane was incubated with Tris-buffered saline containing 0.1% Tween-20 (TBST) and 5% (w/v) non-fat milk (Marvel) in for 1h. The blot was then incubated overnight at 4°C in the blocking buffer containing polyclonal rabbit anti-SLC39A8 antibody (Abcam, ab103182). On the next day, the membrane was washed 3 times at 10 min intervals with TBST and subsequently incubated with anti-rabbit IgG HRP-conjugated secondary antibody (Cell Signalling, 7074S). Immunoreactivity was developed by using enhanced chemiluminescence (ECL, components listed in **A2.4**) and visualized on the autoradiography film. Mouse anti-β-actin was used as the loading control antibody (Abcam, ab8226).

The initial immunoblotting experiments were presented with dark background on the X-ray films. Therefore we focused on optimization of the primary and secondary antibody concentration, as well as their inbucation time. In the end, the best performance was found using a primary antibody concentration of 25ng/ml and a 1:3000 dilution of the secondary antibody with an incubation time of 2h.

Blocking peptide

Non-specific binding is common with polyclonal antibodies. Blocking peptides are peptides of approximately 50 amino acids long which resembles the epitope recognized by the target antibody and block antibody-antigen binding. The peptide resembles the epitope recognized by the antibody. Antibodies bound to the blocking peptide will no longer bind to the epitope on the protein. The remaining signals which are not diminished by blocking peptide will be due to non-specific binding.

To investigate the specificity of ZIP8 proteins upon transfection, immunoblotting analysis was performed with the ZIP8 antibody as described above. Two bands were detected by SDS-PAGE. To test the specificity of the antibody, the rabbit anti-SLC39A8 antibody (0.25mg/ml, 50µl) was pre-incubated with the corresponding excess blocking peptide (ab171521, 1mg/ml, 25 µl), mixed with 5% milk (in TBST) and 0.02% NaN_3 in a total volume of 5ml. One membrane was cut into half with two strips of identical samples, which were placed into two separate tubes containing only ZIP8 antibody and ZIP8 antibody mixed with blocking peptide, respectively. Both strips were blocked overnight at 4°C with rotation, followed by the same immunoblotting procedure as described previously.

2.8 Cloning

2.8.1 Construction of pCDNA3.1(+)-SLC39A8-alanine plasmid

The full-length reference cDNA sequence for human ZIP8 (GenBank Accession No. NM_022154.5) was purchased from Origene (Cat. No. SC112817). It was used as the template to amplify the open reading frame (ORF) of *SLC39A8* by using primers based on the sequences at the 5' and 3' of the ORF, attached with additional EcoRI and HindIII restriction sites sequences (shown in primer sequence table **A1**, primer 11 and 12). The PCR reaction was carried out using Phusion High-fidelity DNA polymerase (NEB, M0530S). The PCR product was first verified by gel electrophoresis, then excised and purified using a PCR clean-up kit (Promega A9281). The DNA was first bound to the column followed by washing and final elution. Subsequently the PCR products and pCDNA3.1 vector were digested using EcoRI and HindIII enzymes, followed by agarose gel electrophoresis. The bands corresponding to the size of the vector and insert were excised and purified by using the PCR clean-up kit. The full-

length *SLC39A8* ORF sequence was ligated to the pCDNA3.1 vector at EcoRI and HindIII restriction sites by using T4 DNA ligase (NEB, M0202S) with incubation at room temperature incubation overnight.

2.8.2 Transformation of *E.coli* bacteria with plasmid vector DNA

JM109 competent *E. coli* cells (Promega, L2001) were thawed from -80°C on ice. Plasmid DNA (200ng/µl) was mixed with bacteria in 1:20 or 1:10 ratio (weight : volume) in a total volume of 10µl containing 100ng or 200ng plasmid DNA. The plasmid/bacteria mix was then incubated on ice for 30 min. Heat shock was performed at 42 °C for 60s on a PCR block, followed by incubation on ice for 1m. The plasmid/bacteria mix was then added to 500µl of pre-warmed LB broth medium without ampicillin and incubated in a thermal shaker at 37 °C for 1h. The LB solution was then centrifuged at 5000 rpm for 5 min, and approximately 460µl of the supernatant was discarded. An aliquot (40-50µl) of the solution was then dispersed on a pre-warmed agar plate (containing 50µg/ml ampicillin) and incubated at 37°C for 16h (can be longer depending on speed of colony formation but no longer than 22h). On the next day, any grown colonies were picked out and propagated in 5ml LB medium containing 100µg/ml ampicillin and incubated in a 37°C rotation incubator (225 rpm) for further 18-22h. On the next day, the plasmid DNA was extracted from the bacterial LB solution by using GenElute™ plasmid miniprep kit according to manufacturer's instruction (Sigma, PLN70-1KT).

2.8.3 Plasmid DNA extraction by mini and midi-preps

The plasmid DNA was extracted by GenElute™ plasmid miniprep kit, and the eluted DNA were quantified with NanoDrop Spectrophotometer before been subjected for

sequencing. The plasmids with confirmed sequence were then subjected to midi-prep (Invitrogen, K210004) extraction to generate higher yields of plasmid DNA.

The mini- and midi- preps were performed according to the manufacturer's protocols. The miniprep kit utilizes a silica-binding technology whereas the midiprep adopts an anion-exchange resin to purify plasmid DNA. First, adequate amount of *E.coli* cells were harvested and re-suspended in the Re-suspension Buffer containing RNaseA. Then the cells were lysed with Lysis Buffer, followed by addition of Precipitation Buffer to neutralize the lysates. At this stage, cell debris, proteins, lipids, and chromosomal DNA should fall out of solution as a cloudy, viscous precipitate. The supernatant of the lysates were then passed through a pre-packed column. Depending on the types of columns used, the DNA was bound to the column resin by different mechanisms. For midiprep extraction, plasmid DNA remains bound to the resin under moderate salt conditions, while RNA, proteins, carbohydrates and other impurities were washed away with the Wash Buffer. After multiple washing, the plasmid DNA was eluted under high salt conditions. Last, desalting and DNA precipitation would be performed with alcohol precipitation. For miniprep extraction, lysates were first adjusted to high salt condition and purification was achieved by adsorption of plasmid DNA on the silica gel column. After washing away the impurities, the plasmid DNA was eluted with nuclease-free H_2O.

2.8.4 Sequencing

The sequence of the insert of the plasmid was verified by Sanger sequencing. Several primers complementary to the sequence located across the cDNA of *SLC39A8* were used in the sequencing reactions to verify in-frame ligation and full sequence of the insert (Primer No.15-19 listed in **A1**). Sequencing result is displayed in **A3**.

2.8.5 Site-directed mutagenesis and generation of pCDNA3.1(+)-SLC39A8-threonine plasmid

Site-directed mutagenesis

The QuickChange® Lightning site-directed mutagenesis kit (Agilent, 210518) was used to mutate the C allele to T allele, which resulted in the change of amino acid alanine to threonine at position 391 on the *SLC39A8* ORF sequence to generate the pCDNA3.1-SLC39A8-threonine plasmid. The primers used are listed in the **A1** (Primer 13 and 14), with the mutation sites underlined. The first step was to perform a PCR reaction to synthesize the mutant strand. The components for the site-directed mutagenesis PCR reaction are listed in **A2.6**. The PCR reaction parameters were denaturation at 95°C for 2 min, 18 cycles of 95°C for 20s, 60°C for 10s, and 68°C for 5 min, followed by a final extension step at 68°C for 10 min. During PCR, the mutation resulting in the desired base changes was incorporated into the amplicon. A schematic representation of the reaction is illustrated in Fig. 2.7.

DpnI digestion

In this step non-mutated parental PCR products were digested by endonuclease DpnI. The DpnI (target sequence: 5'-Gm^{6}ATC-3') is specific for methylated and hemi-methylated (non-mutated) DNA and selectively digests the parental supercoiled dsDNA, while leaving the newly synthesized mutant strands intact. DNA isolated from almost all *E.coli* strains is methylated therefore susceptible to DpnI digestion.[221] Dpn I (20 units) was added to the amplified PCR reaction mixture, followed by incubation at 37°C for 5 min.

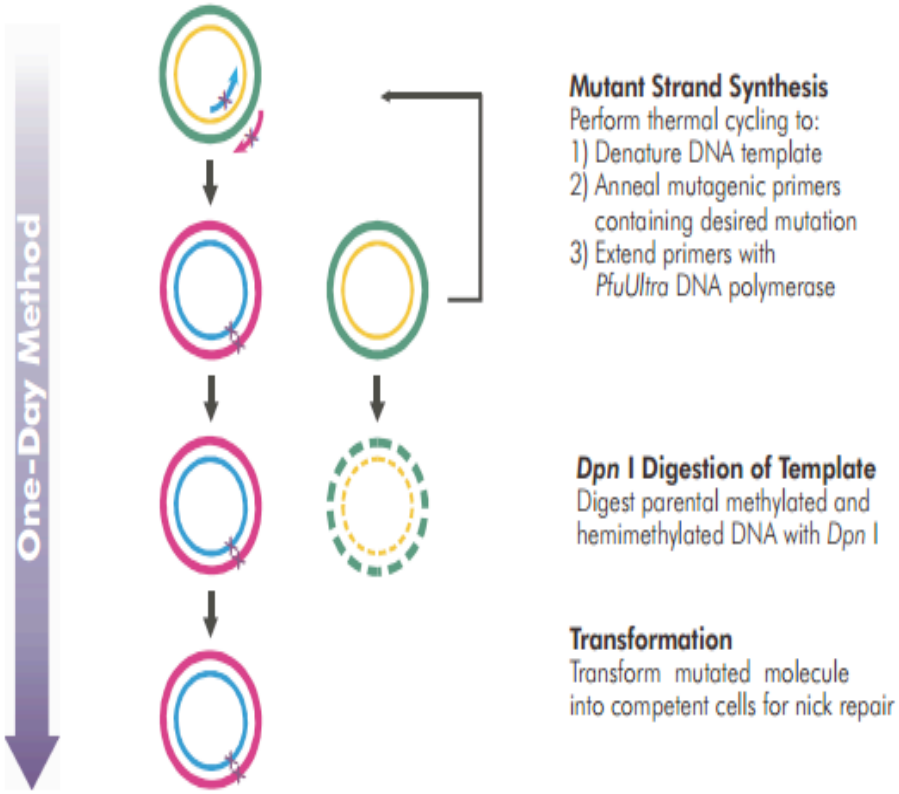

Figure 2.7. Overview of the QuickChange II XL site-directed mutagenesis. Cited from Agilent mutagenesis kit manual

Transformation and generation of the mutant plasmid

The products of the mutagenesis PCR reaction incorporating the desired mutations was then transformed into XL10-Gold® Ultracompetent cells (components of the mutagenesis kit). The plasmid DNA was then extracted by mini-prep, and sequenced to verify the full sequence and the mutated site of the plasmid pCDNA3.1(+)-SLC39A8-threonine. The sequences of the inserts of both plasmids, determined by the DNA sequencing, are listed in **A3**.

2.8.6 Transfection

Transfection of SLC39A8 expression plasmids on HEK293 cells by calcium phosphate transfection

Calcium phosphate transfection was used primarily to transfect HEK293 and MCF-7 cells using the pCDNA3.1-SLC39A8-alanine/threonine plasmids. HEK293 cells were plated in 6-well plates/T-25 flask 12-24h before transfection when the culture reaches 25-30% confluence. For each transfection, two tubes of solutions were required. Tube 1 contained 2 x HEPES (4-(2-hydroxyethyl)-1-piperazineethanesulfonic acid) buffer (pH=7). Tube 2 consisted of a series of solutions: 2M $CaCl_2$, plasmid DNA /vector DNA, filtered ddH_2O (the amount of each component is listed in Table 2.8, with two scales of cell culture vessels listed). The mixture in tube 2 was added to tube 1 in a drop-wise manner, and incubated at room temperature for 5 min. An aliquot of 109µl or 283µl of mixture was then added to each well/flask in small drops. These volumes were sufficient for transfecting cells in one well of a 6-well plate (surface area 9.5cm^2) or one T-25 flask (25cm^2). The cells were cultured for further 48-72h before harvesting for protein extraction or functional assays, respectively.

X-tremeGENE HP DNA transfection optimization

Transfection of ZIP8 expression plasmid on HepG2 cells was carried out by X-tremeGENE HP DNA transfection system (Roche, 06366236001). This method utilizes a multi-component formula that complexes with plasmid DNA, and then transports the complex into animal cells to overexpress the target gene.

	Components	1 well (6-well plate)	T-25
Tube 1	2 X HEPES (µl)	72.3	187
Tube 2	H_2O (µl)	62.1	161
	$CaCl_2$ (µl)	8.82	22.9
	DNA (µg)	1	2
Volume of Tube 1&2 mixture per transfection (µl)		109	283

Table 2.8. Components of calcium phosphate transfection reaction. All the amounts are listed for one transfection.

HepG2 cells were passaged into a 6-well / 12-well plate 24-48h prior to transfection, until they reached 70%-90% confluence on the day of transfection. For optimization purpose, 1µg and 2µg of plasmid DNA (100µl) were mixed with 3µl and 6µl of transfection reagent. The transfection reagent was pipetted directly into the DNA diluent without any contact with the interior walls of the plastic tubes. The ratio of 3:1 of transfection reagent (µl) to microgram (µg) DNA was used because it was shown to be optimal for many cell types. The transfection reagent: plasmid DNA complex was incubated at room temperature for 15 min, then either 100µl or 200µl of the complex was added to the cells in a drop-wise manner. The cells were then kept in the incubator for 48h without any disturbance, before being harvested for protein expression analysis. The total protein of each cell sample was extracted and quantified by BCA protein assay, followed by western blot to quantify the expression of ZIP8.

Transfection of ZIP8 expression plasmid on HepG2 cells by X-tremeGENE HP DNA transfection

HepG2 cells were passaged to 12-well culture plates until a high confluence of 70-90% was achieved on the day of transfection. Plasmid DNA was diluted with serum-free DMEM to a final concentration of 0.01μg/μl. Then the X-tremeGENE HP DNA transfection reagent was added to the diluted DNA (2μl) in the 3:1 ratio (3μl reagent: 1μg DNA). The transfection reagent: DNA complex was incubated for 15 min at room temperature, then been added to the culture medium in a drop-wise manner, followed by gentle swirling to ensure an even coverage of the transfection reagent over the cell surface. Cells were then cultured for 24-48h before harvesting for protein expression measurements or follow-up assays, respectively.

2.9 Cadmium uptake by Measure-iT^{TM} cadmium assay

The Measure-iT^{TM} Cadmium assay kit (Invitrogen, M36353) was used to measure intracellular Cd^{2+} concentration. This assay utilises a fluorescent dye that can fluoresce when bound to Cd^{2+} hence used to quantify Cd^{2+} content, which has a linear detection range of 5-200nM of cadmium in the solution.

2.9.1 Preparation of cadmium standard dilutions

A number of cadmium standard solutions were prepared according to Table 2.9. The stock cadmium chloride standard solution provided by the kit was 8.4μM in deionized H_2O. The stock solution was subjected to serial dilution with lysis buffer.

Concentration of cadmium standard (nM)	Volume of cadmium stock solution (8.4μM) (μL)	Volume of lysis buffer (μL)
0	0	1000
210	25	975
420	50	950
840	100	900
1680	200	800
2520	300	700
3360	400	600
4200	500	500

Table 2.9. Preparation of cadmium standards solutions

A range of 1-10μM of Cd^{2+} has generally been used in the literature for *in vitro* experiments. In order to determine our treatment dose, we used kinetics study as a reference which suggests a K_m value of 0.62 μM for ZIP8-mediated Cd^{2+} transport in mouse fetal fibroblasts that is in line with the Michaelis-Menten model. The K_m value is the concentration of Cd^{2+} at which uptake rate is half of V_{max} (maximum uptake rate). Therefore a concentration close to the K_m value was used (1μM) was used in our assay.

2.9.2 Optimization of lysis buffer

Some lysis buffer produce high background fluorescence, which interfere with the final readout. In order to select the lysis buffer with the lowest fluorescent background, a few lysis buffer was tested, of which the components are listed in Table 2.10.

	Components	Final concentration
1. Tris-HCl 8.0	NaCl	150 mM
	1.0% NP-40 (or 0.1% triton X-100)	1% or 0.1%
	Tris-HCl pH 8.0	50 mM
	Protease inhibitor	1x
2. RIPA buffer	Tris-HCl, pH 7.4	50 mM
	NP-40	1%
	Na-deoxycholate	0.5%
	SDS	0.1%
	NaCl	150 mM
	EDTA	2 mM
	Protease inhibitor mix	1x
3. IP buffer	NaCl	150 mM
	Tris pH 7.5	50 mM
	Nonidet P40	1%
	Sodium deoxycholate	0.5%
	Protease inhibitor mix	1x

Table 2.10. Components of lysis buffer for cadmium uptake assay

2.9.3 Intracellular cadmium concentration measurements

Cadmium solution preparation

Cadmium chloride ($CdCl_2$, Sigma) was dissolved in ddH_2O to a concentration of 500μM for use as the stock solution. The stock solution was dissolved in serum-free culture medium to the required concentrations prior to each experiment.

HEK293 cells were seeded at the number of $0.3x10^6$ cells on six-well plates followed by transfection according to methods in Section 2.7.5. 48h later, the culture

medium was aspirated and replaced with serum-free DMEM containing 1uM Cd^{2+}, followed by incubation of 2h at 37°C in a humidified, 5% CO_2 incubator. After 2h of incubation, the culture medium was aspirated and then cells were washed once with PBS. IP lysis buffer (50µl) was added to each well and transferred to EP tubes, followed by sonication for 1 min and intermittent vortex over 30 min. The tubes were spun down at 13,000 rpm for 10 min, and 10µl of the supernatant was transferred to a well on a 96-well plate, followed by addition of 200µl of the Measure-iT kit reagent containing 1µL of Measure-iT^{TM} cadmium reagent and 200µl of 1x buffer. The fluorescence intensity was recorded for each well at 520nm (λ_{ex}: 490nm). Each sample was analysed in duplicate. A cadmium standard curve was generated for each experiment by using $CdCl_2$ standards ranging between 0 and 4200nM. Each concentration of cadmium standard solution was performed in duplicates of 10µl in volume. The standard curve was used to determine the Cd^{2+} concentration in each sample. The adjusted cadmium uptake was calculated by standardizing the Cd^{2+} content against ZIP8 transfection efficiency as measured in the lysates of each sample in one experiment.

2.10 Zinc uptake assay by flow cytometry

2.10.1 Principle of flow cytometry

Flow cytometry provides rapid analysis of multiple characteristics of single cells by measuring their optical and fluorescence characteristics. The fluidic system (sheath fluid) transports stained cells through the cytometer for interrogation by an illumination system. The fluid surrounds a thin core thread of sample, which space the cells out so that only one passes the laser beam at a time. Detection of cells are achieved by the momentary pulse of fluorescence emitted by the cell measured by photomultipliers at

90° angle from the beam. Typically 2-3 detectors are used with different wavelength bandpass filters to collect fluorescent signals. The resulting light scattering and fluorescence are collected and converted into digital signals, which can be visualized and manipulated on the computer system (shown in Fig. 2.8). Gating allows the operator to extract data only from single, viable cells measured at the desired fluorescence settings, by eliminating data from cell debris, dead cells and clumps of 2 or more cells. The characteristics from a cell population measured by flow cytometry include physical properties, such as size (represented by forward light scatter) and internal complexity (represented by right-angle or side scatter), as well as DNA and RNA content, and proteins. Fluorescent dyes may bind to different cellular components, thus generate quantitative measurements of those components (i.e. intracellular levels of Zn^{2+}).[222]

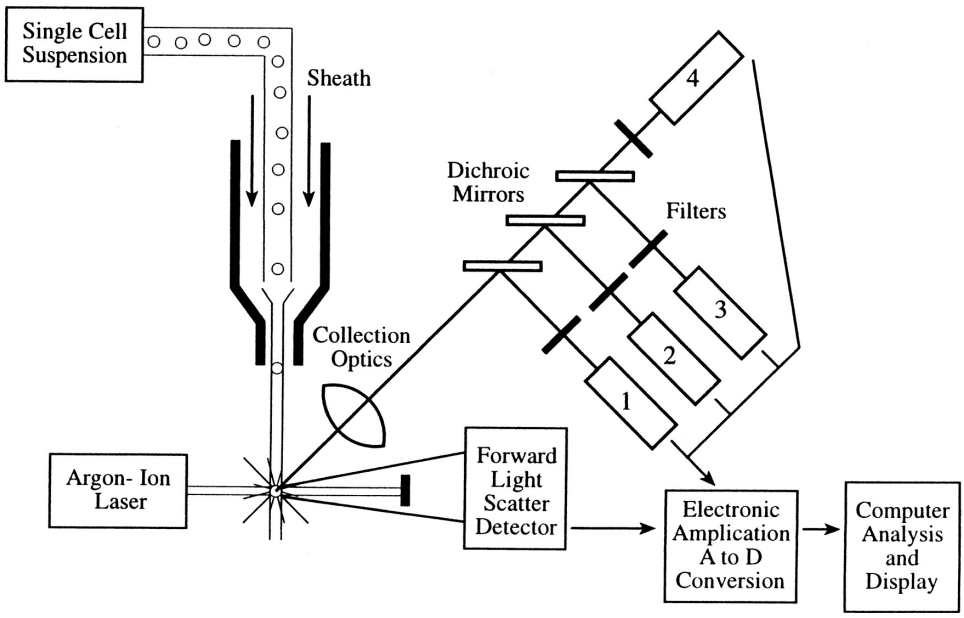

Figure 2.8. Schematic of a flow cytometer

2.10.2 Determination of Zn^{2+} uptake in HepG2 transfected with ZIP8 plasmids

Quantification of intracellular zinc by fluorescent probe - Zinquin ethyl ester

Flow cytometry was used to measure the intracellular level of Zn^{2+} with the incorporation of Zinquin ethyl ester (Santa Cruz, sc-222427). It is a lipophilic, cell-permeable fluorescent probe which is retained within the cell membrane with a negative charge after it has been cleaved by cytosolic esterase. When labelled cells pass through a light source, the fluorescent molecules are excited to a higher energy state (λ_{ex}= 405nm), followed by data collection at emission wavelength at the range of 425-475nm. In order to subtract the auto-fluorescence present in the cell components (such as riboflavin and flavoproteins), a non-stained sample was included for each experiment. The levels of Zinquin fluorescence are correlated with the total cytosolic Zn^{2+} (free or loosely-bound intracellular Zn^{2+}).

Preparation of $ZnCl_2$ treatments and Zinquin working solution

Zinc chloride anhydrous powder ($ZnCl_2$, 208086, Sigma) was dissolved in filtered ddH_2O to generate a stock solution of 1M. The stock solution was further diluted to the desired concentration for each treatment with Opti-MEM (31985062, Life Technologies) on the same day of the Zn^{2+} uptake assay.

One milligram of Zinquin ethyl ester was dissolved in 1ml DMSO to generate stock solution of 2.4mM. The working concentration (25μM) was made up by diluting the stock solution in opti-MEM medium 1h prior to administration. The solution containing the dye was protected from light exposure to prevent bleaching of the

fluorescent dye.

2.10.3 Zinc uptake assay

Cell preparation

HepG2 cells were seeded at 100,000 cells/well on 12-well plates 24h prior to transfection. Cells were then transfected with pCDNA3.1-SLC39A8-Ala391/Thr expression plasmids and vector by X-tremeGENE HP DNA transfection in triplicate, with one set for the Zn^{2+} uptake assay, one set for verification of transfection efficiency, and another set served as a non-stain control. 47h after transfection, cells were treated with 18μM $ZnCl_2$ (a near physiological concentration of 18μM were added to cells in duplicates), while the other half of cells were treated with medium only, followed by 2h incubation at 37°C in the incubator. After incubation, $ZnCl_2$ was removed and cells were washed with PBS twice before incubating with Zinquin dye solution (25μM). A vehicle control was included for the detection of auto-fluorescence present in the cells (no dye control). After 1h incubation, the culture medium was removed and cells were washed with PBS twice. After complete removal of PBS, 500μl of pre-warmed Accutase® (Sigma, A6964) was added to each well and followed by 5-10 min incubation in a 37°C incubator. Upon Accutase® digestion, cells would detach from the cell culture surface into suspension. The suspension from each well was transferred to an ultracentrifugation tube, and then centrifuged at 4500 rpm for 5 min at RT. The supernatant in each tube was removed and cells were re-suspended in 300μl PBS (containing 1% BSA) and transferred to corresponding flow cytometry tubes. The tubes were protected from light exposure prior to flow cytometry analysis.

2.11 Cholesterol efflux

This assay utilizes the fluorescent cholesterol-bound dye BODIPY-cholesterol (Avanti, 810255), which features boron dipyrromethene difluoride linked to sterol carbon-24 (Fig. 2.9). This molecule can bind to the plasma membrane of cells and behaves similarly to cholesterol in normal cells and cells with abnormal cholesterol-storage. In this study, HUVEC/HepG2 cells were cultured to 70-80% confluence, BODIPY-cholesterol was added to the culture medium to the final concentration of 25μM, followed by an incubation at 37°C for 1h. Thereafter, the medium was removed and the cells were washed with serum-free medium. The cells were then incubated with culture medium containing 0.2% BSA for 18h. HDL_3 (Amsbio, A95332H) was diluted in phenol-free DMEM to achieve the final concentration of 25mg/ml (N.B. in vehicle controls, phenol-free medium instead of HDL_3 added). Cells were incubated with HDL_3 at 37°C for 4h, and the culture medium was collected for measurement of fluorescence intensity. After medium removal, cells were lysed by the addition of a solution containing 99.7% (v/v) acetic acid (Sigma, A6283) and 1% (w/v) cholic acid (Sigma, C1129) and followed by incubation at room temperature for 4h with shaking. Fluorescence intensities in the culture medium and cell lysate were determined by a fluorometer (Victor^2 1420 multi-label counter) with excitation and emission wavelengths of 485nm and 535nm, respectively.

$$\text{Cholesterol efflux ratio} = \frac{Fluorescence\ intensity\ in\ cell\ medium}{Total\ fluorescence\ intensity\ (cell\ medium+cell\ lysate)} \text{ X } 100\%$$

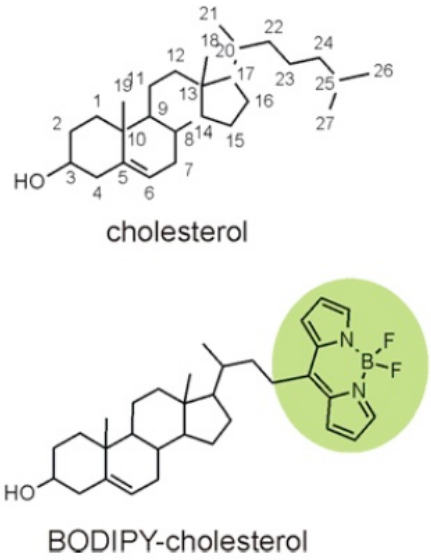

Figure. 2.9. Structures of cholesterol and BODIPY-cholesterol

(http://www.avantilipids.com/index.php?option=com_content&view=article&id=1905&Itemid=306&catnumber=810255)

2.12 Low dose cadmium exposure and ERK1/2 activation

2.12.1 ERK1/2 signalling in HEK293 cells

Cell culture and transfection

HEK293 cells were seeded on 12-well plates at 5 x10^4 cells/well density, and maintained in DMEM supplemented with 10% FBS and 1% antibiotics. Cells were transfected with pCDNA3.1-SLC39A8-Ala/Thr391 plasmids and pCDNA3.1 vector control by calcium phosphate transfection in duplicates. The transfection procedure was carried out with the listed components in Table 2.11

	Components	Volume (µl)
Tube 1	2 x HEPES	144.6
Tube 2	H_2O	121.2
	$CaCl_2$	17.64
	DNA (500ng/µl)	4
Volume of Tube 1&2 mixture per transfection		43.6

Table 2.11 Calcium phosphate transfection for assessing ERK1/2 signalling

Optimization of cadmium treatment

Cadmium chloride salt was dissolved in filtered ddH_2O to 500µM, and then been diluted to 1µM with culture medium on the day of experiment. Cells were then subjected to $CdCl_2$ treatment 24h post transfection. 1ml of DMEM containing 1µM Cd^{2+} was added to the transfected HEK293 cells, followed by 1h, 2h, 4h and 24h incubation in a 37°C, 5% CO_2 incubator.

Detection of phosphorylated ERK1/2 in HEK293

Cells were harvested at the end of incubation with $CdCl_2$. They were washed once with PBS, then lysed with 50µl cold lysis buffer (RIPA) containing protease inhibitor (P.I) and phosphatase inhibitor mixture (2mM Na_4VO_3). Total cellular protein concentrations were determined by BCA assay. Equivalent amounts of proteins were analysed by SDS-PAGE and then transferred onto PVDF membranes. Membranes were blocked in 5% non-fat dried milk in TBST buffer for 1h, followed by several washes with TBST buffer. Membranes were then incubated in antibodies at the following concentrations (developed with no stripping in between the antibodies): first with phospho-p44/42

MAPK (Erk1/2) rabbit polyclonal antibody (Cell Signalling, #9101): 1:1000; then with total ERK (Cell Signalling, #9102) 1:1000. The p44/42(ERK1/2) antibody was diluted in 5% BSA in TBST, and the anti-rabbit secondary antibody was also diluted in 5% BSA at 1:3000 final dilution. Signals were detected by enhanced chemi-luminescence.

2.12.2 ERK1/2 signalling in HuVECs

Cell culture and cadmium treatment

HuVECs were seeded on 12-well plates at density of $0.1x10^6$ cells/well. 24h after seeding, cells were either treated with culture medium containing designated amount of $CdCl_2$ or no $CdCl_2$. For each cell from different human umbilical cords, duplicates were performed on both the treatment and non-treatment group.

Optimization of Cd^{2+} treatment

Two concentrations of Cd^{2+} treatment (1μM and 10μM) and four time points (1h, 2h, 4h, 24h) were assessed on HuVEC to investigate the optimal condition resulting in maximum ERK1/2 activation. HuVEC from one umbilical cord was passaged in a 12-well plate at the densities mentioned above. After incubating with cadmium for the designated length of time, cells were then lysed with 50μl chilled lysis buffer (RIPA) containing protease (P.I) and phosphatase inhibitor mixture (2mM Na_4VO_3). The rest of the procedures were consistent with described above.

Quantification of pERK1/2 in HUVECs of Ala/Ala and Ala/Thr genotypes for rs13107325

ERK1/2 activation was assessed in HUVEC cell lines of either Ala/Ala or Ala/Thr

genotype under Cd^{2+} treatment. Each HuVEC cell line was passaged to 4 wells on 12-well plates, two for cadmium treatment and two for non-cadmium controls. 24h after passage, 1ml of M199 supplemented with 15% FBS and 1μM cadmium and vehicle control were added to the corresponding wells, respectively, followed by incubation of 2h at 37°C, 5% CO_2. After incubation, cells were then been lysed with 50μl chilled lysis buffer (RIPA) containing 1x protease (P.I) and phosphatase inhibitor (2mM Na_4VO_3). The rest of the procedures were consistent with described in Section 2.7.2.

2.13 NF-κB dual luciferase reporter assay

κB-luciferase reporter assays employ the co-transfection of two reporter plasmids. One reporter plasmid expresses the firefly (*Photinus pyralis*) *luciferase* gene under control of a minimal promoter (essentially a TATA box) and one or more copies of a κB *cis*-element, whereas the other 'control' plasmid expresses the Renilla (*Renilla reniformis*) *luciferase* gene that is served as an internal control for transfection efficiency. The activities of firefly and renilla are measured sequentially from a single sample. The luciferase protein encoded by the κB-luciferase plasmid and renilla-luciferase plasmids display luminescence that is detected by spectrophotometry.

This assay allows detection of two individual reporter enzymes within a single sample. The dual-reporter assay produces more reliable interpretation of the experimental data by eliminating variability. Normalizing the activity of the experimental reporter to that of the internal control minimizes experimental variability caused by differences in cell viability or transfection efficiency.

2.13.1 Co-transfection of reporter plasmids and pCDNA3.1-SLC39A8 plasmids

At Day 1, HEK293 cells were seeded onto wells of 24-well tissue culture plates (5 x 10^4 cells/well) in 0.5mL pre-warmed DMEM, and incubated at 37°C in 5% CO_2. The assay was performed in triplicate. After 24h (Day 2), cells were subjected to transient co-transfection of the according to the formulation listed in Table 2.12 by using the calcium phosphate transfection method.

Preparation of cadmium treatment

24h after transfection (day 2), $CdCl_2$ (1μM) solution was prepared using pre-warmed DMEM containing 10% FBS, after aspirating old medium, 0.5mL $CdCl_2$ solution was added to the cells in 18 of the 24 wells. The remaining 6 wells were added with only DMEM containing 10% FBS.

	Tube 1	Tube 2
2 x HEPES	47.1	
pCDNA3.1-SLC39A8-Ala/Thr or pcDNA3.1 plasmid (500 ng/μl) (μl)		1
NF-κB-luci plasmid(150ng/μl) (ul)		1
Renilla-luci plasmid (1.5 ng/μl) (μl)		1
H_2O (μl)		38.5
$CaCl_2$ (μl)		5.75

Table 2.12 Calcium phosphate transfection reagents components used for one 24-well plate. A volume of 71.01μl of the final mixture was added to each well on the 24-well plate

Luciferase activity detection

Cells were incubated at 37°C in 5% CO_2 for 2h. During treatment, 1x luciferase lysis buffer were prepared by adding four volumes of ddH_2O to one volume 5 x passive lysis buffer, and pre-equilibrated to room temperature. After 2h $CdCl_2$ treatment, the culture medium was aspirated from the wells, followed by PBS wash once (without disturbing the cells).

The luciferase activity was measured by Dual-Luciferase reporter assay kit (Promega, E1910). The volume of 100μl 1 x luciferase lysis buffer was added to each well, the plate was wrapped in a sealed plastic bag (to avoid excess evaporation) and shaken for 30 min at room temperature. Cells were then detached from the bottom of

the wells by using a single-use cell lifter and transferred to sterile 0.8mL ultracentrifuge tubes, followed by centrifugation at 13,000 rpm for 30s at 4°C. An aliquot of 20μL of the supernatants was harvested and transferred to new 1.5mL tubes. Lyophilized luciferase assay substrate was re-suspended in luciferase assay buffer II (LAR II, Cat.1910), Stop & Glo® substrate was diluted with Stop & Glo reagent in 1:50 ratio. Both reagents were protected from light before and during the luciferase assay.

The firefly luciferase intensity was first measured by adding 100μL of the LAR II to the cell lysates and the luciferase was measured immediately with time delays of less than 10s. The first reading showed NF-κB-dependent transcriptional activities within each sample lysate. The reaction was quenched and the Renilla luciferase reaction was simultaneously initiated by adding 100μL of the Stop&Glo reagent to the same cell lysates in the same manner, which indicated the Renilla luciferase intensity. For each sample, the luminescence intensity was normalized by dividing the Firefly luciferase reading of NF-κB by Renilla luciferase levels.

2.14 Immunoblotting for detecting NF-κB activation

HUVECs of Ala/Ala and Ala/Thr genotypes were cultured on 12-well plates and were exposed to various durations of cadmium treatments (1μM Cd^{2+} for 2h, 4h and 24h). Cells were lysed in RIPA lysis buffer containing proteinase inhibitor and phosphatase inhibitor on ice for 45 min. Total protein concentrations were quantified by BCA assay. Proteins were separated by SDS-polyacrylamide gel electrophoresis, blotted onto PVDF membrane and probed with IkBα (Santa Cruz, sc-371, 1:1000), pIkkα/β (Cell Signalling, 2697, 1:1000), and phosphor-p65 (Cell Signalling, 30335, 1:200) antibodies. The rest of the protocol was in accordance with the immunoblotting assay described in 2.7.3.

2.15 Cell toxicity assay

2.15.1 LDH cytotoxicity assay

Lactate dehydrogenase (LDH) cytotoxicity assay is a colorimetric method for quantification of cellular cytotoxicity mediated by chemical compounds. LDH is a cytosolic enzyme which is released from cells into the culture medium when plasma membrane damage occurs. LDH acts as the catalyst for the conversion of lactate to pyruvate via NAD^+ reduction to NADH. Diaphorase then uses NADH to reduce a Tetrazolium salt (INT) to a red formazan product with a colorimetric absorbance at 490nm which can be measured by a spectrophotometry. The level of formazan formation is directly proportional to the amount of LDH released into the medium, which indicates the cytotoxicity. (Fig. 2.10)

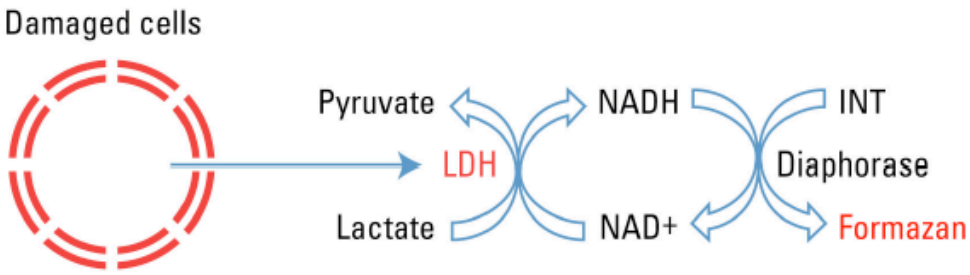

Figure 2.10. Principle reaction of LDH cytotoxicity assay

HuVECs were seeded on 96-well plates at a density of 5,000 cells/well with 100µl medium in 6 wells for each cell line. On the following day, $CdCl_2$ stock solution (500µM) was diluted in M199 medium containing 0.1% FBS and loaded to cells to induce cytotoxicity which led to the release of LDH. Culture medium containing equivalent amounts of H_20 were added to another set of duplicate to be served as

Spontaneous LDH activity controls. For maximum LDH activity controls, 10 µl of lysis buffer (10x) were added to another set of duplicate wells and mixed by gentle tapping, followed by incubation at 37°C, 5% CO_2 for 45 min. After incubation, 12.5µl of the cell culture medium was transferred to a new 384-well plate and mixed with 12.5µl reaction mixture (assay buffer: substrate=1:19). After a 30 min incubation at room temperature protected from light, reactions were stopped by adding 12.5µl Stop Solution. Absorbance at 490nm and 630nm was measured by a plate reader spectrophotometer. To determine LDH activity, 630nm absorbance value (background) was subtracted from the 490nm absorbance before calculation of % cytotoxicity. Net LDH= [(LDH at 490nm)-(LDH at 630nm)]. Additional wells containing M199 (supplemented with 0.1% FBS) and serum free medium without cells were also included for detection of the amount of basal LDH activity in sera.

Calculation of cytotoxicity

$$\% \text{ Cytotoxicity} = \frac{(Cadmium\text{-}treated\ LDH\ activity) - (spontaneous\ LDH\ activity)}{(Maximum\ LDH\ activity) - (spontaneous\ LDH\ activity)} \times 100\%$$

2.15.2 CellTiter 96® Aqueous One solution cell proliferation assay

In order to test the toxicity of Cd^{2+} on HUVEC and HEK293 cells, the CellTiter 96® AQueous One Solution reagent (Promega, G3582) was used to determine the number of viable cells, as an indicator for cytotoxicity of Cd^{2+}. The reagent contains a novel tetrazolium compound [3-(4,5-dimethylthiazol-2-yl)-5-(3-carboxymethoxyphenyl)-2-(4-sulfophenyl)-2H-tetrazolium, inner salt; MTS] and an electron coupling reagent (phenazine ethosulfate; PES). The MTS tetrazolium compound (Owen's reagent) is bio-reduced by cells into a brown formazan product that is soluble in tissue culture

medium. The conversion is presumably accomplished by NADPH or NADH produced by dehydrogenase enzymes in metabolically active cells.[223] The chemical reaction is listed in Fig. 2.11. The quantity of formazan products as measured by the colorimetric absorbance at 490nm is directly proportional to the number of viable cells in culture.

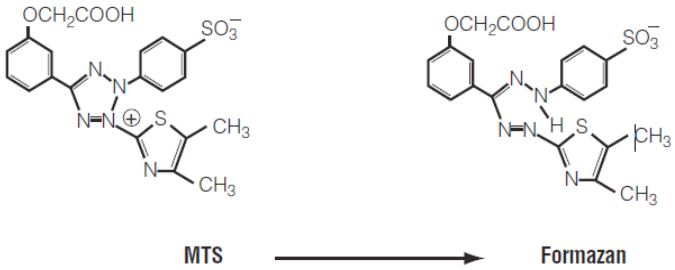

Figure 2.11. Structure of MTS tetrazolium and its formazan product[223]

HEK293 cells were passaged on a 96-well plate and a 6-well plate 24h prior to transfection at confluency of 20-30%. On day 1, cells were transfected by calcium phosphate method with pCDNA3.1–SLC39A8-Ala391/Thr plasmids and pCDNA3.1 vector control. The volume of transfection reagent/DNA mixture was adjusted according to the surface area of each well, therefore 1/30 of the transfection reagent/DNA mixture volume for a well on the 6-well plate was used for one well on the 96-well plate. $CdCl_2$ aqueous solution was diluted in phenol-free DMEM (to avoid binding of Cd^{2+} with components of the serum) to the final concentration of 1μM. 48h later, the culture medium was aspirated and replaced with phenol-free DMEM containing 1 μM $CdCl_2$, followed by incubation of 2h at 37°C in a humidified, 5% CO_2 incubator. By the end of the incubation, 20μl/well of CellTitre 96® AQueous One Solution reagent was added to each well, followed by approximately 1.5h incubation at 37°C in a humidified, 5% CO_2 incubator, to allow a sufficient development of the colour. The colorimetric absorbance at 490nm was recorded using a plate reader. The cells cultured on the 6-well plate were harvested for testing of transfection efficiency, which

is representative of the 96-well plate by sharing the same transfection reagent.

Viable cells percentage= $\frac{(Ab490nm\ of\ cadmium-treated\ cells)-(Ab490nm\ of\ medium\ background)}{(Ab490nm\ of\ control\ cells)-(Ab490nm\ of\ medium\ background)}$ x100%

2.16 Bioinformatics analysis

2.16.1 Prediction of Ala391Thr variation on ZIP8 function

At the beginning of this project, we conducted intensive bioinformatics search to predict the potential functional impact of Ala391Thr variation on ZIP8 function. A number of bioinformatics tools included Phenotype Polymorphism (PolyPhen 2.0), Sorting Intolerant from Tolerent (SIFT), SNPs&Go, Screening for Non-Acceptable Polymorphisms (SNAP), Panther, dbSNP, Pmut, PROVEAN, iMutant, Mutpred. (The links for each of these tools have been listed in Results section Table 4.3) They usually use features based on sequence, structure, or known function. Some of these tools used learning algorithms to predict protein structure (use a training set of positive and negative examples to 'learn' sites). Others use substitutions based on disease-associated human alleles.

It is now been recognized that transcription factor (TF) binding can occur at exonic regions within the genome, in which codons that are highly conserved may also specify TF recognition sites.[224] Protein-coding DNA also often contains enhancers functioning at the transcriptional level.[225] Two algorithms have been used with an attempt to detect any overlapping of potential TF binding site within the polymorphic region, which are listed as follows:

Patch (http://www.gene-regulation.com/cgi-bin/pub/programs/patch/bin/patch.cgi), and

P-match (http://www.gene-regulation.com/cgi-bin/pub/programs/pmatch/bin/p-match.cgi).

2.16.2 Prediction of Ala391Thr variation on ZIP8 structure

At the later stage of the project, more bioinformatics tools have been employed to predict the impact of Ala391Thr variation on the transmembrane structure of ZIP8. Conservation analysis was performed at both the nucleotide and amino acid position, followed by protein secondary structure prediction based on a structurally similar homologue.

In the conservation analysis, protein sequences for human ZIP8 were retrieved from Ensembl version 78 (http://www.ensembl.org/index.html).[226] The longest isoform (ENST00000356736), deemed as canonical, was chosen for further analysis. Conservation analysis was performed on Ensembl using 23 way alignment of high-coverage amniote vertebrate genomes. The ConSurf server (http://consurf.tau.ac.il/) was used to predict functional domains based on the evolutionary conservation of amino acid positions.[227] This technique relies on UniRef protein clusters to infer the phylogenetic relations between homologous sequences.

The Robetta approach was employed to predict the secondary structure of the ZIP8 protein containing either the Ala391 or the Thr amino acid.[228] (http://robetta.bakerlab.org/queue.jsp) This method segments the protein into domains that are homologous to proteins with known structure, before an optional structure refinement stage. Both the full protein sequences containing the Ala391 and Thr391 residues were submitted for structure prediction. The domain containing amino acid 391 for both variants were fully processed and analyzed using PyMol to assess the

predicted structural effects of the amino acid substitution in the respective functional domain.[93] Further to the full structural reconstruction, Prediction of Transmembrane Helices In Proteins (TMHMM) v2 was used to predict transmembrane helical domains within the input sequences.[229] (http://www.cbs.dtu.dk/services/TMHMM/)

3. Results

3.1 Investigation of effect of rs13107325 on *SLC39A8*/ZIP8 expression

3.1.1 Identification of human umbilical artery smooth muscle cells and umbilical vein endothelial cells of relevant genotypes for functional study

In order to identify cells of the appropriate genotypes for subsequent gene expression studies, the DNA from human umbilical artery smooth muscle cells (HUASMCs) and umbilical vein endothelial cells (HUVECs) from different individuals were genotyped for SNP rs13107325 by KASPar, TaqMan and restriction enzyme digestion. The KASPar SNP genotyping assay was mainly used for HUASMCs, whereas TaqMan was used for HUVECs. The results of KASPar and TaqMan SNP genotyping were analysed by the SDS 2.4 software (Applied Biosystems), which produced an output display shown in Fig. 3.1 A. Genotype distributions of SNP rs13107325 in the HUASMC and HUVEC collections are summarized in Fig. 3.1 C. KASPar genotyping achieved a call rate of 97.2% in HUASMC samples, but was lower in HUVEC, hence TaqMan and restriction enzyme digestion methods were employed, which resulted in a 98.3 and 100% call rate, respectively. In the HUASMC samples, the frequencies of the C/C, C/T and T/T genotypes determined by KASPar were 93.8%, 5.8% and 0.4%, respectively. In the HUVEC DNA samples, the frequencies of the C/C, C/T and T/T genotypes determined by TaqMan were 93.1%, 7.5% and 0, respectively. However after sequencing of predicted heterozygous samples in HUVEC (n=13), only 3.4% (n=6) were proven to be true heterozygotes, with the rest being common homozygotes. The observed genotype distribution of the HUASMC collection was in agreement with Hardy-Weinberg equilibrium (HWE) (P = 0.7955, Chi-squared test).[230] The observed genotype distributi on in the HUVEC collection was in agreement with the expected distribution in HWE calculation (P = 0.9597, Chi-squared test). The restriction enzyme digestion of the PCR

A

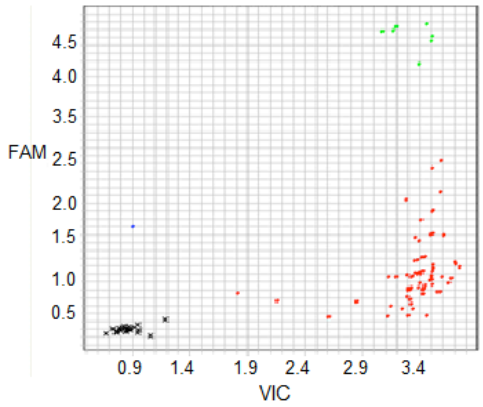

B

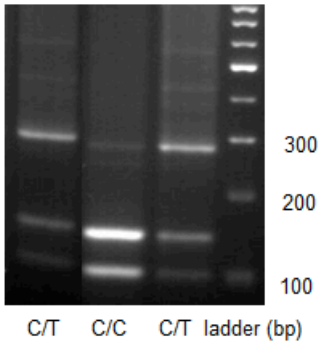

C

	KASPar	TaqMan
Genotype	HUASMC (n=282)	HUVEC (n=178)
C/C	257	162
C/T	16	13
T/T	1	0
Unclassified	8	3

Figure 3.1. Genotyping of rs13107325 in HUASMC and HUVEC DNA. (A) A representative SDS2.4 output of KASPar genotyping assay on HUASMC DNA samples. Each red dot is part of a selected cluster which has a predominantly VIC fluorescence signal, representing C/C genotype; each blue dot indicates a cluster of largely FAM fluorescence signal and thus the T/T genotype, whereas each green dot indicates both the detection of both VIC and FAM signals and thus the C/T genotype (B) A representative image of agarose gel electrophoresis of restriction enzyme digests of PCR products. The presence of the 121bp, 153bp and 274bp bands of similar intensity indicates the sample to be C/T genotype, whereas the presence of only the 121bp and 153bp bands indicates the C/C genotype (C) Genotype distribution of rs13107325 in HUASMCs and HUVEC DNA samples.

products method was used to facilitate genotyping, as shown in Fig. 3.1 B, which resulted in high success rate but ambiguity for distinguishing genotypes. The genotypes of all heterozygous samples were confirmed by Sanger sequencing. The rare homozygote sample in HUASMC was not pursued for further experimentation due to lack of cDNA or cell stock.

Overall, both KASPar and TaqMan genotyping methods have yielded some false positive results in genotype determination. This could be due to poor hybridization of the probes with gDNA, or the relatively small sample size (100-200) used in our projects. Definitive clustering was not achieved when small number of samples were used. Restriction enzyme digestion served as a more efficient method which allow individual sample detection. However, the ambiguity of results interpretation in some samples have affected its reliability in application.

3.1.2 Comparison of the relative *SLC39A8* mRNA expression levels of the T and C alleles

In order to investigate whether SNP rs13107325 has an allelic effect on *SLC39A8* expression, allelic expression imbalance (AEI) assays were performed to determine whether there was a difference in mRNA expression levels between the T and C alleles in the HUASMCs. PCR was performed to amplify the sequence (~200bp) flanking SNP rs13107325 in genomic DNA and cDNA in five HUASMC samples of C/T genotype. The PCR products from genomic DNA and cDNA were subsequently sequenced for AEI analysis (representative sequencing result is shown in Fig. 3.2 A). The relative heights of the peaks for T and C alleles at the rs13107325 SNP site were quantified with the use of PeakPicker software. In 5 pairs of samples which were heterozygous for rs13107325, the mean ratio of the peak height of allele T and allele C

at the polymorphic site was not significantly greater in cDNA than in genomic DNA (p=0.06 by Wilcoxon test), as shown in Fig. 3.2 B.

A

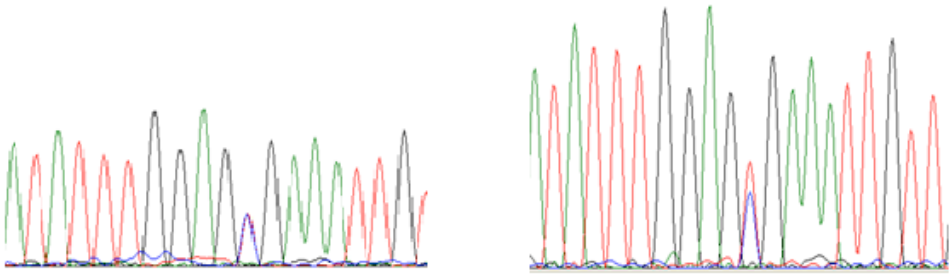

gDNA cDNA

B

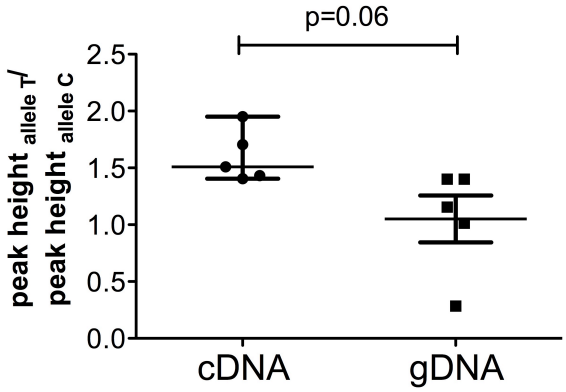

Figure 3.2 Effect of rs13107325 on *SLC39A8* mRNA transcription in HUASMC. (A) Representative of sequencing chromatograms from genomic DNA and cDNA of the same individual. The arrow points the polymorphic site of rs13107325 (B) Median ratio (± range) of allele T over allele C in cDNA and genomic DNA, respectively, in HUASMC of individuals heterozygous for rs13107325 (n=5 for each column)

The allelic imbalance analysis in HUVEC samples was hindered by an insufficient number of samples that were heterozygous for rs13107325. Two samples subjected to sequencing resulted in no major difference of the C/T ratio between cDNA and genomic DNA, as shown in Fig. 3.3. Therefore there is not enough evidence to demonstrate an allelic difference in mRNA expression in HUVECs.

A

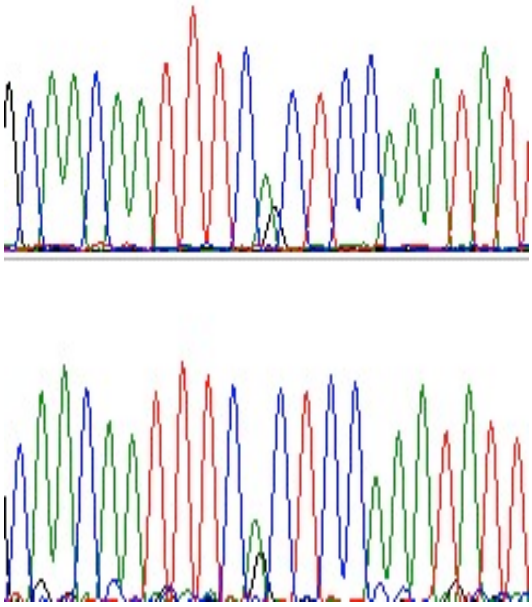

B

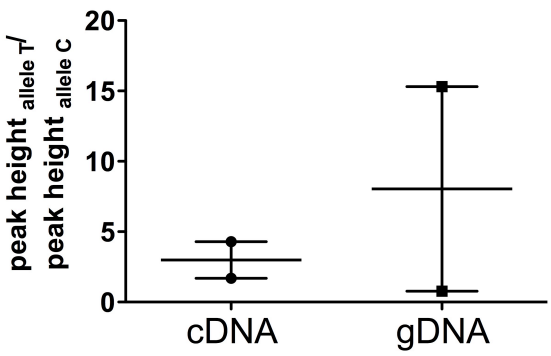

Figure 3.3 Effect of rs13107325 on *SLC39A8* mRNA transcription in HUVEC. (A) Representative of sequencing chromatograms from genomic DNA and cDNA of the same HUVEC sample. The arrow points the polymorphic site of rs13107325 (B) Ratio of allele T over allele C in cDNA and genomic DNA (n=2 for each column). Each bar represents median (± range) of each sample.

AEI appears to be a reliable method for assessing cis-acting regulatory elements when compared to eQTL for the reasons below: 1. AEI minimizes the intra-sample variation by correction with genomic DNA. When comparing mRNA levels between different individuals, other trans-acting regulators or different genetic background may contribuate to the differences in gene expression; 2. AEI also offers the advantage of assessing such interaction in more relavant tissue samples, as to generate a tissue-specific expression pattern. Standard eQTL mapping is done to test the linkage between variation in expression and genetic polymorphism. The available eQTL (expression quantitative trait loci) association of rs13107325-SLC39A8 is shown in Fig. 3.4. These data were obtained from the Genevar program at the Wellcome Trust Sanger Institute which can be downloaded from www. Sanger.ac.uk/resources/software/genevar/. These results were performed mainly on adipose, lateral collateral ligament (LCL) and skin tissues, and have not shown a significant difference in mRNA transcription levels among the three genotypes.

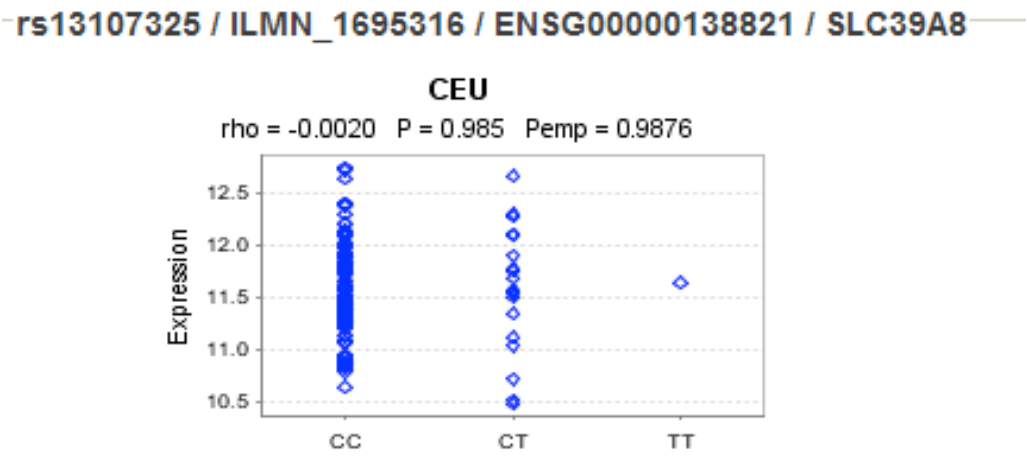

Figure 3.4. eQTL results of the association between rs13107325 and mRNA expression of *SLC39A8*. Data obtained from Genevar.

3.1.3 Comparison of ZIP8 protein levels among cells of the C/C and C/T genotypes

Total ZIP8 protein expression levels in HUASMC and HUVEC

The total ZIP8 protein expression levels were examined in HUASMCs and HUVECs of C/T and C/C genotypes. Immunoblotting with the polyclonal anti-ZIP8 antibody showed multiple bands of around 150kDa and 60kDa for all the cell lines tested (HUASMC, HUVEC and MCF-7) (Fig. 3.5 A, C, F). ZIP8 was reported to be expressed in MCF-7 cells, which was used as a positive control. (Fig. 3.5 F). Quantification of the two bands (~60kDa and 150kDa) in HUASMC showed approximately 1.6 fold higher expression in C/T samples than C/C samples, as shown in Fig. 3.5 B. However the difference was not significant, which might be due to insufficient sample numbers. The experiment was repeated twice, and similar results were seen. The trend was consistent with the previous finding in AEI, however needs to be validated in larger number of samples.

Although AEI failed to reveal any trend of expression difference on mRNA level in HUVECs. Given the small number of samples tested, the possible effect of this SNP on protein expression still can not be ruled out. HUVEC proteins were probed with the anti-ZIP8 antibody pre-incubated with a specific blocking peptide to verify the specificity of the antibody and nature of the multiple bands. The blocking peptide reduced the intensity of most of the bands, this could be due to incomplete blocking of the primary antibody at a high concentration. The band above the 100 kDa was greatly abolished by the blocking peptide, as indicated by the double arrow in Fig. 3.5 D. This suggested that the band of >100kDa was most specific to ZIP8, hence was used for further quantification of ZIP8 expression in HUVEC (Fig. 3.5 E). The expression level

of ZIP8 in HUVECs of C/T and C/C genotype was not significantly different.

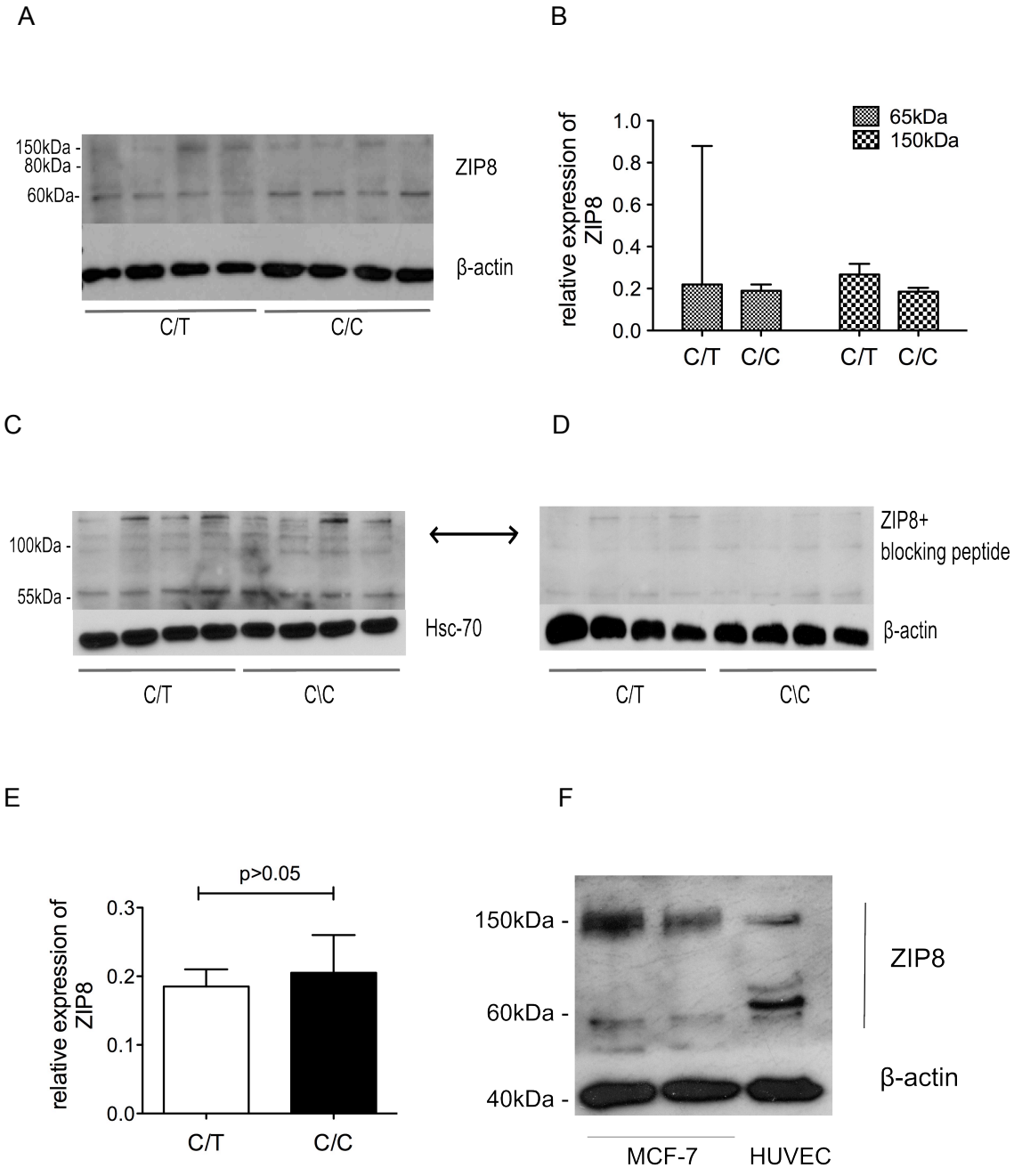

Figure 3.5. Immunoblotting image of total proteins in HUASMC and HUVEC cells of C/T and C/C genotypes. (A) Immunobloting analysis for the detection of ZIP8 expression in HUASMC (B) Quantification of relative ZIP8 expression in HUASMCs of C/C and C/T genotypes, n=4 for each genotype (C) Immunoblotting analysis for the detection of ZIP8 expression in HUVEC (D) Specificity of the ~100kDa bands was determined by preincubating the respective antibody with a ZIP8 specific peptide

solution (E) Quantification of relative ZIP8 expression in HUVEC cells of C/C and C/T genotype, n=4 for each genotype, p>0.5 by paired Student's t test (F) ZIP8 expression in other positive control cell line (MCF-7). Each bar represents the median value (± range) of each sample.

ZIP8 protein in subcellular fractions of HUVECs of C/T and C/C genotypes

In order to determine the ZIP8 expression was further determined in protein fractions extracted from different cellular compartments, including membrane, nucleus, mitochondrial and organelles. As shown in Fig. 3.6, protein of different sizes were observed in these fractions, which may suggest different post-translational modification in these cell compartments. The majority of the ZIP8 signals detected were larger than 130kDa, suggesting that ZIP8 exists as a dimer or multimer in HUVECs. On top of that, some of these proteins may be glycosylated, which may explain the presence of multiple signals. In the cytosolic fraction, the presence of bands above 250 kDa indicates that ZIP8 proteins may exist in heterodimers. The expression levels were lower in the 10,000 x g (organelles) and 900 x g (nuclear + cell debris) fractions, which was to be expected for membrane proteins.

3.2 Investigation of effect of Ala391Thr on ZIP8 function

3.2.1 Generation of pCDNA3.1-SLC39A8-Ala/Thr391 plasmids

In order to investigate the effect of Ala391Thr substitution caused by SNP rs13107325 on ZIP8 protein function, two plasmids for expressing either ZIP8-Ala391 or ZIP8-Thr391 were generated by a series of molecular cloning experiments. First of all, the full open-reading-frame (ORF) sequence of ZIP8 was amplified using a plasmid

containing the full-length human ZIP8 cDNA (C allele-containing) as the template

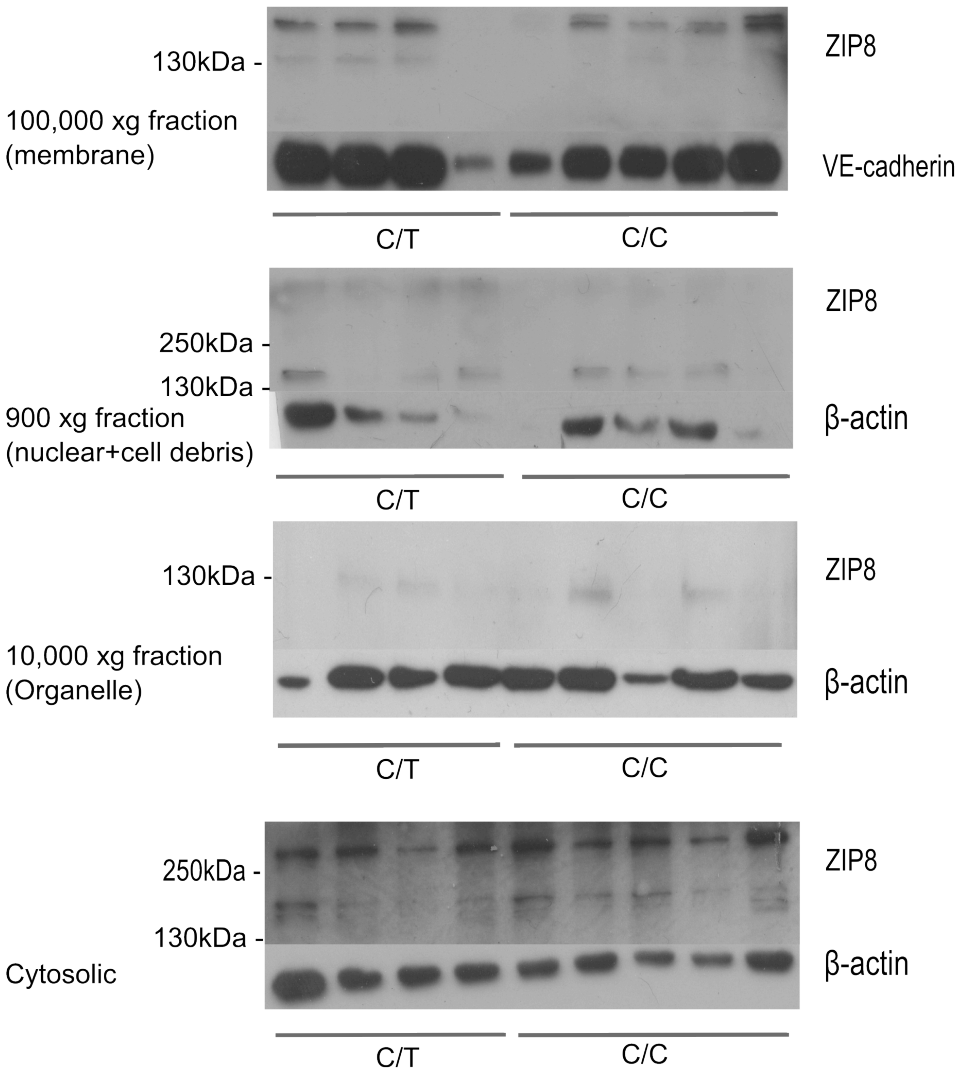

Figure 3.6. Immunoblotting image of ZIP8 expression in HUVEC cellular fractions. $n_{C/T}$=4, $n_{C/C}$=5.

followed by digestion with *EcoRI* and *HindIII* restriction enzymes (Fig. 3.7 A, B and C). The digested products were then ligated overnight using T4 ligase and subsequently transformed into JM109 competent cells.

Positive colonies were further propagated followed by plasmid extraction and verification by sequencing. The insert of the pCDNA3.1-SLC39A8-alanine (Ala)

plasmid was sequenced to be in line with the *SLC39A8* ORF (corresponding to the C allele) without any nucleotide change compared to the reference sequence. This plasmid was then subjected to site-directed mutagenesis to generate a corresponding pCDNA3.1-SLC39A8-Thr plasmid. Following mutagenesis, the insert of the second plasmid was sequenced to verify that nucleotide C had been changed to T at the SNP rs13107325 site (Fig. 3.7 D; full sequence shown in **Appendix 3**).

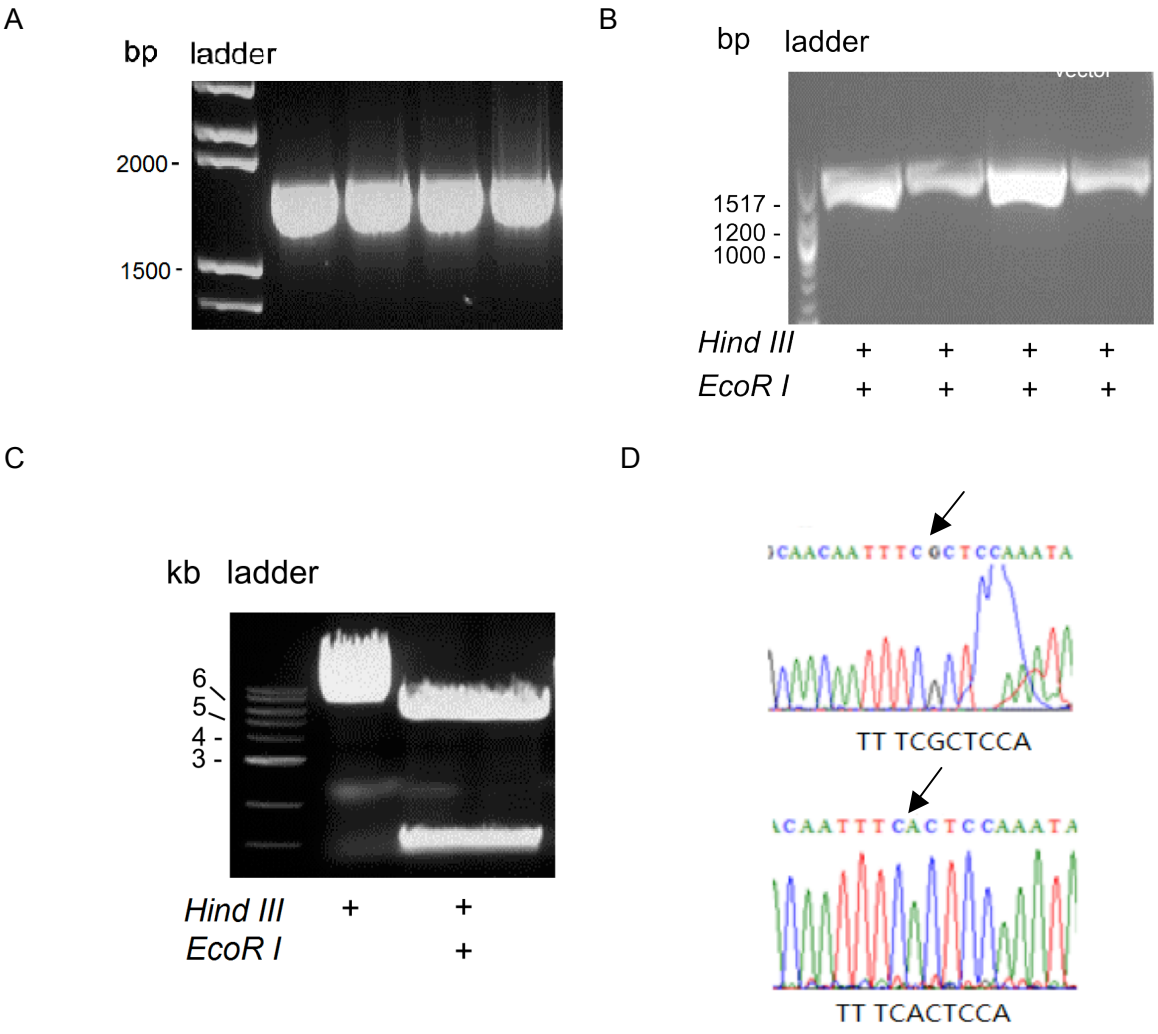

Figure 3.7. Gel electrophoresis results of PCR products for cloning. (A) PCR amplicon of the *SLC39A8* ORF insert, each lane represents one selected colony (B) PCR amplicons of ZIP8 ORF digested by EcoR I and Hind III enzymes: Lane 1 and 2 represent C allele (Ala391) containing insert, lane 3 and 4 represent T allele (Thr391)

containing insert (C) pCDNA 3.1 plasmid vector digested by Hind III enzyme (lane 1) or by both EcoR I and Hind III enzymes (lane 2) (D) Sequencing chromatograms of the pcDNA3.1-SLC39A8-Ala and –Thr plasmid containing the C→T mutation.

3.2.2 Transfection of cultured cells with pCDNA3.1-SLC39A8-Ala/Thr391 plasmids

Different transfection methods were used for different cell lines. The calcium phosphate method was used to transfect HEK293 with the SLC39A8 expression plasmids or the plasmid vector. Subsequent immunoblotting analyses using a polyclonal hZIP8 antibody generated two bands (~100 and 150kDa) in transfected HEK293 cells (Fig. 3.8, left half), which showed higher intensities in the cells transfected with the pCDNA3.1-SLC39A8-Ala/Thr plasmids than cells transfected with the vector. Co-incubation of ZIP8 antibody with the ZIP8 antigen peptide resulted in a significant reduction of the 100kDa and 150kDa bands (Fig. 3.8, right half), indicating that those two bands derived from ZIP8 proteins. Preliminary data showed that 1μg of the plasmid DNA produced a good transfection efficiency. Therefore 1μg of plasmid was used for subsequent transfections conducted in 6-well plates. The amount of plasmid was adjusted proportionally according to the surface area of the culture plate when other types of plates were used.

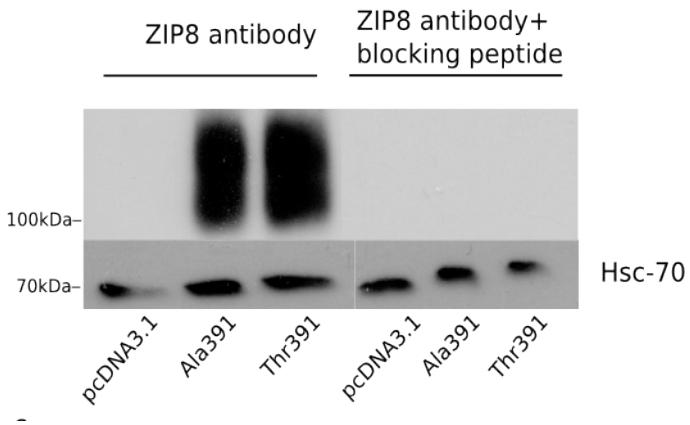

Figure 3.8. Immunoblotting of calcium phosphate transfection on HEK293 cells. HEK293 cells transfected with the ZIP8 expression plasmids, incubated with a ZIP8 antibody in the presence or absence of a ZIP8 blocking peptide

X-tremeGENE HP DNA method was used to transfect HepG2 cells, as the calcium phosphate method yielded very low transfection efficiency and electroporation resulted in severe cell death in this cell line. X-tremeGENE HP DNA method did not change the morphology or the number of cells (Fig.3.9 A) and caused minimum cell death. This method has yielded high transfection efficiency for both plasmids (Fig. 3.9 B). Without detecting any monomer form of ZIP8, this protein seems to be present in dimer or multimer form which is consistent with the previous finding in HUASMC and HUVECs (bands ~ 150kDa). The smeary bands shown in Fig. 3.9 B indicate the possible presence of more than one band upon transfection.

A

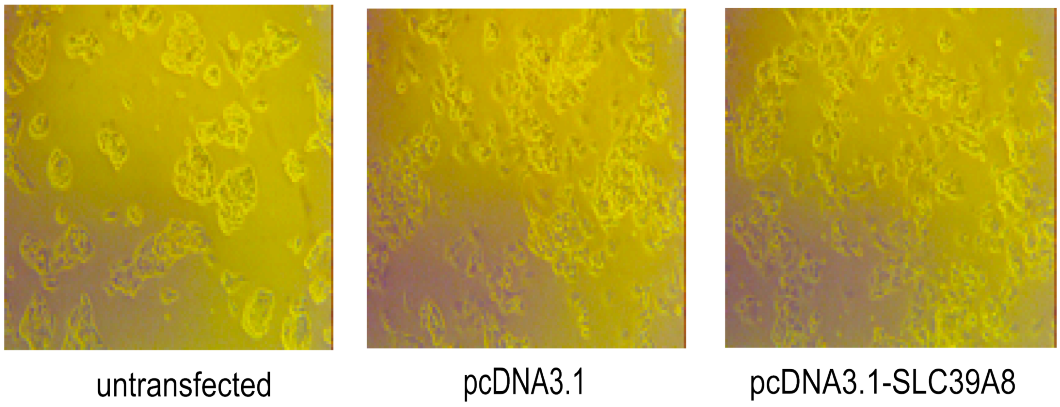

B

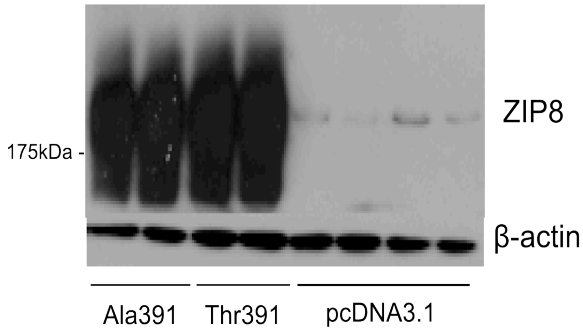

Figure 3.9. X-tremeGENE HD transfection in HepG2 cells. (A) Morphology of transfected and untransfected cells 24h after transfection (B) Immunoblot result of HepG2 cells transfected with 1µg of ZIP8 plasmid DNA or vector

3.2.3 The effect of *SLC39A8* genotype on metal ion uptake

SLC39A8-Ala391 variant is associated with higher levels of Cd^{2+} uptake in HUVEC and HEK293 cells

The kidney is the one of the primary targets for deposition of Cd^{2+}. Using a human embryonic kidney model, only a very low level of endogenous ZIP8 was found in

HEK293 cell (Fig. 3.10 A: lanes pCDNA3.1, upper panel). This makes HEK293 cell a good cellular model for the study of the genotypic impact of *SLC39A8* on cellular function. Transfection yielded ZIP8-specific bands of around 100kDa, which are similar in size as the ZIP8 signal in HUVEC. As proven by the blocking peptide experiment, overexpressed ZIP8 is likely to be packed into different complexes in different tissues. Immunoblotting and quantification of ZIP8 expression in HUVECs of Ala/Ala and Ala/Thr genotypes is shown in Fig. 3.10 B. Higher levels of Cd^{2+} uptake were observed in transfected HEK293 cells overexpressing the Ala391 variant (Mean=9.29) compared to the Thr391 (Mean=1.9) (Fig. 3.10 C). In HUVECs, cells of the Ala/Ala genotype (Mean=215) also exhibited higher Cd^{2+} uptake compared with cells of Ala/Thr genotype (Mean=5.1) , as illustrated in Fig. 3.10 D.

A

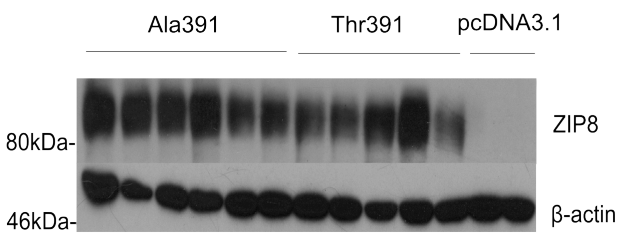

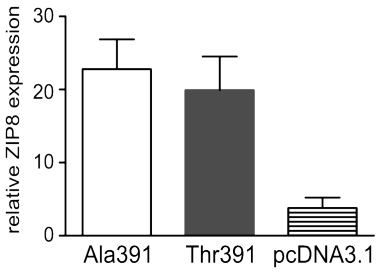

B

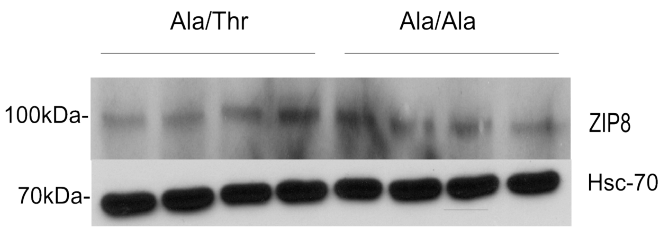

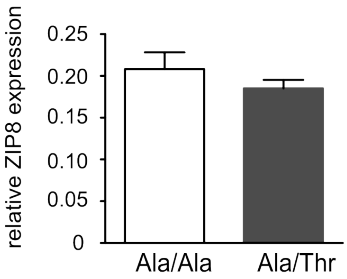

C

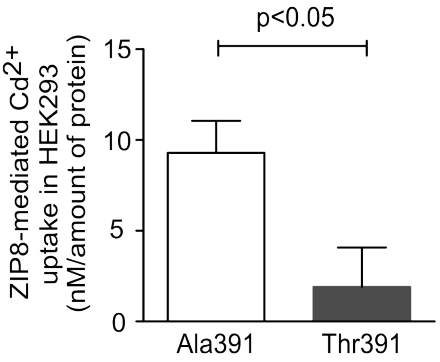

D

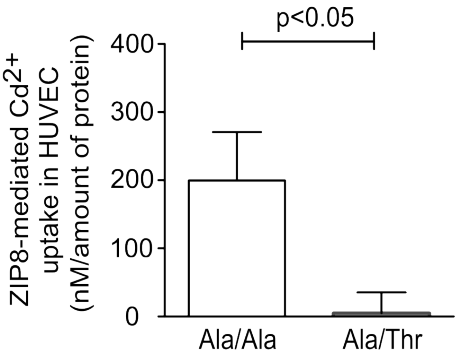

Figure 3.10. Effect of *SLC39A8* genotype on Cd^{2+} uptake. (A) A representative image of immunoblot analysis and the quantification of overexpressed ZIP8 proteins in cultured HEK293 cells transfected with pCDNA3.1-SLC39A8 plasmids containing either alanine or threonine at residue 391 on the protein sequence (B) A representative image of immunoblot analysis and the quantification of ZIP8 proteins in HUVECs of Ala/Ala and Ala/Thr genotypes (C) Intracellular Cd^{2+} levels in transfected HEK293 cells. Each column represents the difference of Cd^{2+} content between Cd^{2+}-treated cells and vehicle-treated cells, standardized against total ZIP8 expression in each HUVEC sample. Each data point represents mean (± SEM) in duplicates from 3 experiments, n=6 for each plasmid (D) Intracellular Cd^{2+} levels in HUVECs. Each column represents the difference of Cd^{2+} content between Cd^{2+}-treated cells and vehicle-treated cells, standardized against total ZIP8 expression in each HUVEC sample. Each data point represents mean (± SEM) in duplicates from 3 experiments, n=4 for each genotype. $p<0.05$ by paired Student's t-test.

SLC39A8-Ala391 variant is associated with higher levels of Zn^{2+} uptake in HepG2 cells

In order to test whether the Ala391Thr substitution may affect the activity of ZIP8 on Zn^{2+} uptake, and to further elucidate the link between Zn^{2+} uptake, NF-κB signalling, and cholesterol efflux, Zn^{2+} uptake assay was performed on HepG2 cells. A fluorescent dye (Zinquin) which binds to labile Zn^{2+} was used and detected by a flow cytometer. HepG2 cells were firstly been transfected with pCDNA3.1-SLC39A8-Ala391, Thr391 plasmid or pCDNA3.1 vector, followed by incubation with zinc chloride and Zinquin. As shown in Fig. 3.11, the Ala391 variant exhibited a higher level of Zn^{2+} uptake under physiological concentration of Zn^{2+} treatment (18μM), compared to pCDNA3.1-SLC39A8- Thr391 plasmid and pCDNA3.1 vector.

A

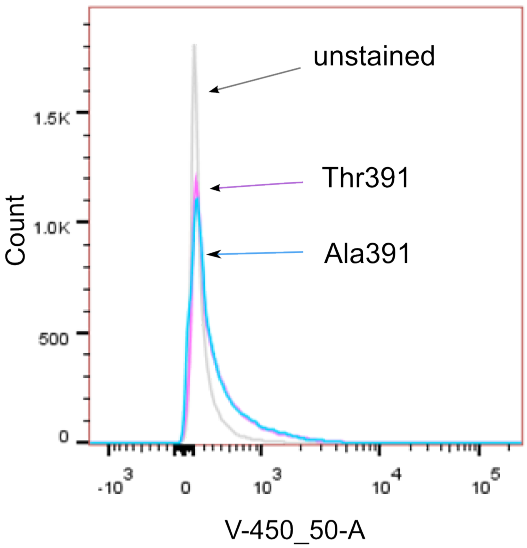

B

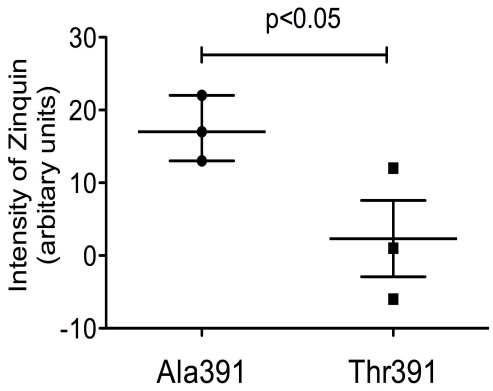

Figure 3.11. Zn^{2+} uptake result in HepG2 cells transfected with pCDNA3.1-Ala/Thr391 plasmids. (A) A representative plot of flow cytometric analysis showing intracellular Zn^{2+} content (B) Quantification of intracellular Zn^{2+} content after 2h of $ZnCl_2$ treatment (18μM), each value is the vector control and unstained sample V450/50 -subtracted reading value, and each bar represents median (± range) from 3 samples.

3.2.4 SLC39A8-Thr391 variant is not associated with HDL_3-mediated cholesterol efflux

To examine whether quantitative cholesterol efflux measurements can be achieved using BODIPY-Ch, a time-course experiment was performed in HUVEC. Efflux of BODIPY-Ch increased over 24h, although significant cell death was also observed. A gradient range of HDL_3 was used to determine the optimal concentration for cholesterol efflux. A positive correlation was observed between increasing amount of HDL_3 and cholesterol efflux, with 25μg/ml of HDL_3 resulting in an efflux rate of 4.27% over 4h efflux (Fig. 3.12). Minimal cell death was seen at this concentration and time period. Therefore 4h efflux period was used for further experiments.

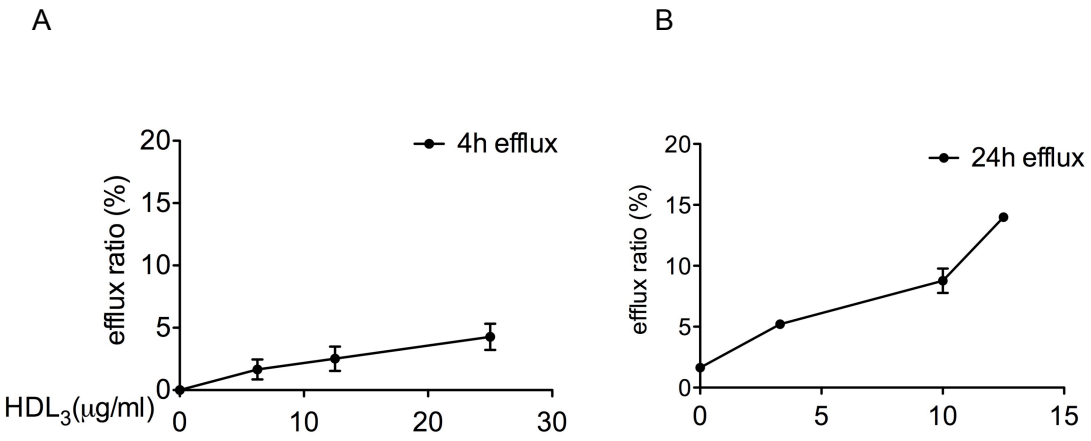

Figure 3.12. Optimization of HDL_3-mediated cholesterol efflux in HUVECs. (A) HDL_3 dose response curve of cholesterol efflux over 4h time period. (B) HDL_3 dose response curve of cholesterol efflux over 24h time period. Efflux ratio was expressed as the percentage of the medium BODIPY-ch fluorescence from the total BOBIPY-ch fluorescence measured from the medium and cells. Each value was generated by subtraction of value from the vehicle-treated sample from the HDL_3-treated sample which were transfected by the same plasmid or vector. Data represent median (± range) of duplicates from two experiments.

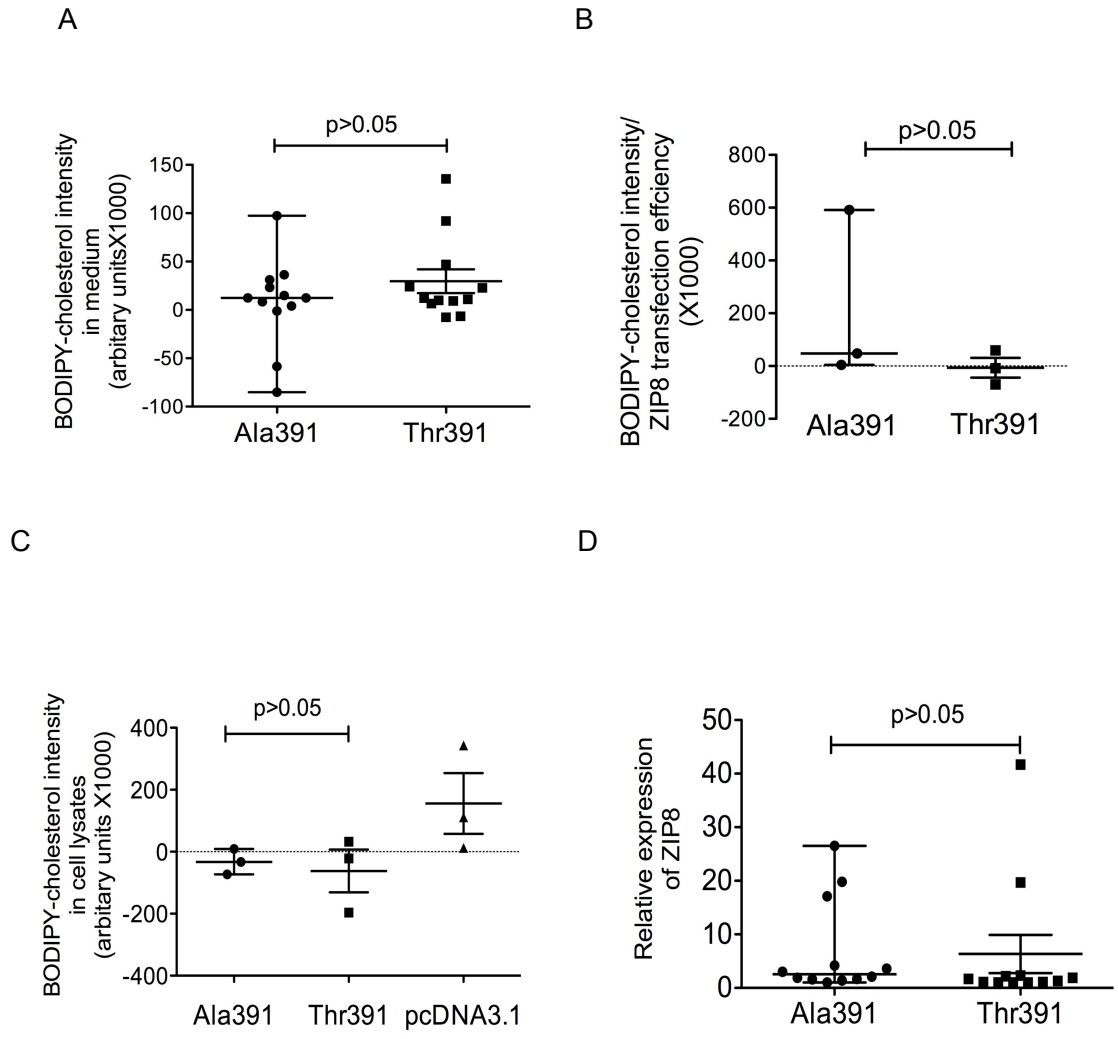

Figure 3.13. HDL_3-induced cholesterol efflux in HepG2 cells transfected with pCDNA3.1-SLC39A8-Ala/Thr391 plasmids. Cells were transfected with pCDNA3.1-SLC39A8-Ala391, Thr391 and pCDNA3.1 vector, then treated with BODIPY-ch for 4h, followed by HDL_3 (25μg/ml), or BODIPY-ch followed by vehicle. (A) Culture medium fluorescence intensity in samples with HDL_3 treatment minus vehicle in cells transfected with the same plasmid. Experiments were conducted in duplicates from six independent experiments (n=12) (B) Each bar represents the transfection efficiency adjusted value for each plasmid shown in (A) subtract the value for vector control (n=6) (C) Levels of BODIPY-cholesterol in cell lyates (n=6) (D) Transfection efficiency of pcDNA3.1-SLC39A8 plasmids on HepG2 cells that were subjected to cholesterol efflux assay (n=12). Each bar represents median value (± range) of each sample.

In order to test whether the Ala391Thr substitution has any effect on cholesterol efflux capacity, HepG2 cells transfected with pCDNA3.1-SLC39A8-Ala/Thr391 plasmids were used. Cells overexpressing the Thr variant showed a trend of higher cholesterol efflux levels, compared to Ala391 and vector control (Fig. 3.13 A). The intra-sample variability of intracellular cholesterol was large (Fig. 3.13 C), which could be due to interference of acidity with the fluorescence dye when acetic acid lysing was used. Therefore only medium cholesterol concentration was used for further analysis. Similar method can be found in the cholesterol efflux calculation published by S. Sankaranarayanan *et al.* [231] However, when the cholesterol efflux was adjusted against ZIP8 transfection efficiency, the mean value of adjusted cholesterol efflux appeared to be higher in Ala391 variant, as shown in Fig. 3.13 B. This could be caused by variations in each transfection, shown by the large SEM bars in Fig. 3.13 D. Overexpression of ZIP8 has enhanced the overall cholesterol efflux in HepG2 cells, however no conclusions can be drawn on any allelic influence as the difference between Ala391 and Thr391 variant was not significant.

3.2.5 Effect of Ala391Thr variation on cadmium-induced activation of cell signalling pathway

Allele-dependent modulation of cadmium-induced ERK activation in HEK293 cells

The potential involvement of Ala391Thr variation in MAPK pathway activation (ERK1/2 phosphorylation) following treatment with low dose Cd^{2+} was assessed in HEK293 cells. Cells were exposed to 1μM Cd^{2+} for different lengths of time and analysed for ERK1/2 phosphorylation over a period of 24h. An early ERK response to Cd^{2+} stimulation was detected as early as 1h, and remained elevated up to 24h. Phosphorylation of ERK2 was significantly higher in HEK293 overexpressing the SLC39A8-Ala391 variant, compared to cells expressing the SLC39A8-Thr391 variant and pCDNA3.1 vector at 24h (Fig. 3.14 C), whereas the lowest ERK activation was detected in cells transfected with vector control (Fig. 3.14 A). ERK1 phosphorylation was also elevated in cells transfected with *SLC39A8* expression plasmids, however the difference between the Ala391 and Thr391 variant was not statistically significant at all time points (Fig. 3.14 D). ZIP8 expression levels in both Ala391 and Thr391-transfected cells were similar at earlier treatment time points (up to 1h, shown in Fig. 3.14 B), however gradually reduced after 1h up to 24h. This suggests degradation of overexpressed ZIP8 in transfected cells, possibly due to its interaction with Cd^{2+}. The Ala391 variant, which is associated with higher Cd^{2+} uptake levels shown in Fig. 3.10, corresponds to a significantly greater activation of ERK2 at a longer incubation time. Hereby it is plausible that the activation in ERK2 is caused by higher intracellular accumulation of Cd^{2+}.

A

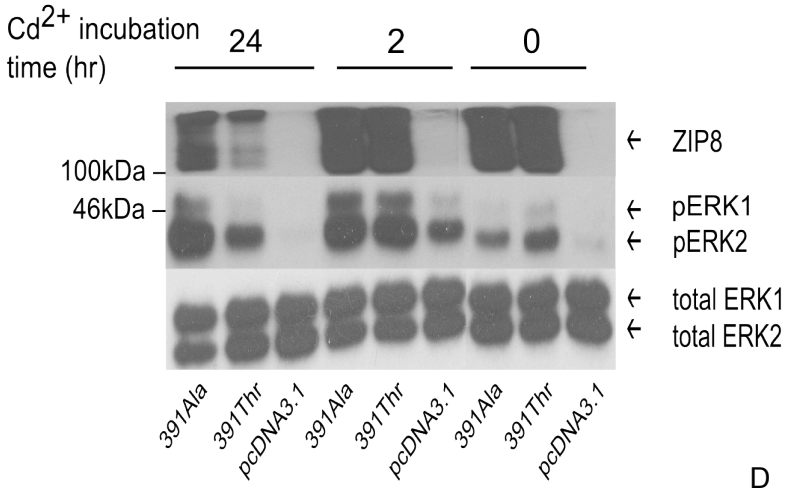
Cd2+ incubation time (hr)
24
2
0
100kDa
46kDa
ZIP8
pERK1
pERK2
total ERK1
total ERK2
391Ala
391Thr
pcDNA3.1
391Ala
391Thr
pcDNA3.1
391Ala
391Thr
pcDNA3.1

B

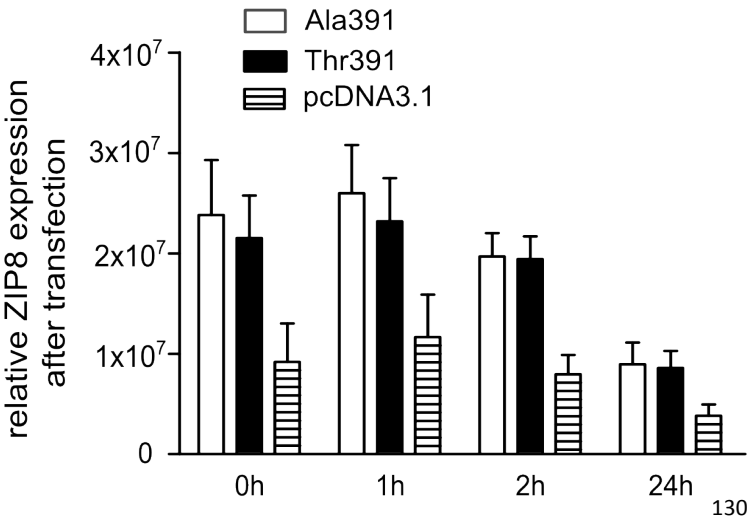
Ala391
Thr391
pcDNA3.1
relative ZIP8 expression after transfection
4x10^7
3x10^7
2x10^7
1x10^7
0
0h
1h
2h
24h

C

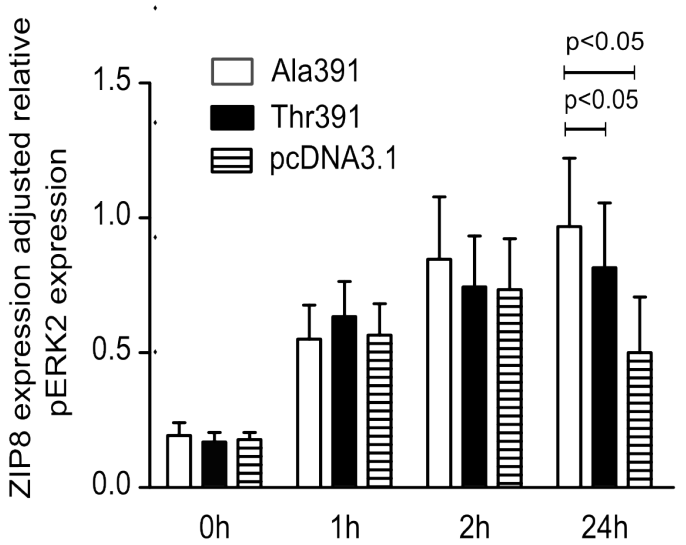
Ala391
Thr391
pcDNA3.1
p<0.05
p<0.05
ZIP8 expression adjusted relative pERK2 expression
1.5
1.0
0.5
0.0
0h
1h
2h
24h

D

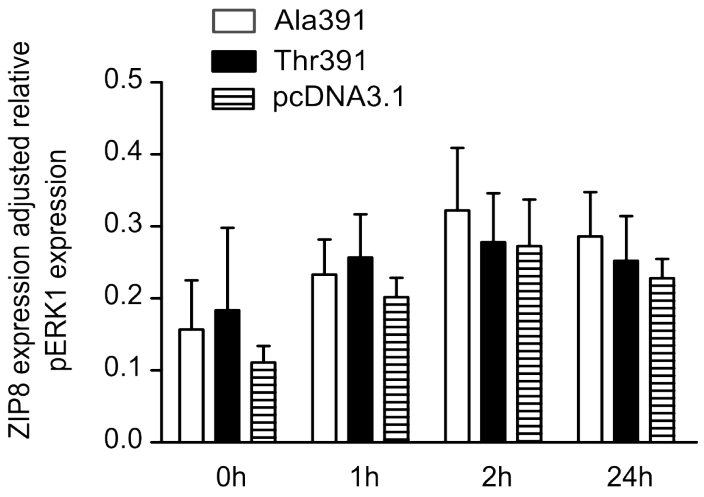
Ala391
Thr391
pcDNA3.1
ZIP8 expression adjusted relative pERK1 expression
0.5
0.4
0.3
0.2
0.1
0.0
0h
1h
2h
24h

Figure 3.14. Phosphorylation of ERK1/2 in HEK293 cells transfected with pCDNA3.1-SLC39A8-Ala/Thr391 or pcDNA3.1 vector. (A) A representative immunoblotting image of expression of pERK1/2, total ERK1/2 and ZIP8 at different time points (B) Quantification of relative ZIP8 expression after different incubation periods of $CdCl_2$ (C) and (D) quantification of immunoblots of phosphorylation of ERK2 and ERK1 after 0h, 1h , 2h, 24h of $CdCl_2$ treatment (1μM). Data shown are mean (± SEM) each genotype was done in duplicates from at least 3 separate experiments

Cadmium-induced ERK activation in HUVEC

In order to investigate whether there is a genotypic effect of ERK1/2 activation in HUVEC induced by Cd^{2+}, phospho-ERK1/2 expression was detected after 4 and 24 hours of Cd^{2+} treatment (1μM). The expression change of pERK1/2 at 24h was bidirectional comparing to basal level, with a trend for upregulation observed at 4h of Cd^{2+} treatment (Fig. 3.15 B), although no significant difference was detected between the Ala/Ala and Ala/Thr genotypes (n=4) (Fig. 3.15 C&D). A larger number of sample for each genotype is a required to validate this finding, with a minimum sample size of 13 being estimated by G*Power calculation. (critical t = 2.17881, power = 0.96).

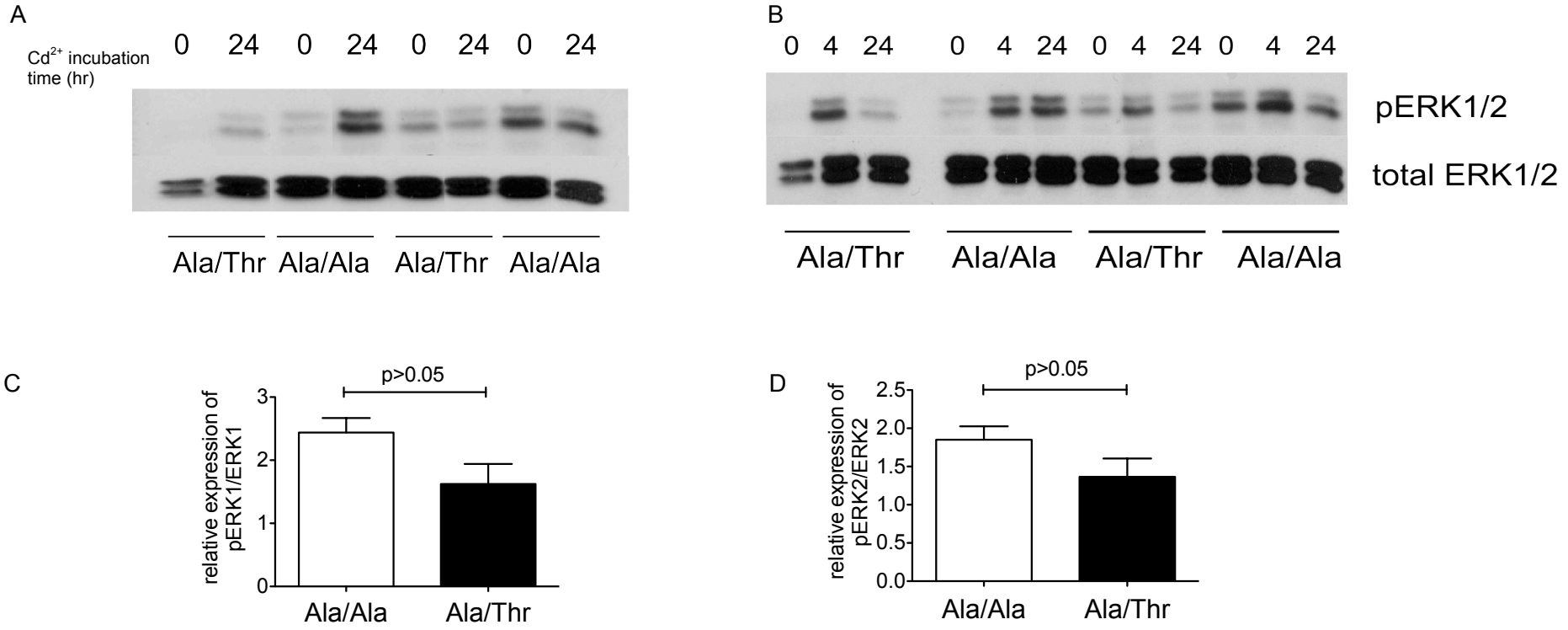

Figure 3.15. Phosphorylation of ERK1/2 in HUVEC of Ala/Ala and Ala/Thr genotypes after 4h of cadmium treatment (1µM). (A) A representative immunoblot image of phospho-ERK1/2 and total ERK1/2 protein expression in cells of different genotypes (B) A representative immunoblot image of phospho-ERK1/2 and total ERK1/2 protein expression in cells been treated with $CdCl_2$ for 0h, 4h and 24h (C) and (D) Quantification of pERK1 and pERK2 normalized to total ERK1 and ERK2 expression after 4h of Cd^{2+} incubation. Value represents mean (±SEM) of each genotype done in duplicates from 4 separate experiments.

3.2.6 Different modulation of NF-κB activation of SLC39A8-Ala391 and Thr391 variant in response to cadmium

Cadmium induced NF-κB activation in HEK293 cells

To further examine the potential signalling pathway triggered by cellular uptake of Cd^{2+}, activation of transcription factor NF-κB was detected by dual-luciferase reporter assay in HEK293 cells. We performed transient transfection using pCDNA3.1-SLC39A8-Ala/Thr391 plasmids and κB-dependent firefly luciferase reporter plasmids to investigate whether the Ala391Thr variation mediates NF-κB activation through differences in the amount of Cd^{2+} uptake. As shown in Fig. 3.16 A, cadmium (1μM) induced a 10-fold increase in κB-dependent luciferase activity in HEK293 cells overexpressing ZIP8 compared with vector control after 2h of Cd^{2+} incubation. The SLC39A8-Ala391 variant associated with higher Cd^{2+} uptake showed stronger NF-κB activation compared to the Thr391 variant. However, longer Cd^{2+} treatment of 24h was shown to conversely inhibit NF-κB activation comparing to no Cd^{2+} control (Fig. 3.16 B).

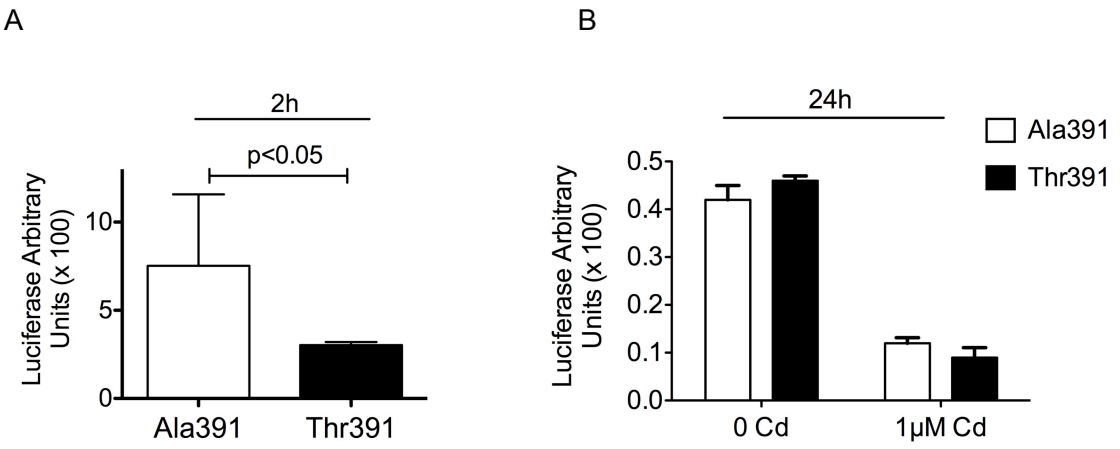

Figure 3.16. Relative promoter activity of the NF-κB mediated by SLC39A8-Ala/Thr391 plasmids following Cd^{2+} treatment. HEK293 cells were co-transfected with the mixture of luciferase plasmids, and pCDNA3.1-SLC39A8-Ala/Thr391 expression plasmids. $CdCl_2$ were added 24h after transfection. (A) NF-κB luciferase activities after 2h incubation with 1μM Cd^{2+}. Data are normalized ratios of firefly luciferase and renilla luciferase activity. Data are mean (±SEM) values from triplicates, repeated in 3 experiments (B) Luciferase activity after 24h incubation with $CdCl_2$. Data is generated from triplicates from one experiment, each bar represents median value with range of each sample.

Inhibition of NF-κB in HUVEC of Ala/Ala and Ala/Thr under Cd^{2+} treatment

In order to study whether there is any genotypic effect on NF-κB activation in HUVEC exposed to cadmium, cells of Ala/Ala and Ala/Thr genotype were used for detection of NF-κB effector elements such as IkBα, pIkkα/β. Cells were treated with $CdCl_2$ (1μM) for 2h, 4h or 24h before been harvested for immunoblotting assays. Served as an inhibitory protein, IkB α expression level is usually negatively correlated with NF-κB

activation. As shown in the immunoblot image after 2h of cadmium incubation (Fig. 3.17 A), the expression level of IkBα was not clear enough to show any activation or inhibition of the NF-κB pathway in repsonse to Cd^{2+}. Despite the overall inhibition, Ala/Thr genotype exhibited a greater level of NF-κB inhibition comparing to Ala/Ala genotype at 2h and 4h time points (Fig. 3.17 C). To further test our hypothesis, additional upstream regulator pIkkα/β was quantified. Depite the relatively high basal level of pIkkα/β in HUVECs (Fig. 3.17 B, lane 3, 6, 9, 12), difference in the change of pIkkα/β relative expression between 4h and 24h time points was detected in HUVECs of Ala/Ala and Ala/Thr genotypes. As shown in the immunoblot quantification at 24h over 4h (Fig. 3.17 D), a sustained elevation of pIkkα/β level was found in HUVECs of the Ala/Ala genotype. This partially agrees with the previous findings on HEK293 cells, whereas significantly higher level of NF-κB activation was found in the Ala391 variant at a shorter Cd^{2+} exposure time (2h). These findings indicate that NF-κB pathway signalling may be differentially regulated in different cell lines under Cd^{2+} exposure. The variability of NF-κB effector elements expression may have also been affected by occurrence of cell death under longer Cd^{2+} exposure.

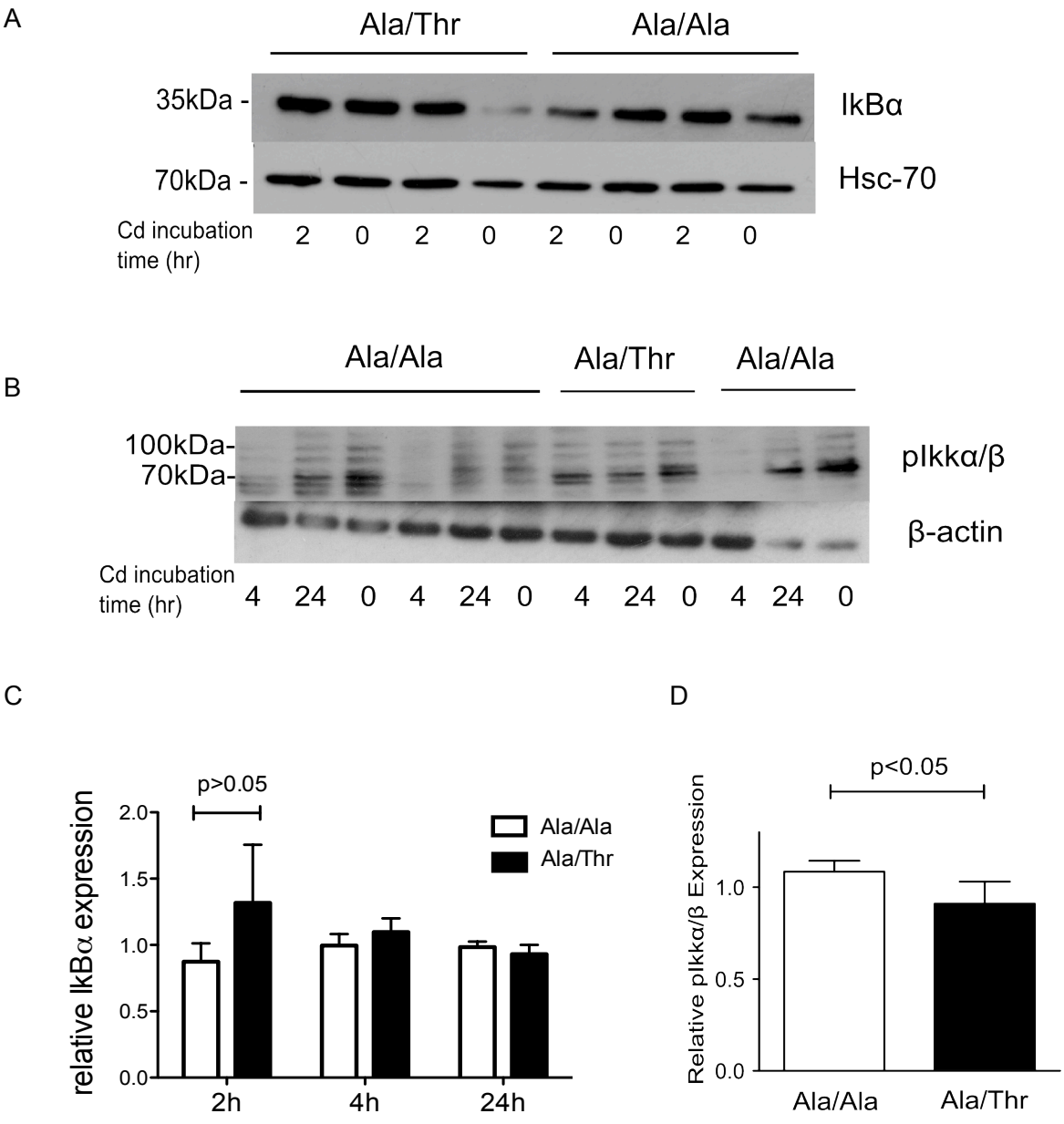

Figure 3.17. Immunoblotting of NF-κB activation related elements in HUVECs of Ala/Ala and Ala/Thr genotypes. (A) A representative immunoblot image of IkBα expression after 2h of $CdCl_2$ (1μM) incubation (B) A representative immunoblot image of pIkkα/β expression after 4h and 24h of $CdCl_2$ (1μM) incubation (C) Quantification of relative IkBα expression at 2h, 4h and 24h time points. Each value in been normalized to t_0 value of each sample. Data are mean (±SEM) values from duplicates from at least 3 separate experiments (D) Quantification of the ratio of relative pIkkα/β expression between 24h and 4h Cd^{2+} treatment in HUVECs. Data are mean (±SEM) values of 4 samples for

each genotype, conducted in duplicates

3.2.7 SLC39A8-Ala391 variant is associated with higher cytotoxicity under Cd^{2+} exposure

It has been proven by many studies that cadmium exposure causes cell deaths.[232] Cell toxicity assays were conducted in order to investigate whether there is any difference in cytotoxicity associated with different Cd^{2+} uptake levels caused by Ala391Thr variation. We used LDH and MTS assays on HEK293 and HUVEC to test this hypothesis.

SLC39A8-Ala variant is associated with higher cytotoxicity in HEK293 and HUVEC

Following the finding on the SLC39A8-Ala391 variant being associated with an elevation in Cd^{2+} uptake in HEK293 and HUVECs. We further studied the viability of these cells in the presence of low dose Cd^{2+} (1μM). After 24h of $CdCl_2$ incubation, HEK293 overexpressing both Ala/Thr391 variants have undergone a morphological change by becoming smaller and changed from spindle-shaped to spherical-shaped, compared to the vector control (Fig. 3.18 A). This was accompanied by the presence of more floating cells in the culture medium. Cd^{2+} exposure resulted in higher levels of LDH in supernatant of the cells transfected with the pcDNA3.1-SLC39A8-Ala391 plasmid compared with the pcDNA3.1-SLC39A8-Thr391 plasmid and vector control (Fig. 3.18 C), which indicates higher cell death. HUVECs of Ala/Ala genotype also exhibited higher cell death compared to Ala/Thr genotype (Fig. 3.18 C).

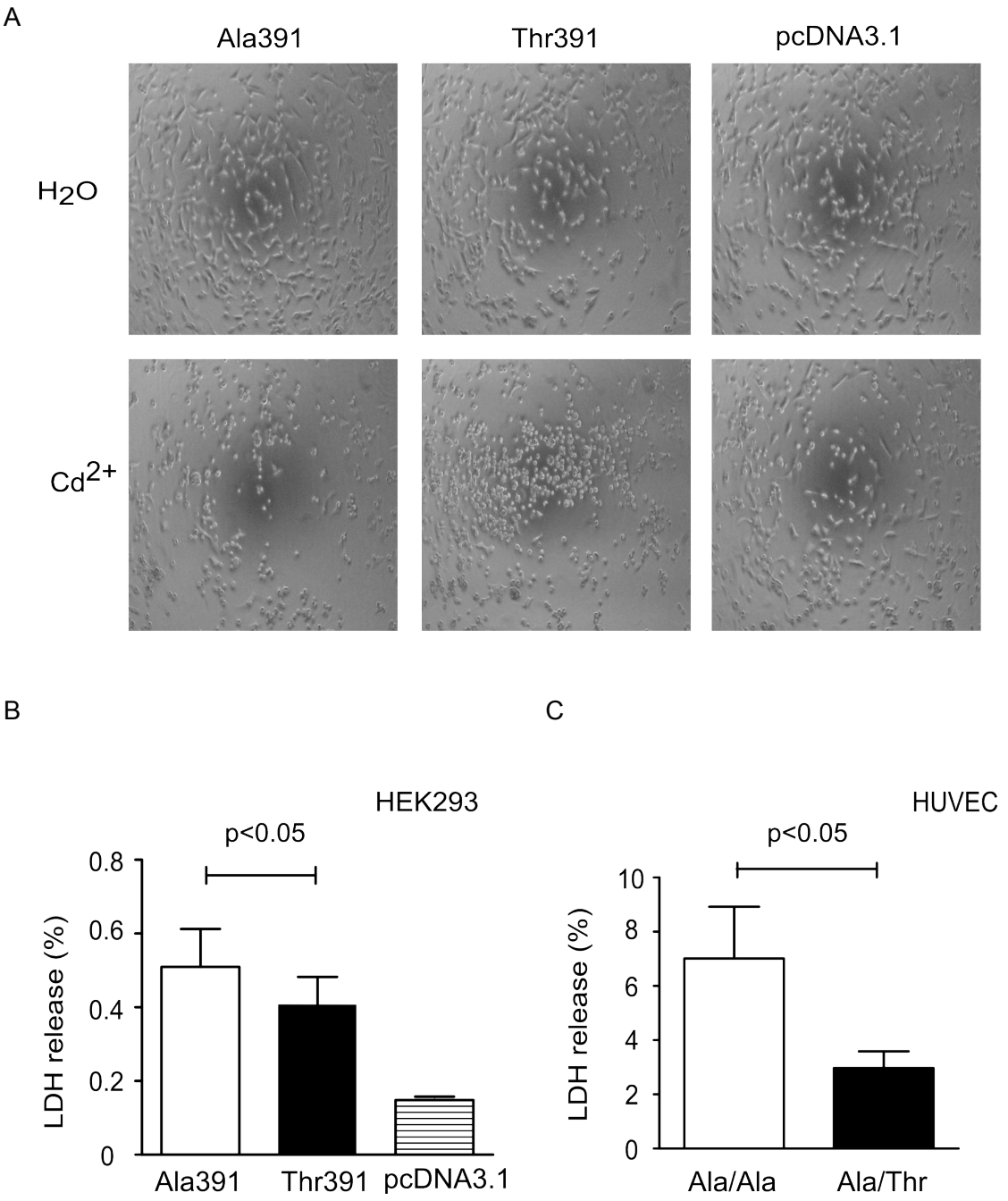

Figure 3.18. Effect of *SLC39A8* genotype on cell death induced by cadmium. (A) Pictures illustrating phenotypic changes of HEK293 cells transfected with pCDNA3.1-SLC39A8-Ala/Thr391 and vector control plasmids following 24h incubation with $CdCl_2$ (1μM) (B) Cd^{2+}-induced LDH release in HEK293 cells transfected with pCDNA3.1-SLC39A8-Ala/Thr391 plasmids, cells were loaded with $CdCl_2$ 48h after transfection. Each experiment was done in triplicates or more and repeated 3 times (C) Cd^{2+}-

induced LDH release in HUVECs of Ala/Ala and Ala/Thr genotypes. Both cell lines were subjected to 24h incubation of $CdCl_2$. The level of toxicity, as measured by LHD levels in the cell medium. Value of each bar = LDH $_{(Cd^{2+}\text{-treated samples-H2O-treated samples})}$. Data are mean (±SEM) values from 3 experiments (n=4 for each genotype).

SLC39A8-Ala391 variant is associated with lower cell proliferation in HEK293 and HUVECs

In the CellTiter 96 AQ_{ueous} One solution cell proliferation assay (MTS), a low dose of Cd^{2+} (1μM) showed varied cell proliferation patterns depending on the experimental condition. The number of proliferative (viable) cells was lower in Ala391 variant overexpressing cells, comparing to Thr391. However in HUVECs, cell proliferation seemed to be increased after 2h or 24h of $CdCl_2$ incubation, with lower proliferation rate seen at 24h (Fig. 3.19 B). In HEK293 cells transfected with pCDNA-SLC39A8-Ala/Thr391 plasmids, both 2h and 24h $CdCl_2$ incubation decreased the cell proliferation comparing to no Cd^{2+} controls (Fig. 3.19 C&D). Transfection efficiency was checked by immunoblot assay, as shown in Fig. 3.19 A. Cell proliferation rate indicates metabolically active cells, which usually reflects viable cells, but not necessarily. A second cytotoxicity assay is preferred to validate the toxic effect of Cd^{2+}.

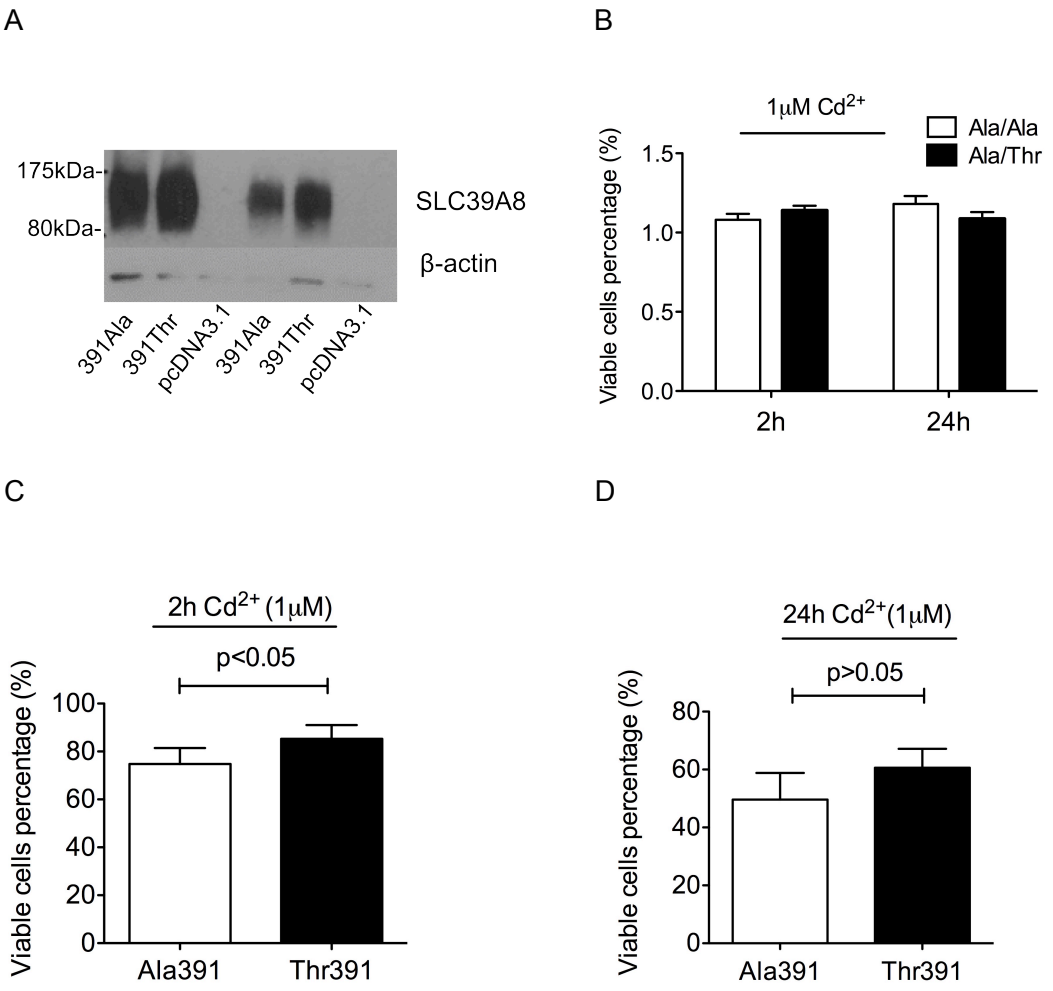

Fig.3.19. CellTiter 96 AQ_{ueous} One Solution cell proliferation assay (MTS). (A) Immunoblot image showing transfection efficiency of pCDNA3.1-SLC39A8-Ala/Thr391 plasmids in HEK293 cells (B) Viable cell percentage in HUVECs of Ala/Ala and Ala/Thr genotype after 2h or 24h of $CdCl_2$ incubation Each value was standardized against vector control. Data are mean (±SEM) of duplicates from 2 experiment (n=4 for each genotype) (C) Viable cell percentage in transfected HEK293 cells after 2h $CdCl_2$ incubation (D) Viable cell percentage in transfected HEK293 cells after 24h $CdCl_2$ incubation**.** Data are mean (±SEM) of duplicates from 4 experiments. Data are calculated by Wilcoxon test.

3.2.8 Real-time qPCR quantification of downstream gene expression regulated by ZIP8-mediated cholesterol efflux

We further investigated the expression levels of cholesterol transporter genes and transcription factors after conducting cholesterol efflux in HepG2 cells. Data were generated from the pooled results from samples treated with HDL_3 and vehicles. There were no major differences between these two groups hence allowing combination of these data. The biggest difference in transcript levels of cholesterol transporters was observed in *ABCA1*. There seemed to be a trend of higher mRNA transcription levels of *ABCA1* and *PPAR-γ* in Thr391 variant than in the Ala391 variant, however the difference between the two variants are not significant. Therefore there is not enough evidence showing preferential upregulation of any of these downstream genes (Fig. 3.20). There was a 5000~15,000-fold change in *SLC39A8* transcript level in the samples transfected with *SLC39A8* expression plasmids. This could be due to a low power in small sample size or true findings. If this was a true finding, apart from the low expression of ABCG1 in HepG2 cells, the major cholesterol transporters ABCA1 and SR-BI have not shown any major transcriptional difference in the cells overexpressing *SLC39A8* of genotypes. This finding can not be expanded to other cell lines, as macrophage and arterial wall efflux are also known to contribute to the overall cholesterol transported by HDL particles. If this was an issue of insufficient power, a more sensitive assay as well as optimitized assay conditions need to be developed. Knocking-down of *SLC39A8* in HepG2 cells might be necessary prior to overexpression to reduce the background signal and to produce a cleaner cut-off point. The Thr391 variant is reported to be associated with lower levels of HDL-C in the GWAS. However recent studies have indicated cholesterol efflux capacity to be a better indicator of carotid intima-media thickness and angiographic coronary artery disease, comparing to HDL-C level.[54] Therefore more robust experiments are required

to fully interpret the lipid GWAS result.

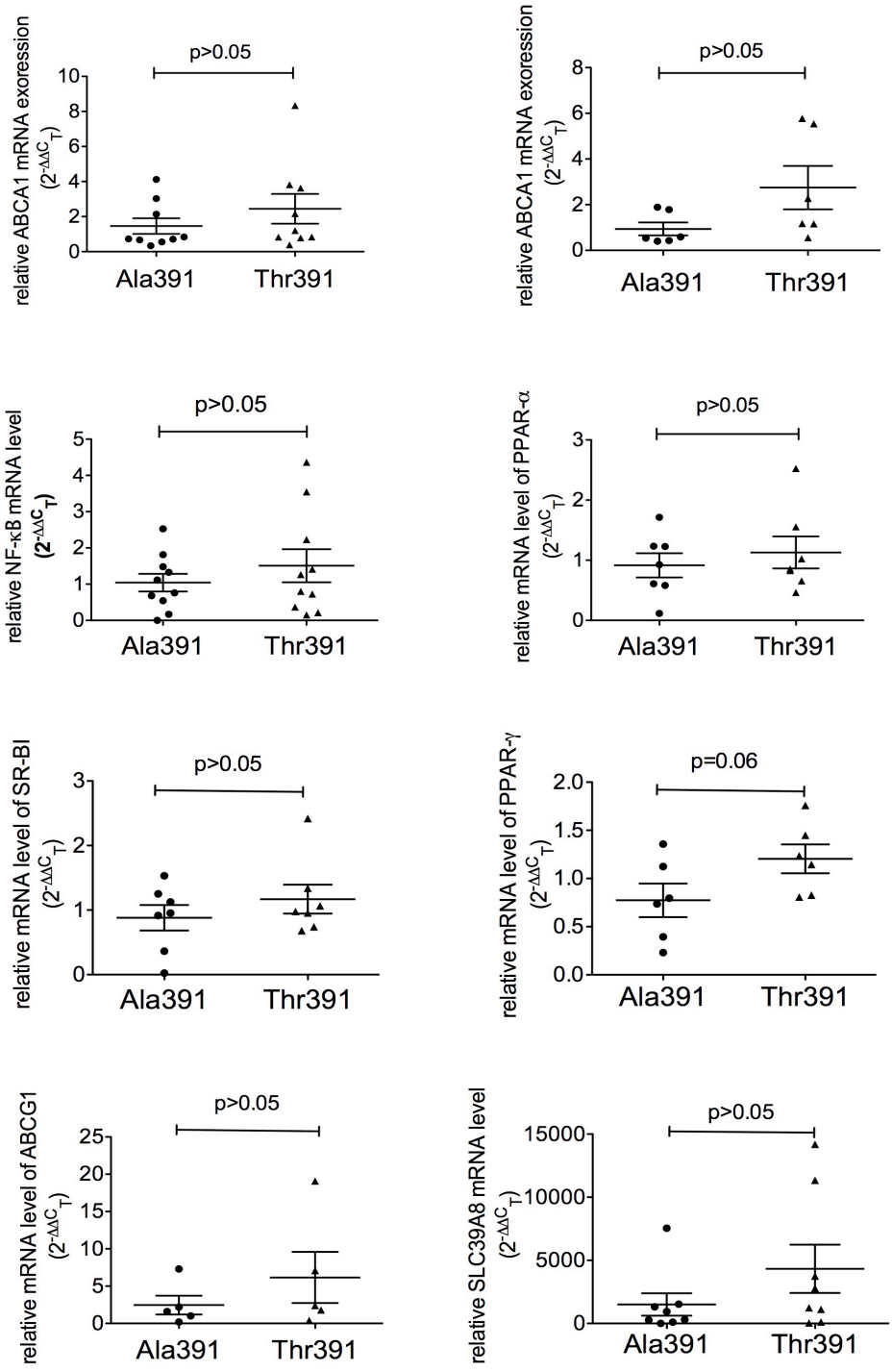

Figure 3.20. Relative mRNA levels of *ABCA1, ABCG1, SR-BI, PPAR-α, PPAR-γ, NF-κB1* in pCDNA-3.1-SLC39A8-Ala/Thr391 transfected HepG2 cells subjected to cholesterol efflux. Each value is relative to the vector control value and was normalized to 18s rRNA. Data are means (± SEM) of one experiment (n≥6 for each

genotype)

3.3 Investigation of effect of rs13107325 on ZIP8 function and structure

3.3.1 Bioinformatics prediction of Ala391Thr on ZIP8 function

An intensive bioinformatics search was conducted to investigate the influence of the Ala391Thr substituiton on ZIP8 funtion. We applied a combination of *in silico* tools and molecular dynamics simulation to predict the structural and functional impact of the missense SNP on activity or stability of the ZIP8 protein. Different algorithms have been used for functional prediction, as listed below (Table 3.1). Out of the 10 algorithmss used, 5 have predicted possible damaging effect, including PolyPhen 2.0, SIFT, SNAP, Panther and iMutant, 5 predicted either neutral or not damaging.

SIFT indicated the amino acid change (Ala391Thr) in all three ZIP8 isoforms could cause a deleterious effect on the protein function. PolyPhe-2 suggested this SNP was benign in two of the isoforms and possibly damaging in the third isoform. Panther also predicted a possible deleterious effect from this SNP on the protein function. iMutant indicated a decrease in protein stability with reliability index of 7. However, SNP&Go and Mutpred both suggested neutral effect for this SNP. Overall, most of the tools predicted a possible change of protein function caused by the Ala391Thr substitution on ZIP8. The transcription factor binding site prediction tool Patch predicted the SNP either created or abolished binding sites of E2F, E2F-4, and E2F-1, whereas P-match predicted possible differences in binding of C-EBP, C/EBP-α, CREB and SP1. Experiments with the use of EMSA (electrophoretic mobility shift assay) and other techniques will be required to test these predictions.

Programs	Prediction result (score)	Notes	Link	Algorithms
SIFT	Deleterious (0.01-0.02)	Damaging, however low confidence	http://sift.jcvi.org	based on evolutionary information
PolyPhen-2	Possibly damaging	Score=0.589 (sensitivity: 0.87; specificity 0.91)	http://genetics.bwh.harvard.edu/pph2/	combine both protein structural/functional parameters and sequence analysis derived information
SNAP	Non-neutral	Expected accuracy 78%	https://www.rostlab.org/services/SNAP/submit	uses *in silico* derived protein information based on the protein sequence
Panther	$P_{deleterious}$= 0.75638	subPSEC=-4.13(<-3 deleterious)	http://pantherdb.org	evolutionary analysis of coding SNPs
iMutant	Protein stability decrease	Reliability index 7.0	http://folding.biofold.org/i-mutant/i-mutant2.0.html	change in structural stability
SNPs&Go	Neutral (6)		http://snps.biofold.org/snps-and-go/pages/method.html	information based on protein sequence
Mutpred	No hypothesis Probability of deleterious=0.147 (>0.5)	Gain of glycosylation at A391 (P = 0.0443) Loss of helix (P = 0.1299) Loss of stability (P = 0.1922) Gain of loop (P = 0.2045) Gain of sheet (P = 0.4423)	http://mutpred.mutdb.org	based upon SIFT, and a gain/loss of 14 different structural and functional properties
dbSNP	not damaging		http://www.snps3d.org/	based on structure and sequence analysis
Pmut analysis from mmb2	neutral		http://mmb.irbbarcelona.org/PMut/	based on neutral networks and sequence/structural information, high success rate for predicting Mendelian's mutations
PROVEAN	neutral		http://provean.jcvi.org/seq_submit.php	based on top 30 clusters of closely related sequences (>75% global sequence identity) to

				generate the prediction

Table 3.1. Bioinformatics predicion of the effect of Ala391Thr variation on ZIP8 function

3.3.2 Bioinformatics prediction of Ala391Thr on ZIP8 structure

Our functional data prompted further bioinformatics investigations into the impact of the Ala391Thr variation on ZIP8 structure. According to TMHMM prediction, in the protein containing the Ala residue at position 391, Ala is packed inside the α-helical transmembrane domain, whereas the Thr residue locates just outside the α-helix domain in the mutant protein sequence (Fig. 3.21 A).

A homology-based 3D protein structure modelling was performed using the Robetta approach. Secondary structure analysis was performed to predict *in silico* the effect of Ala391Thr on the structure and dynamics of ZIP8. This was performed both on the Ala391 containing wild-type ZIP8 protein sequence and the mutant sequence containing Thr. The results revealed a total of 7 α-helical domains for both sequences. A noticeable change was observed at the α-helical structural transition (residues 390-392) in the Thr391 mutant when overlapped with the Ala391 sequence. It is interesting to note that other transmembrane α-helical domain in close proximity with the mutation also shifted their position within the membrane as illustrated in Fig. 3.21 B. We speculate that the conformational transition also resulted in an increased solvent exposure of Thr391, in agreement with the higher hydrophilicity of this residue compared to Ala391.

A

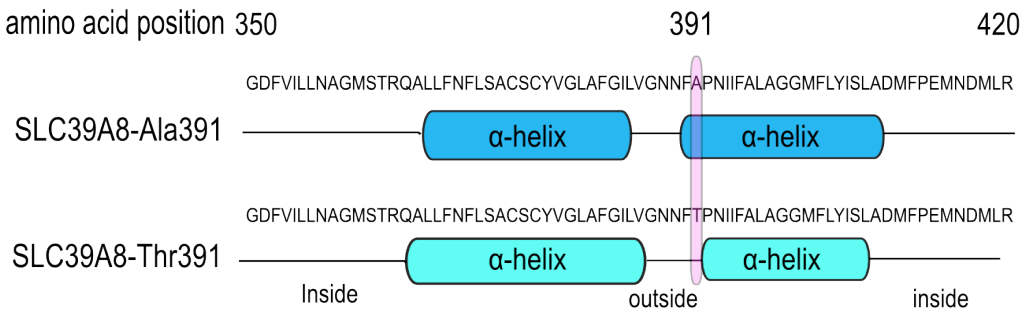

B

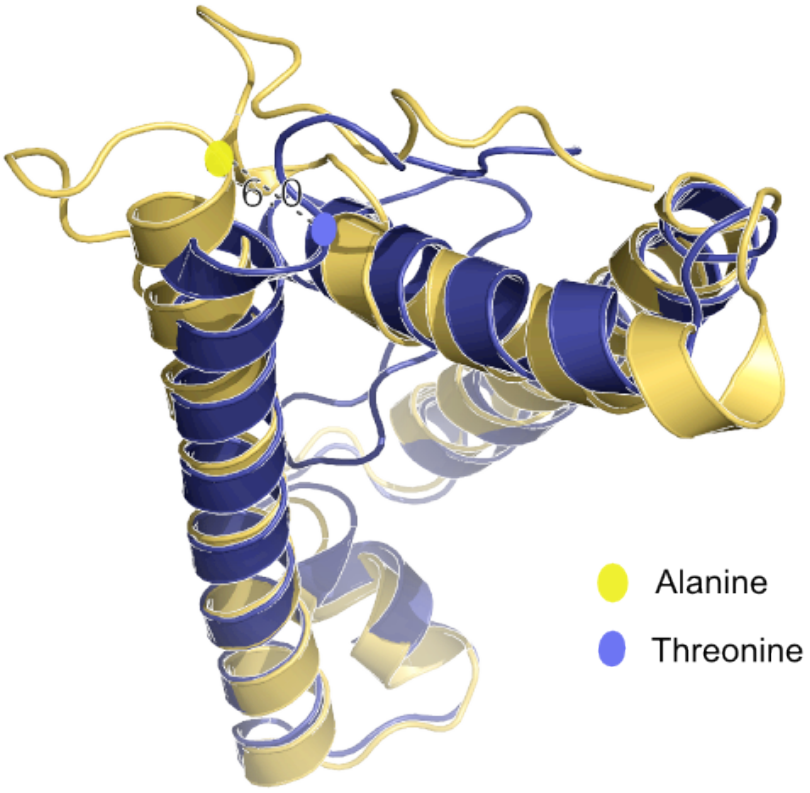

Figure 3.21. Bioinformatics prediction of Ala391Thr variation in relation to ZIP8 protein structure. (A) Graphical interpretation of the transmembrane helical domains predicted by TMHMM (B) Structural perturbation promoted by the Ala391Thr variation as shown by Robetta secondary protein structure prediction. The wild-type protein (Ala391) is displayed in yellow, and the mutatn protein (Thr391) is shown in blue. The image shows an overlapped simulation of the two protein structures. The Thr391 residue (representated by the blue circle) shows a distance of 6Å from the Ala391 residue (represented by the yellow circle).

4. Discussion

Several different GWAS studies have reported association between a non-synonymous SNP (rs13107325, Ala391Thr) in *SLC39A8* and various CVD and non-CVD traits.[22; 57-59] The rare allele T has been associated with lower blood pressure and lower circulating HDL-C. *SLC39A8* is one of the 14 members of the *SLC39* gene family of metal ion transporters, which transport these ions from the cell exterior or lumen of intracellular organelles into the cytoplasm.[69] This gene has not been previously linked with CVD pathogenesis, neither is it involved in any established pathways contributing to the disease. The physiological role of *SLC39A8* remains to be elucidated.

I sought to investigate the possible mechanisms of the association between *SLC39A8* and blood pressure and HDL-C, including the impact of Ala391Thr variation on the expression and function of the gene product.

This study demonstrated the impact of SNP rs13107325 in *SLC39A8*, and the corresponding Ala391Thr substitution on Cd^{2+} accumulation, activation of downstream signalling pathways and cell phenotype. In the latter part of study, the genetic impact of *SLC39A8* on cholesterol efflux was assessed, as well as the downstream regulation of cholesterol transporter proteins. Based on the association of cadmium and cardiovascular disease, this study has provided some potential biological mechanisms for the reported BP GWAS association. The Ala391Thr variation reduced cellular uptake of Cd^{2+}, which may further influence the developmenet of hypertension. It is hoped that these findings will facilitate more advanced studies on development of potential therapeutic target for prevention and treatment of hypertension.

4.1 Genetic investigation of Ala391Thr variation on *SLC39A8* expression

I first conducted gene expression studies to compare the mRNA and protein levels of *SLC39A8* in HUASMC and HUVEC of the C/C (Ala/Ala) and C/T (Ala/Thr) genotypes. A trend of a higher mRNA transcript level for T allele comparing to C allele in HUASMC was observed (n=5) (Section 3.1.2, Fig. 3.2 B), suggesting that T allele is possibly preferentially transcribed over C allele. However at protein level, no significant difference was seen between cells of the Ala/Thr and Ala/Ala genotype in HUASMCs or HUVECs. The result is not statistically significant potentially due to the limited sample size for the heterozygous genotype, and the absence of rare homozygote genotype in both the HUASMC and HUVEC samples. A power calculation estimated a sample size of approximately 565 to obtain one rare homozygote (rare allele frequency: 0.15, α error: 0.05, power: 0.95), which is more than double the size of our current dataset. The trend was not seen in HUVECs which had an even smaller sample size for each genotype, in which the direction of effect, if any, was unclear. Immunoblotting of four protein sub-fractions revealed a difference in cell localization and post-translational modification of ZIP8 in different cell compartments, for instance the most modified form (possibly glycosylation) of ZIP8 was seen in the cytosolic fraction. The appearance of multiple bands detected in each fraction suggests co-existence of various multimers. All the bands can be reduced by a ZIP8 specific blocking peptide to different extent, which suggest the specificity of these bands.

The potential mechanism of how exonic SNP might affect gene expression can be explained by two points: one is through the alternative splicing of the transcript. The polymorphic site is within a common region for all three transcripts of *SLC39A8*, therefore this SNP is unlikely to affect splicing; the second is through the change of transcription factor (TF) binding sites which can sometimes occur at highly conserved

genomic regions. Protein-coding DNA have been reported to contain enhancer sequences functioning at the transcriptional level.[225] Based on available ENCODE data, this SNP is not within any conserved transcription factor (TF) binding site, or TF ChIP-seq region, neither is it involved in any epigenetic regulation. The mechanistic evidence supporting the regulation of this exonic SNP on gene regulation is weak.

4.2 *In-vitro* investigation of Ala391Thr variation on ZIP8 function

Cadmium and zinc ions are both reported to be transported by ZIP8, which co-transports 1 molecule of the metal divalent cation with 2 molecules of HCO_3^- in an electroneutral manner. Critical Cd^{2+} concentration in the kidney cortex is 1mM, above which kidney dysfunction appears, such as defective protein, amino acid, glucose, bicarbonate and phosphate reabsorption, a condition similar to features of Fanconi syndrome. The average circulating levels of Cd^{2+} in humans vary because the exposure can be environmental or dietary dependent. In order to determine the experimental dose, we used kinetics study as a reference which suggests a K_m value of 0.62 μM for ZIP8-mediated Cd^{2+} transport in mouse fetal fibroblasts that fits the Michaelis-Menten model. The K_m value is the concentration of Cd^{2+} at which uptake rate is half of V_{max} (maximum uptake rate). A range of 1-10μM of Cd^{2+} has generally been used in the literature. In our assay, a concentration close to the K_m value was used (1μM). The physiological concentration of Zn^{2+} is 18μM, which is the concentration we used in the Zn^{2+} uptake assay.

The Cd^{2+} uptake assay conducted on transfected HEK293 cells and HUVECs showed a higher intracellular accumulation of Cd^{2+} in cells overexpressing the Ala391 variant, and HUVECs of the Ala/Ala genotype after 2h of incubation with 1μM Cd^{2+}.

The significant difference between Ala/Ala and Ala/Thr genotype in HUVECs (Fig. 3.10 D) suggests a potentially cumulative model for the ZIP8-mediated Cd^{2+} transport. Our results suggest that Ala391Thr caused a reduced but not abolished ZIP8 function in Cd^{2+} uptake, as shown by the detectable intracellular Cd^{2+} in the Thr391 variant after adjustment with vector control (Fig. 3.10 C). This could also be due to the endogenous expression of Ala391-containing ZIP8 found in HEKs, which was not readily detectable by immunoblotting, or existence of other endogenous cadmium transporters.

The Zn^{2+} uptake assay in transfected HepG2 cells also demonstrated a higher intracellular accumulation of Zn^{2+} in cells overexpressing the Ala391 variant compared to Thr391 after 2h of Zn^{2+} incubation (Fig. 3.11 B). Although more replications are needed to confirm this finding, this is consistent with the previous Cd^{2+} uptake result on that ZIP8 containing the Thr391 variant attenuates the protein's function of metal ion transport. The association of rs13107325 T allele (Thr391) with lower SBP and DBP by the ICBP-GWAS[30] may be linked with its reduced metal ion transport activity, particularly in Cd^{2+}.

A recent study has reported an association of rs13107325 with blood levels of Mn^{2+} (p=5.1 x 10^{-11}, β= -0.77).[233] ZIP8 was also shown to have a high affinity for Mn^{2+}[234] and may be a preferred transporter in specific tissues or cell types.[73; 235] In mouse kidney proximal tubule cells, Cd^{2+} uptake can be significantly inhibited by 10 times the concentration of Mn^{2+} or Zn^{2+}, whereas Mn^{2+} uptake can only be inhibited by 30 times the concentration of Cd^{2+} or Zn^{2+}. This suggests ZIP8-mediated Cd^{2+} uptake may be inhibited in the presence of Mn^{2+} in certain cell types.[95] There is already some prior knowledge on the association between Mn^{2+} levels and various CVD outcomes, for example, low blood Mn^{2+} has been reported to be associated with renal dysfunction in the cross-sectional general population study in Korea;[236] In the same study, higher Pb^{2+} and Cd^{2+} levels were found in the individuals with renal dysfunction (OR_{Pb} 1.344,

95% CI=1.157-1.162; OR $_{Cd}$ 1.467, 95% CI=1.077-1.999);[237] dietary Mn intake was negatively correlated with DBP, serum cholesterol and triglycerides;[238] in a PM2.5 air pollution study from Beijing, Mn content in the air was associated with a reduction in SBP.[239] Despite the unstandardized measurements in the existing reports, majority of the studies indicated a negative correlation between Mn and unfavourable CVD outcome. Assuming the Ala391Thr variation on *SLC39A8* has a similar effect on Mn^{2+} transport (reduction of Mn^{2+} uptake), the resulting effect is likely to cause adverse CVD outcome (including SBP). Therefore Mn^{2+} is unlikely to be the confounder of the link between Cd^{2+} and blood pressure mediated by ZIP8, although this need to be further validated by the intracellular measurement of Mn^{2+} in ZIP8 expressing cell lines.

In order to assess the inhibitory effect of other divalent metals which may be transported by ZIP8, we searched for relevant evidence in the literature. In RNA-injected Xenopus oocytes, ZIP8 can significantly transport radiolabelled Cd^{2+}, Co^{2+}, Fe^{2+}, Zn^{2+} > Mn^{2+}, but not Cu (I or II).[81] Zn^{2+} was shown to be the best inhibitor of Cd^{2+} influx, whereas Mn^{2+} didn't block the Cd^{2+} influx. In mouse fetal fibroblast cultures stably overexpressing ZIP8 (rvZIP8 cells), Cd^{2+} influx can be competitively inhibited by other divalent metals in the following order: Mn^{2+} > Hg^{2+} >> Pb^{2+} = Cu^{2+} = Zn^{2+} = Cs^{2+}.[95] However competition assays for Cd^{2+} and Zn^{2+} uptake cannot prove absolutely that ZIP8 can transport other metal ions; competitive inhibitors might have blocked the Cd^{2+} or Zn^{2+} uptake via interaction with thiol groups or by plugging up the transport channel.[82] There are limitations to either of these systems in their relevance to the *in vivo* system. Oocytes are not the native cells where the ion channels are normally expressed, therefore it is often difficult to make a direct comparison because the native cells usually contain multiple types of channels. Mouse fetal fibroblasts are probably a better model, however cellular trafficking can be different between mice and humans. Overall, other than Mn^{2+}, the inhibitory effects of other divalent metals on Cd^{2+} uptake seem to be moderate on these cell lines.

4.3 *In-vitro* investigation of Ala391Thr variation on Cd^{2+}-induced signalling pathway activation

Cadmium is a non-essential metal with no known biological functions. The entry of Cd^{2+} into cells have proven to be toxic to many cells, even at lower concentrations (e.g. 0.1-10μM).[232] Cadmium has been shown to activate the mitogen-activated protein kinases (MAPKs) which include ERK, c-Jun N-terminal kinases (JNK) and p38 kinase, albeit showing varied effects in different cell types.[179; 240; 241] ERK is often activated following growth factor stimulation which stimulates cell proliferation, and protecting cells against apoptosis. We have shown in our study that Ala391Thr variation in SLC39A8 causes different levels of activation of the ERK1/2 pathway, particularly at 24h after Cd^{2+} stimulation in HEK293 cells (Fig. 3.14). Recent studies showed sustained activation of ERK can be associated with or at least partly responsible for cell death signalling.[193] A similar trend was seen in HUVECs of Ala/Ala and Ala/Thr genotypes, although the difference was not significant. It is intriguing to note that the strongest phosphorylation of ERK1//2 were found at the 4h time point in HUVECs, but remained elevated after 24h of Cd^{2+} treatment (Fig. 3.15). The reason for this observation may be attributed to the biphasic activation pattern of ERK, with a first peak at 2-6h after M phase, and a second peak at 14-20h, as reported in Chinese hamster ovary cells.[242] The different regulation of ERK signalling may partially contribute to the observed phenotypic difference in different cell lines.

ERK1 and 2 proteins are two kinases with similar identities and regulation mechanisms. Despite their similarities, recent studies have shown some apparent biological differences driven by these two kinases. Functional differences between ERK1 and ERK2 proteins are implicated in zebrafish development, as the two kinases target distinct genes during early embryogenesis and are involved in different

developmental processes.[243] In mice, disruption of the *ERK2* locus led to early embryonic lethality while those lacking in *ERK1* didn't cause death or affect living and reproductive ability; silencing of only *ERK2* slowed down cell proliferation in mouse embryonic fibroblasts.[244] Furthermore, *ERK2* seems to have a positive role in controlling normal and Ras-dependent cell proliferation, whereas *ERK1* may affect the overall signalling output by antagonizing *ERK2* activity.[245] From immunoprecipitation studies with MEK antibodies (shown in Fig. 4.1), in the absence of ERK1, binding of ERK2 to MEK appears slightly but significantly increased.[245] Our data suggests that the effect of Cd-induced MAPK pathway activation is more profound via *ERK2* signalling.

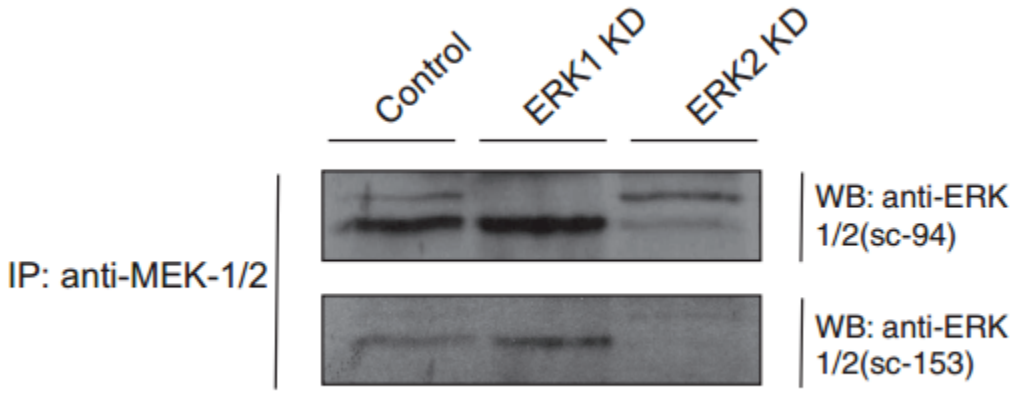

Figure 4.1. ERK-specific gene silencing in NIH 3T3 cells differentially affects MEK-ERK interactions

The other signalling pathway we investigated was NF-κB, which is a prominent factor in the cell death/survival balance. In response to inflammation stimuli, the canonical NF-κB pathway is activated to induce anti-apoptotic and/or survival genes; however other stimuli may result in repression of anti-apoptotic genes and induction of proapoptotic genes. The dominance of either of these processes is dependent on the cell type and nature of the inducing stimulus, which will determine the subsequent

biological events.[208] The majority of *in vitro* and *in vivo* studies suggest Cd^{2+} induces a NF-κB dependent transactivation of oxidative stress genes, anti-apoptotic and protective target genes at concentration range of 10-50 μM for a period of 4-48 hrs.[208]

In my dual luciferase reporter assay, NF-κB activation was detected in transfected HEK293 cells after 2h of exposure to 1μM Cd^{2+} (Fig. 3.16 A), however an inhibitory effect of NF-κB was seen after 24h of Cd^{2+} exposure (Fig. 3.16 B). Oscillation in the temporal response of NF-κB activity has been reported in IκBβ and ε knockout mouse embryonic fibroblast cells, suggesting a dynamic mechanism by period and/or amplitude to regulate transcription of target genes.[246; 247] IκBα was reported to be responsible for the negative feedback mechanisms that allow the turn-off of the NF-κB response. In HEK293 cells transfected with pcDNA3.1-SLC39A8-Ala391/Thr391 plasmids, we have detected a significantly higher activation of NF-κB in cells overexpressing Ala391. Therefore we conclude that Ala391 initiates a higher activation of NF-κB after 2h of Cd^{2+} treatment, with a treatment dose and duration consistent with the previous Cd^{2+} uptake assay and ERK signalling analysis.

A different approach was employed in assessing the Cd-induced NF-κB response in HUVECs, which was immunoblotting of NF-κB effector elements (IκBα, phospho-Ikkα/β, phospho-p65). After 2h incubation with Cd^{2+}, a fluctuation of IκBα signal was seen in HUVECs of either genotypes, the deprivation of serum in the culture did not seem to have any effect on the outcome. At longer time points of 4h and 24h, reduction in both phospho-Ikkα/β and phosphor-p65 were detected compared to basal level, which suggests the effect of Cd^{2+} on NF-κB signalling might be cell type dependent, or treatment dose/length dependent. More comprehensive assessments are needed to rule out the involvement of NF-κB signalling in HUVECs under stimulation of Cd^{2+}.

In summary, in the cells with abundant ZIP8 expressions (HEK293), intracellular accumulation of Cd^{2+} may result in a sustained activation of ERK1/2 kinases, with higher levels of ERK2 in cells expressing Ala391, suggesting the ERK and NF- κB are involved in the cellular response of Cd^{2+} entry which might trigger further regulatory elements that are responsible for the subsequent cell phenotype. However, we do not yet have enough evidence suggesting the cell phenotypic change induced by ZIP8-mediated Cd^{2+} uptake is ERK1/2 or NF-κB dependent in HUVECs.

4.4 *In-vitro* investigation of Ala391Thr variation on HDL_3-mediated cholesterol efflux and regulation of downstream gene expression

The ICBP-GWAS study also reported an association between Ala391Thr and HDL-C.[57] HDL particles are critical acceptors of cholesterol from lipid-laden macrophages, and HDL-C levels have been found to be inversely related to CHD risk.[248] Some of the attributes of HDL in mitigating CHD risk include mediating cholesterol efflux, promoting nitric oxide production, and having anti-inflammatory properties.[249] We aimed to investigate the possible involvement of ZIP8 in cholesterol efflux pathways, possibly through its ability of transporting Zn^{2+}.

HDL is highly heterogeneous in size and composition. Approximately 65% of the HDL protein mass is apoA-I with 12-15% apoA-II.[250] HDL_3 is the small-medium sub-fraction of HDL with a density of 1120-1180 g/ml. HDL_3 has been shown to be an efficient cholesterol acceptor with high portion of apolipoprotein A (apoA) I-II.[47] ATP-binding cassette (ABC) transporters are the main mediators of cholesterol efflux from cells to apoA-I and HDL.[251] ABCA1 deficiency causes both Tangier disease and familial HDL deficiency, two pathologies characterized by very low levels of plasma HDL.[252] The expression of *ABCA1* has been reported to be induced by peroxisome

proliferator-activated receptor γ (*PPAR-γ*) activators through a possible upregulation of liver-x-receptor α.[253] The potential role of ZIP8 in these observations warranted further study with an improved cell model. Recent studies pointed out that circulating HDL-C levels being an inadequate measurement for CVD risk,[54] supported by failures in the clinical trials of HDL increasing drugs (i.e. nicotinic acid and fibric acid derivatives). HDL-C fractions or cholesterol efflux capacity may appear to be a more precise metric associated with the CVD outcome considering the heterogeneous functions of HDL *in vivo*. Overexpression of ZIP8 on HepG2 cells has significantly promoted cholesterol efflux over a period of 4h, however the difference between Ala391 and Thr391 can be differentially interpreted with or without adjustment for transfection efficiency (Fig. 3.13). The high level of transfection efficiency together with endogenous ZIP8 expression may have confounded the results and masked any potential net difference between the two alleles. Studies in HUVECs have been aborted due to the lack of samples with the rare allele genotype. Therefore it is not clear at this stage whether the Ala391Thr variation on SLC39A8 have any influence on HDL_3-mediated cholesterol efflux.

The enhanced cholesterol efflux by overexpressing ZIP8 prompted further investigation into the study of downstream gene expression by real-time qPCR, including key cholesterol transporters, i.e. *ABCA1*, *ABCG1*, *SR-BI*, and transcription factors i.e. *PPAR-α*, *PPAR-γ* and *NF-κB*. There was a trend towards increased transcription levels of *ABCA1* and *PPAR-γ* in cells overexpressing the Thr391 variant (Fig. 3.20), however no major difference between the Ala391 and Thr391 variants was seen in the expression levels in all the genes tested. These observations may be true, or may be not due to the lack of sensitivity in our experimental design which was not optimal for capturing the differential expression regulation pattern of these genes. We have not developed a method that allows simultaneous measurements of cholesterol efflux, gene expression and intracellular content of Zn^{2+}. Therefore the relationship between Zn^{2+} and cholesterol efflux has not been validated in this study.

4.5 Cadmium-induced cell death mediated by ZIP8

In 1950, the focus of cadmium toxicity was initially on its damage to lungs and kidneys, and subsequently testicles were also identified to be another target organ under low dose cadmium exposure.[254] The WHO identified renal dysfunction as the critical effect of cadmium in the International Program on Chemical Safety.[255] The Cadmibel study including 2327 subjects have reported a 10% probability of tubular dysfunction when UCd reaches 2 μg/day.[256] However the effect of low environmental exposure of Cd on kidney is low as men with UCd and BCd of 7.5 nM and 6.1 nM showed no progressive renal damage. The critical concentration in the organ is defined as the concentration when adverse functional changes, reversible or irreversible, occur in the most sensitive cells of the organ.[257] The critical Cd^{2+} concentration in the kidney cortex is 1mM, above which kidney dysfunction appears.[258] Morphological changes were observed in transfected HEK293 cells under Cd^{2+} treatment (1μM for 24h), compared to a vehicle control. This phenotypic change was accompanied with LDH and MTS cytotoxicity assays showing a higher cytotoxicity in cells transfected with SLC39A8-Ala391 plasmid, compared to SLC39A8-Thr391 (Fig. 3.18). With the same allele being associated with higher blood pressure and higher Cd^{2+} uptake, this phenotypic change may be directly associated with entry of Cd^{2+}. This direct link between Cd^{2+} uptake and cell toxicity has already been established in other cell lines such as hepatocytes and renal tubular MDCK cells.[259; 260] The expression levels of ZIP8 have been shown to be the highest in kidney, lung and testis in mice,[89; 235] which appear to be the main target organs for Cd toxicity. It is postulated that ZIP8 may play a critical role in Cd-induced cell death and dysfunction in these organs, which remains to be proven in future experiments.

The vascular endothelium system has also emerged to be a main target of Cd^{2+} toxicity for both acute injury and disease progression.[261] Cadmium can exert its toxicity

to the vascular endothelium through direct vasoconstriction and inhibition of nitric oxide,[262] peroxidation of membrane lipids,[263] inhibition of tube formation,[264] increase of endothelial permeability and other endothelial dysfunction.[261] These actions can lead to the initiation and promotion of atherosclerosis. This is supported by the epidemiological observation of higher frequencies of atherosclerosis in a Cd-contaminated area in the Netherlands.[141] Additionally, Cd^{2+} level has been observed to be independently associated with early atherosclerotic vessel wall thickening in healthy female individuals.[265] With experimental studies, Cd-fed $apoE^{-/-}$ mice showed a marked increase in plaque area with upregulation of VCAM-1 and Hsp60, and endothelial leakage.[125] In line with the allele encoding Thr391 being associated with lower blood pressure, our findings in HUVECs identified cell of the Ala/Thr genotype having a lower Cd^{2+} uptake and Cd^{2+}-induced cell death when compared to cells of the Ala/Ala genotype. These morphology and viability changes may alleviate the toxicity of Cd^{2+} and restore normal endothelial function.

We have not been able to distinguish the type of cell death in this study, whether being apoptosis or necrosis. Expression of apoptotic marker (cleaved form of caspase-3) and anti-apoptotic marker Bcl-2 expression were assessed in cells treated with Cd^{2+} of various concentrations and durations by immunoblotting. The cleaved caspase-3 signal was not detected after various designated Cd^{2+} treatment, and similar levels of Bcl-2 expression were in the two groups of different genotypes. A time course study is required in the future as caspase-3 activity may peak at different time-points depending on cell type. It is too early to conclude the type of cell death yielded by Cd is non-apoptotic.

4.6 Bioinformatics investigation of Ala391Thr variation on ZIP8 secondary structure

In a study on nonsynonymous SNPs in the proteins for which structures were known, 45% of the missense variants were mapped to structurally and functionally important regions, suggesting that a large fraction of nonsynonymous SNPs can affect the encoded proteins.[266] Conservation analysis revealed a high degree of conservation of the Ala391 amino acid among known homologues (Fig. 1.3 D). The degree to which amino acid position is evolutionarily conserved, is strongly dependent on its structural and functional importance. This missense substitution has a high possibility of causing a deleterious effect on the protein function.

Various algorithms such as Robetta, Uniprot and TMHMM Server V.2.0 have all predicted 7 transmembrane domains (α-helices) within the ZIP8 protein. According to Robetta's predicted configuration, α-helix 6 undergoes a conformational change that corresponds to the substitution of the amino acid (AA) 391 (Fig. 3.21 B). The substitution from a hydrophobic amino acid (Ala) to a hydrophilic polar amino acid (Thr) may change the position of the amino acid across the phospholipid bilayers of the cell membrane. The non-polar AAs cause proteins to be embedded in the membrane while polar AAs cause portions of the proteins to protrude from the membrane. Some polar AAs are also found inside membranes and create a channel through which hydrophilic molecules can pass through. Most transporters have a single substrate binding site with activity following the Michaelis-Menten kinetics.[267] My *in vitro* results on Cd^{2+} transport warrants further study on the ZIP8 structure-function relationships by the study of specific sequence for substrate recognition, to investigate whether the Ala391Thr is directly involved in specific interaction with the substrate transport.

. The prediction of the secondary structure was based on protein homologues with a known structure. The fundamental pitfall in homology modelling is that the differences between the target and template will reduce the accuracy of the model. Therefore the quality of the resulting model primarily depends on the sequence similarity between the template and target.[268] The sequence similarity between the template and the known homologue is around 28%.

4.7 Alternative approach and future work

Looking back on this project, there are a few areas which can be improved. Along with the study of Zn^{2+} and Cd^{2+} uptake mediated by ZIP8, the uptake of other metal ions (i.e. Mn^{2+}, Fe^{2+}) could also have been investigated. A universal approach such as inductively coupled plasma mass spectrometry (ICP-MS) may be ideal for the detection of the majority of the trace metals in the cells. With regards to the lack of primary cells with the rare genotype (Thr/Thr), the recent launch of CRISPR-CAS9 technology will be able to overcome this limitation by editing the genome to introduce single nucleotide mutation in the desired cell lines. The results generated from primary cells with endogenous Thr/Thr genotype would complement our functional experiments on the overexpression system.

There are certain limitations to this study as cell lines do not always mimic the behaviour of primary cells, therefore it is crucial to validate our findings *in vivo*. To our knowledge, the global *SLC39A8(-/-)* knockout mice was prone to be early embryonic-lethal, and died between 48 hours postnatal and gestational day 18.5.[83] It is therefore impossible to test whether mice lacking *SLC39A8* will develop a hypertension phenotype over time. Other models with either knockdown or knock-in of *SLC39A8* can be used in the future to study the relationship between long term Cd exposure and the

development of hypertension. [33; 269]

5. Summary

This study characterised the functional impact of SNP rs13107325 in *SLC39A8* leading to the subsequent Ala391Thr substitution in the gene product, in particular the effect of ZIP8-mediated Cd^{2+} accumulation, downstream activation of the signalling pathways and cell behaviour. A genetic difference was observed in both the overexpression system as well as the primary cells, although the majority of the pathway activities was more apparent in the transfected HEK293 cells. The phenotype difference was more likely to be caused by change in protein function rather than gene expression, given that the evidence gained on the effect of the Ala391Thr variation on gene expression was inconclusive.

Bioinformatics analysis further supported the hypothesis that Ala391Thr substitution induced structural changes on the protein, specifically through a shift of the transmembrane α-helical domain, changing the biochemical properties of the exposed residues. High conservation degree of Ala391 on ZIP8 suggests its importance for the correct protein function. Further advances in structural biology for membrane proteins will be necessary before further details on these changes can be reliably assessed.

Epidemiologically, high levels of cadmium were found to be associated with numerous adverse cardiovascular effects such as hypertension, atherosclerosis, abnormal cardiac function, myocardial infarction, and peripheral arterial disease.[116; 141; 143; 270] Chronic Cd^{2+} exposure is associated with HTN in animal models,[148] although this relationship is somewhat inconclusive in humans.[116; 127; 133] Conflicting findings call for

future studies for the genetic mechanisms underlying these observations/ interactions. Most of these studies have focused on the relationship between extracellular levels (blood and urine) of Cd^{2+} and blood pressure, however the impact of intracellular Cd^{2+} content has not been investigated on the population level. The findings in this study may prompt more investigations to assess the tissue specific accumulation of Cd^{2+} in the general population in relationship to BP.

This study advances our understanding of the genetic impact on the protein function of ZIP8 in metal ion transport, and provides preliminary mechanistic investigations into the GWAS association. Although the precise mechanism for Cd^{2+} as a risk factor for CVD remains unresolved, it does provide functional characterization of a BP associated non-synonymous SNP within *SLC39A8*. Pharmacological inhibition of SLC39A8 may be of benefit to the risk allele-bearing individuals, particularly if heavy metal exposure was present in the surrounding environment. However, given the small effect size of common hypertension-associated variants, the therapeutic benefit gained from one biological target may be moderate. In that context it is important to note that even a 2 mmHg lowering of SBP result in 10% lower stroke mortality and about 7% lower mortality from IHD or other vascular causes in middle aged people (40-69 years old).[6] Therefore producing persistent reduction in BP of even just a few mmHg will have a large impact on the general population in preventing hypertension related events like stroke or IHD. The knowledge gained from our study may encourage and facilitate the development of novel therapeutic interventions with stratified healthcare potential.

Reference

1. WHO. (2015). Cardiovascular diseases (CVDs) Fact sheet No. 317.
2. Kearney, P.M., Whelton, M., Reynolds, K., Muntner, P., Whelton, P.K., and He, J. (2005). Global burden of hypertension: analysis of worldwide data. Lancet 365, 217-223.
3. Lim, S.S., Vos, T., Flaxman, A.D., Danaei, G., Shibuya, K., Adair-Rohani, H., Amann, M., Anderson, H.R., Andrews, K.G., Aryee, M., et al. (2012). A comparative risk assessment of burden of disease and injury attributable to 67 risk factors and risk factor clusters in 21 regions, 1990-2010: a systematic analysis for the Global Burden of Disease Study 2010. Lancet 380, 2224-2260.
4. Mendis S, P.P., Norrving B. (2011). Global Atlas on cardiovascular disease prevention and controls. In. (Geneva, World Health Organization.
5. WHO. (2013). A global brief on hypertension In. (WHO press
6. Lewington, S., Clarke, R., Qizilbash, N., Peto, R., Collins, R., and Prospective Studies, C. (2002). Age-specific relevance of usual blood pressure to vascular mortality: a meta-analysis of individual data for one million adults in 61 prospective studies. Lancet 360, 1903-1913.
7. Vasan, R.S., Larson, M.G., Leip, E.P., Evans, J.C., O'Donnell, C.J., Kannel, W.B., and Levy, D. (2001). Impact of high-normal blood pressure on the risk of cardiovascular disease. The New England journal of medicine 345, 1291-1297.
8. Berry, J.D., Dyer, A., Cai, X., Garside, D.B., Ning, H., Thomas, A., Greenland, P., Van Horn, L., Tracy, R.P., and Lloyd-Jones, D.M. Lifetime risks of cardiovascular disease. The New England journal of medicine 366, 321-329.
9. Lawes, C.M., Bennett, D.A., Feigin, V.L., and Rodgers, A. (2004). Blood pressure and stroke: an overview of published reviews. Stroke 35, 1024.
10. Mayet, J., and Hughes, A. (2003). Cardiac and vascular pathophysiology in hypertension. Heart 89, 1104-1109.
11. Swales, J.D. (1994). Textbook of hypertension.(Oxford ; Boston: Blackwell Scientific Publications).
12. Carretero, O.A., and Oparil, S. (2000). Essential hypertension. Part I: definition and etiology. Circulation 101, 329-335.
13. Carretero, O., and Oparil, S. (2000). Essential hypertension. Part I: definition and etiology. Circulation 101, 329-335.
14. Banegas, J.R., Lopez-Garcia, E., Dallongeville, J., Guallar, E., Halcox, J.P., Borghi, C., Masso-Gonzalez, E.L., Jimenez, F.J., Perk, J., Steg, P.G., et al. (2011). Achievement of treatment goals for primary prevention of cardiovascular disease in clinical practice across Europe: the EURIKA study. Eur Heart J 32, 2143-2152.
15. Havlik, R.J., Garrison, R.J., Feinleib, M., Kannel, W.B., Castelli, W.P., and McNamara, P.M. (1979). Blood pressure aggregation in families. American journal of epidemiology 110, 304-312.
16. Williams, R.R., Hunt, S.C., Hopkins, P.N., Wu, L.L., Hasstedt, S.J., Berry, T.D., Barlow, G.K., Stults, B.M., Schumacher, M.C., Ludwig, E.H., et al. (1993). Genetic basis of familial dyslipidemia and hypertension: 15-year results from Utah. Am J Hypertens 6, 319S-327S.
17. Altm √ º ller, J., Palmer, L., Fischer, G., Scherb, H., and Wjst, M. (2001). Genomewide scans of complex human diseases: true linkage is hard to find. American journal of human genetics 69, 936-950.
18. Cowley, A.W., Jr. (2006). The genetic dissection of essential hypertension. Nature reviews Genetics 7, 829-840.
19. Lifton, R.P., Gharavi, A.G., and Geller, D.S. (2001). Molecular mechanisms of human hypertension. Cell 104, 545-556.
20. Lifton, R.P., Dluhy, R.G., Powers, M., Rich, G.M., Gutkin, M., Fallo, F., Gill, J.R., Jr., Feld, L., Ganguly, A., Laidlaw, J.C., et al. (1992). Hereditary hypertension caused by chimaeric gene duplications and ectopic expression of aldosterone synthase. Nature genetics 2, 66-74.
21. Shimkets, R.A., Warnock, D.G., Bositis, C.M., Nelson-Williams, C., Hansson, J.H., Schambelan, M., Gill, J.R., Jr., Ulick, S., Milora, R.V., Findling, J.W., et al. (1994). Liddle's syndrome: heritable human hypertension caused by mutations in the beta subunit of the epithelial sodium channel. Cell 79, 407-414.

22. Ehret, G.B. Genome-wide association studies: contribution of genomics to understanding blood pressure and essential hypertension. Curr Hypertens Rep 12, 17-25.
23. Newton-Cheh, C., Larson, M.G., Vasan, R.S., Levy, D., Bloch, K.D., Surti, A., Guiducci, C., Kathiresan, S., Benjamin, E.J., Struck, J., et al. (2009). Association of common variants in NPPA and NPPB with circulating natriuretic peptides and blood pressure. Nature genetics 41, 348-353.
24. Hirschhorn, J.N., Lohmueller, K., Byrne, E., and Hirschhorn, K. (2002). A comprehensive review of genetic association studies. Genetics in medicine : official journal of the American College of Medical Genetics 4, 45-61.
25. (2004). Integrating ethics and science in the International HapMap Project. Nature reviews Genetics 5, 467-475.
26. Wellcome Trust Case Control, C. (2007). Genome-wide association study of 14,000 cases of seven common diseases and 3,000 shared controls. Nature 447, 661-678.
27. International Consortium for Blood Pressure Genome-Wide Association, S., Ehret, G.B., Munroe, P.B., Rice, K.M., Bochud, M., Johnson, A.D., Chasman, D.I., Smith, A.V., Tobin, M.D., Verwoert, G.C., et al. (2011). Genetic variants in novel pathways influence blood pressure and cardiovascular disease risk. Nature 478, 103-109.
28. Hong, E.P., and Park, J.W. (2012). Sample size and statistical power calculation in genetic association studies. Genomics Inform 10, 117-122.
29. Patel, R.S., and Ye, S. (2011). Genetic determinants of coronary heart disease: new discoveries and insights from genome-wide association studies. Heart 97, 1463-1473.
30. Ehret, G.B., Munroe, P.B., Rice, K.M., Bochud, M., Johnson, A.D., Chasman, D.I., Smith, A.V., Tobin, M.D., Verwoert, G.C., Hwang, S.J., et al. Genetic variants in novel pathways influence blood pressure and cardiovascular disease risk. Nature 478, 103-109.
31. Newton-Cheh, C., Johnson, T., Gateva, V., Tobin, M.D., Bochud, M., Coin, L., Najjar, S.S., Zhao, J.H., Heath, S.C., Eyheramendy, S., et al. (2009). Genome-wide association study identifies eight loci associated with blood pressure. Nat Genet 41, 666-676.
32. Dean, M. (2003). Approaches to identify genes for complex human diseases: lessons from Mendelian disorders. Hum Mutat 22, 261-274.
33. Manolio, T.A., Collins, F.S., Cox, N.J., Goldstein, D.B., Hindorff, L.A., Hunter, D.J., McCarthy, M.I., Ramos, E.M., Cardon, L.R., Chakravarti, A., et al. (2009). Finding the missing heritability of complex diseases. Nature 461, 747-753.
34. Wang, X., and Snieder, H. (2010). Genome-wide association studies and beyond: what's next in blood pressure genetics? Hypertension 56, 1035-1037.
35. (2013). The Atlas of Heart Disease and Stroke. In. (
36. Mackay, J.a.M., G.A. (2004). The atlas of Heart disease and stroke (World Health Organization, Geneva, 2004).
37. Libby, P., and Theroux, P. (2005). Pathophysiology of coronary artery disease. Circulation 111, 3481-3488.
38. Fuster, V., Badimon, L., Badimon, J., and Chesebro, J. (1992). The pathogenesis of coronary artery disease and the acute coronary syndromes (1). The New England journal of medicine 326, 242-250.
39. Maldonado, N., Kelly-Arnold, A., Vengrenyuk, Y., Laudier, D., Fallon, J., Virmani, R., Cardoso, L., and Weinbaum, S. (2012). A mechanistic analysis of the role of microcalcifications in atherosclerotic plaque stability: potential implications for plaque rupture. American journal of physiology Heart and circulatory physiology 303, 28.
40. Law, M., Wald, N., and Rudnicka, A. (2003). Quantifying effect of statins on low density lipoprotein cholesterol, ischaemic heart disease, and stroke: systematic review and meta-analysis. BMJ (Clinical research ed) 326, 1423.
41. Clarke, R., Emberson, J., Parish, S., Palmer, A., Shipley, M., Linksted, P., Sherliker, P., Clark, S., Armitage, J., Fletcher, A., et al. (2007). Cholesterol fractions and apolipoproteins as risk factors for heart disease mortality in older men. Archives of internal medicine 167, 1373-1378.
42. Gotto, A.M., Jr., and Brinton, E.A. (2004). Assessing low levels of high-density lipoprotein cholesterol as a risk factor in coronary heart disease: a working group report and update. Journal of the American College of Cardiology 43, 717-724.
43. Libby, P. (2001). Current concepts of the pathogenesis of the acute coronary syndromes. Circulation 104, 365-372.
44. Barter, P.J., Caulfield, M., Eriksson, M., Grundy, S.M., Kastelein, J.J., Komajda, M., Lopez-Sendon, J.,

Mosca, L., Tardif, J.C., Waters, D.D., et al. (2007). Effects of torcetrapib in patients at high risk for coronary events. The New England journal of medicine 357, 2109-2122.
45. Schwartz, G.G., Olsson, A.G., Abt, M., Ballantyne, C.M., Barter, P.J., Brumm, J., Chaitman, B.R., Holme, I.M., Kallend, D., Leiter, L.A., et al. (2012). Effects of dalcetrapib in patients with a recent acute coronary syndrome. The New England journal of medicine 367, 2089-2099.
46. Genest, J. HDL, Atherosclerosis and Emerging Therapies.
47. Fang, L., Choi, S.-H., Baek, J., Liu, C., Almazan, F., Ulrich, F., Wiesner, P., Taleb, A., Deer, E., Pattison, J., et al. (2013). Control of angiogenesis by AIBP-mediated cholesterol efflux. Nature 498, 118-122.
48. Glomset, J.A. (1968). The plasma lecithins:cholesterol acyltransferase reaction. Journal of lipid research 9, 155-167.
49. Zhang, J., Cai, S., Peterson, B., Kris-Etherton, P., and Heuvel, J. (2011). Development of a cell-based, high-throughput screening assay for cholesterol efflux using a fluorescent mimic of cholesterol. Assay and drug development technologies 9, 136-146.
50. Low, H., Hoang, A., and Sviridov, D. (2012). Cholesterol efflux assay. Journal of visualized experiments : JoVE, e3810.
51. Yvan-Charvet, L., Wang, N., and Tall, A.R. (2010). Role of HDL, ABCA1, and ABCG1 transporters in cholesterol efflux and immune responses. Arterioscler Thromb Vasc Biol 30, 139-143.
52. Phillips, M.C. (2014). Molecular mechanisms of cellular cholesterol efflux. J Biol Chem 289, 24020-24029.
53. Noguchi, T., Yamada, N., Higashi, M., Goto, Y., and Naito, H. (2011). High-intensity signals in carotid plaques on T1-weighted magnetic resonance imaging predict coronary events in patients with coronary artery disease. Journal of the American College of Cardiology 58, 416-422.
54. Khera, A.V., Cuchel, M., de la Llera-Moya, M., Rodrigues, A., Burke, M.F., Jafri, K., French, B.C., Phillips, J.A., Mucksavage, M.L., Wilensky, R.L., et al. (2011). Cholesterol efflux capacity, high-density lipoprotein function, and atherosclerosis. The New England journal of medicine 364, 127-135.
55. Kitsios, G.D., Dahabreh, I.J., Trikalinos, T.A., Schmid, C.H., Huggins, G.S., and Kent, D.M. (2011). Heterogeneity of the phenotypic definition of coronary artery disease and its impact on genetic association studies. Circulation Cardiovascular genetics 4, 58-67.
56. Consortium, C.A.D., Deloukas, P., Kanoni, S., Willenborg, C., Farrall, M., Assimes, T., Thompson, J., Ingelsson, E., Saleheen, D., Erdmann, J., et al. (2013). Large-scale association analysis identifies new risk loci for coronary artery disease. Nature genetics 45, 25-33.
57. Waterworth, D.M., Ricketts, S.L., Song, K., Chen, L., Zhao, J.H., Ripatti, S., Aulchenko, Y.S., Zhang, W., Yuan, X., Lim, N., et al. Genetic variants influencing circulating lipid levels and risk of coronary artery disease. Arterioscler Thromb Vasc Biol 30, 2264-2276.
58. Carrera, N., Arrojo, M., Sanjuan, J., Ramos-Rios, R., Paz, E., Suarez-Rama, J.J., Paramo, M., Agra, S., Brenlla, J., Martinez, S., et al. Association study of nonsynonymous single nucleotide polymorphisms in schizophrenia. Biol Psychiatry 71, 169-177.
59. Speliotes, E.K., Willer, C.J., Berndt, S.I., Monda, K.L., Thorleifsson, G., Jackson, A.U., Allen, H.L., Lindgren, C.M., Luan, J., Magi, R., et al. Association analyses of 249,796 individuals reveal 18 new loci associated with body mass index. Nat Genet 42, 937-948.
60. Solovieff, N., Cotsapas, C., Lee, P.H., Purcell, S.M., and Smoller, J.W. (2013). Pleiotropy in complex traits: challenges and strategies. Nature reviews Genetics 14, 483-495.
61. Pritchard, J.K., and Przeworski, M. (2001). Linkage disequilibrium in humans: models and data. American journal of human genetics 69, 1-14.
62. Girijashanker, K., He, L., Soleimani, M., Reed, J.M., Li, H., Liu, Z., Wang, B., Dalton, T.P., and Nebert, D.W. (2008). Slc39a14 gene encodes ZIP14, a metal/bicarbonate symporter: similarities to the ZIP8 transporter. Mol Pharmacol 73, 1413-1423.
63. Taylor, K.M., and Nicholson, R.I. (2003). The LZT proteins; the LIV-1 subfamily of zinc transporters. Biochim Biophys Acta 1611, 16-30.
64. Guo, L., Deshmukh, H., Lu, R., Vidal, G.S., Kelly, J.A., Kaufman, K.M., Dominguez, N., Klein, W., Kim-Howard, X., Bruner, G.R., et al. (2009). Replication of the BANK1 genetic association with systemic lupus erythematosus in a European-derived population. Genes Immun 10, 531-538.
65. Trott, D.W., and Harrison, D.G. (2014). The immune system in hypertension. Adv Physiol Educ 38, 20-24.
66. LaMarca, B., Wallace, K., Herse, F., Wallukat, G., Martin, J.N., Jr., Weimer, A., and Dechend, R. (2011).

Hypertension in response to placental ischemia during pregnancy: role of B lymphocytes. Hypertension 57, 865-871.
67. Garret Powell, J.K. ChemWiki: Membrane transport
68. Wang, C.Y., Jenkitkasemwong, S., Duarte, S., Sparkman, B.K., Shawki, A., Mackenzie, B., and Knutson, M.D. (2012). ZIP8 is an iron and zinc transporter whose cell-surface expression is up-regulated by cellular iron loading. The Journal of biological chemistry 287, 34032-34043.
69. Eide, D.J. (2004). The SLC39 family of metal ion transporters. Pflugers Archiv : European journal of physiology 447, 796-800.
70. Girijashanker, K., He, L., Soleimani, M., Reed, J., Li, H., Liu, Z., Wang, B., Dalton, T., and Nebert, D. (2008). Slc39a14 gene encodes ZIP14, a metal/bicarbonate symporter: similarities to the ZIP8 transporter. Molecular pharmacology 73, 1413-1423.
71. Ryu, M.S., Lichten, L.A., Liuzzi, J.P., and Cousins, R.J. (2008). Zinc transporters ZnT1 (Slc30a1), Zip8 (Slc39a8), and Zip10 (Slc39a10) in mouse red blood cells are differentially regulated during erythroid development and by dietary zinc deficiency. J Nutr 138, 2076-2083.
72. Taylor, K.M., Morgan, H.E., Smart, K., Zahari, N.M., Pumford, S., Ellis, I.O., Robertson, J.F., and Nicholson, R.I. (2007). The emerging role of the LIV-1 subfamily of zinc transporters in breast cancer. Mol Med 13, 396-406.
73. He, L., Girijashanker, K., Dalton, T.P., Reed, J., Li, H., Soleimani, M., and Nebert, D.W. (2006). ZIP8, member of the solute-carrier-39 (SLC39) metal-transporter family: characterization of transporter properties. Mol Pharmacol 70, 171-180.
74. Aydemir, T.B., Liuzzi, J.P., McClellan, S., and Cousins, R.J. (2009). Zinc transporter ZIP8 (SLC39A8) and zinc influence IFN-gamma expression in activated human T cells. J Leukoc Biol 86, 337-348.
75. Liu, Z., Li, H., Soleimani, M., Girijashanker, K., Reed, J., He, L., Dalton, T., and Nebert, D. (2008). Cd2+ versus Zn2+ uptake by the ZIP8 HCO3--dependent symporter: kinetics, electrogenicity and trafficking. Biochemical and biophysical research communications 365, 814-820.
76. Besecker, B., Bao, S., Bohacova, B., Papp, A., Sadee, W., and Knoell, D.L. (2008). The human zinc transporter SLC39A8 (Zip8) is critical in zinc-mediated cytoprotection in lung epithelia. Am J Physiol Lung Cell Mol Physiol 294, L1127-1136.
77. Aiba, I., Hossain, A., and Kuo, M.T. (2008). Elevated GSH level increases cadmium resistance through down-regulation of Sp1-dependent expression of the cadmium transporter ZIP8. Mol Pharmacol 74, 823-833.
78. Begum, N., Kobayashi, M., Moriwaki, Y., Matsumoto, M., Toyoshima, K., and Seya, T. (2002). Mycobacterium bovis BCG cell wall and lipopolysaccharide induce a novel gene, BIGM103, encoding a 7-TM protein: identification of a new protein family having Zn-transporter and Zn-metalloprotease signatures. Genomics 80, 630-645.
79. Hooper, N.M. (1994). Families of zinc metalloproteases. FEBS letters 354, 1-6.
80. Taylor, K.M., Morgan, H.E., Smart, K., Zahari, N.M., Pumford, S., Ellis, I.O., Robertson, J.F., and Nicholson, R.I. (2007). The emerging role of the LIV-1 subfamily of zinc transporters in breast cancer. Mol Med 13, 396-406.
81. Wang, C.Y., Jenkitkasemwong, S., Duarte, S., Sparkman, B.K., Shawki, A., Mackenzie, B., and Knutson, M.D. (2012). ZIP8 is an iron and zinc transporter whose cell-surface expression is up-regulated by cellular iron loading. J Biol Chem 287, 34032-34043.
82. Nebert, D.W., Galvez-Peralta, M., Hay, E.B., Li, H., Johansson, E., Yin, C., Wang, B., He, L., and Soleimani, M. (2012). ZIP14 and ZIP8 zinc/bicarbonate symporters in Xenopus oocytes: characterization of metal uptake and inhibition. Metallomics 4, 1218-1225.
83. Galvez-Peralta, M., He, L., Jorge-Nebert, L.F., Wang, B., Miller, M.L., Eppert, B.L., Afton, S., and Nebert, D.W. (2012). ZIP8 zinc transporter: indispensable role for both multiple-organ organogenesis and hematopoiesis in utero. PloS one 7, e36055.
84. He, L., Girijashanker, K., Dalton, T.P., Reed, J., Li, H., Soleimani, M., and Nebert, D.W. (2006). ZIP8, member of the solute-carrier-39 (SLC39) metal-transporter family: characterization of transporter properties. Mol Pharmacol 70, 171-180.
85. Wang, C.-Y., Jenkitkasemwong, S., Duarte, S., Sparkman, B., Shawki, A., Mackenzie, B., and Knutson, M. (2012). ZIP8 is an iron and zinc transporter whose cell-surface expression is up-regulated by cellular iron loading. The Journal of biological chemistry 287, 34032-34043.
86. Zheng, D., Kille, P., Feeney, G.P., Cunningham, P., Handy, R.D., and Hogstrand, C. (2010). Dynamic transcriptomic profiles of zebrafish gills in response to zinc depletion. BMC genomics 11, 548.
87. Aydemir, T.B., Liuzzi, J.P., McClellan, S., and Cousins, R.J. (2009). Zinc transporter ZIP8 (SLC39A8) and

zinc influence IFN-gamma expression in activated human T cells. J Leukoc Biol 86, 337-348.
88. Aydemir, T., Liuzzi, J., McClellan, S., and Cousins, R. (2009). Zinc transporter ZIP8 (SLC39A8) and zinc influence IFN-gamma expression in activated human T cells. Journal of leukocyte biology 86, 337-348.
89. Wang, B., Schneider, S.N., Dragin, N., Girijashanker, K., Dalton, T.P., He, L., Miller, M.L., Stringer, K.F., Soleimani, M., Richardson, D.D., et al. (2007). Enhanced cadmium-induced testicular necrosis and renal proximal tubule damage caused by gene-dose increase in a Slc39a8-transgenic mouse line. American journal of physiology Cell physiology 292, C1523-1535.
90. Uhlen, M., Fagerberg, L., Hallstrom, B.M., Lindskog, C., Oksvold, P., Mardinoglu, A., Sivertsson, A., Kampf, C., Sjostedt, E., Asplund, A., et al. (2015). Proteomics. Tissue-based map of the human proteome. Science 347, 1260419.
91. Besecker, B., Bao, S., Bohacova, B., Papp, A., Sadee, W., and Knoell, D. (2008). The human zinc transporter SLC39A8 (Zip8) is critical in zinc-mediated cytoprotection in lung epithelia. American journal of physiology Lung cellular and molecular physiology 294, 36.
92. Nasim, A.B., Mika, K., Yasuhiro, M., Misako, M., Kumao, T., and Tsukasa, S. (2002). Mycobacterium bovis BCG Cell Wall and Lipopolysaccharide Induce a Novel Gene, BIGM103, Encoding a 7-TM Protein: Identification of a New Protein Family Having Zn-Transporter and Zn-Metalloprotease Signatures. Genomics 80.
93. Liu, M.-J., Bao, S., G √ ° lvez-Peralta, M., Pyle, C., Rudawsky, A., Pavlovicz, R., Killilea, D., Li, C., Nebert, D., Wewers, M., et al. (2013). ZIP8 regulates host defense through zinc-mediated inhibition of NF-ℂ ∫ B. Cell reports 3, 386-400.
94. Fukada, T., and Kambe, T. (2011). Molecular and genetic features of zinc transporters in physiology and pathogenesis. Metallomics : integrated biometal science 3, 662-674.
95. Fujishiro, H., Yano, Y., Takada, Y., Tanihara, M., and Himeno, S. (2012). Roles of ZIP8, ZIP14, and DMT1 in transport of cadmium and manganese in mouse kidney proximal tubule cells. Metallomics 4, 700-708.
96. Dalton, T., He, L., Wang, B., Miller, M., Jin, L., Stringer, K., Chang, X., Baxter, C., and Nebert, D. (2005). Identification of mouse SLC39A8 as the transporter responsible for cadmium-induced toxicity in the testis. Proceedings of the National Academy of Sciences of the United States of America 102, 3401-3406.
97. Dalton, T.P., He, L., Wang, B., Miller, M.L., Jin, L., Stringer, K.F., Chang, X., Baxter, C.S., and Nebert, D.W. (2005). Identification of mouse SLC39A8 as the transporter responsible for cadmium-induced toxicity in the testis. Proceedings of the National Academy of Sciences of the United States of America 102, 3401-3406.
98. Ajjimaporn, A., Botsford, T., Garrett, S.H., Sens, M.A., Zhou, X.D., Dunlevy, J.R., Sens, D.A., and Somji, S. (2012). ZIP8 expression in human proximal tubule cells, human urothelial cells transformed by Cd+2 and As+3 and in specimens of normal human urothelium and urothelial cancer. Cancer Cell Int 12, 16.
99. He, L., Wang, B., Hay, E., and Nebert, D. (2009). Discovery of ZIP transporters that participate in cadmium damage to testis and kidney. Toxicology and applied pharmacology 238, 250-257.
100. G √ ° lvez-Peralta, M., He, L., Jorge-Nebert, L., Wang, B., Miller, M., Eppert, B., Afton, S., and Nebert, D. (2012). ZIP8 zinc transporter: indispensable role for both multiple-organ organogenesis and hematopoiesis in utero. PloS one 7.
101. Wang, B., He, L., Dong, H., Dalton, T., and Nebert, D. (2011). Generation of a Slc39a8 hypomorph mouse: markedly decreased ZIP8 Zn¬≤, Å ∫ /(HCO, ÇÉ, Åª), ÇÇ transporter expression. Biochemical and biophysical research communications 410, 289-294.
102. Schneider, S.N., Liu, Z., Wang, B., Miller, M.L., Afton, S.E., Soleimani, M., and Nebert, D.W. (2014). Oral cadmium in mice carrying 5 versus 2 copies of the Slc39a8 gene: comparison of uptake, distribution, metal content, and toxicity. Int J Toxicol 33, 14-20.
103. Alberts, B. (2002). Molecular biology of the cell.(New York: Garland Science).
104. Little, P.J., Bhattacharya, R., Moreyra, A.E., and Korichneva, I.L. (2010). Zinc and cardiovascular disease. Nutrition 26, 1050-1057.
105. Hirano, T., Murakami, M., Fukada, T., Nishida, K., Yamasaki, S., and Suzuki, T. (2008). Roles of zinc and zinc signaling in immunity: zinc as an intracellular signaling molecule. Advances in immunology 97, 149-176.
106. Zheng, D., Kille, P., Feeney, G.P., Cunningham, P., Handy, R.D., and Hogstrand, C. (2010). Dynamic

transcriptomic profiles of zebrafish gills in response to zinc supplementation. BMC genomics 11, 553.
107. Bao, S., Liu, M.-J., Lee, B., Besecker, B., Lai, J.-P., Guttridge, D., and Knoell, D. (2010). Zinc modulates the innate immune response in vivo to polymicrobial sepsis through regulation of NF-kappaB. American journal of physiology Lung cellular and molecular physiology 298, 54.
108. Karagulova, G., Yue, Y., Moreyra, A., Boutjdir, M., and Korichneva, I. (2007). Protective role of intracellular zinc in myocardial ischemia/reperfusion is associated with preservation of protein kinase C isoforms. J Pharmacol Exp Ther 321, 517-525.
109. Hambidge, K.M., and Krebs, N.F. (2007). Zinc deficiency: a special challenge. The Journal of nutrition 137, 1101-1105.
110. Jarup, L., Berglund, M., Elinder, C.G., Nordberg, G., and Vahter, M. (1998). Health effects of cadmium exposure--a review of the literature and a risk estimate. Scand J Work Environ Health 24 Suppl 1, 1-51.
111. Daud, M.K., Sun, Y., Dawood, M., Hayat, Y., Variath, M.T., Wu, Y.X., Raziuddin, Mishkat, U., Salahuddin, Najeeb, U., et al. (2009). Cadmium-induced functional and ultrastructural alterations in roots of two transgenic cotton cultivars. J Hazard Mater 161, 463-473.
112. J. C. Merrill, J. J. P. Morton, and S. D. Soileau, “Metals: cadmium,” in Principles and Methods of Toxicology, A. W. Hayes, Ed., pp. 665–667, Taylor and Francis, London, UK, 2001
113. Foulkes, E.C. (2000). Transport of toxic heavy metals across cell membranes. Proc Soc Exp Biol Med 223, 234-240.
114. Organization, W.H. (1992). Cadmium. Environmental Health Criteria. . In Wolrd Health Organization, Geneva. (
115. Lalor, G.C. (2008). Review of cadmium transfers from soil to humans and its health effects in the Jamaican environment. Science of the Total Environment 400, 162-172.
116. Tellez-Plaza, M., Navas-Acien, A., Crainiceanu, C.M., and Guallar, E. (2008). Cadmium exposure and hypertension in the 1999-2004 National Health and Nutrition Examination Survey (NHANES). Environ Health Perspect 116, 51-56.
117. Zalups, R., and Ahmad, S. (2003). Molecular handling of cadmium in transporting epithelia. Toxicology and applied pharmacology 186, 163-188.
118. Gunshin, H., Mackenzie, B., Berger, U.V., Gunshin, Y., Romero, M.F., Boron, W.F., Nussberger, S., Gollan, J.L., and Hediger, M.A. (1997). Cloning and characterization of a mammalian proton-coupled metal-ion transporter. Nature 388, 482-488.
119. Hinkle, P., Kinsella, P., and Osterhoudt, K. (1987). Cadmium uptake and toxicity via voltage-sensitive calcium channels. The Journal of biological chemistry 262, 16333-16337.
120. Liu, J.e.a. (2001). Genetic background but not metallothionein phenotype dictates sensitivity to cadmium-induced testicular injury in mice. . Toxicology and applied pharmacology 176, 1-9.
121. Ishikawa, T., Bao, J.J., Yamane, Y., Akimaru, K., Frindrich, K., Wright, C.D., and Kuo, M.T. (1996). Coordinated induction of MRP/GS-X pump and gamma-glutamylcysteine synthetase by heavy metals in human leukemia cells. The Journal of biological chemistry 271, 14981-14988.
122. Vestergaard, P., and Shaikh, Z.A. (1994). The nephrotoxicity of intravenously administered cadmium-metallothionein: effect of dose, mode of administration, and preexisting renal cadmium burden. Toxicol Appl Pharmacol 126, 240-247.
123. Morales, A.I., Vicente-Sanchez, C., Jerkic, M., Santiago, J.M., Sanchez-Gonzalez, P.D., Perez-Barriocanal, F., and Lopez-Novoa, J.M. (2006). Effect of quercetin on metallothionein, nitric oxide synthases and cyclooxygenase-2 expression on experimental chronic cadmium nephrotoxicity in rats. Toxicol Appl Pharmacol 210, 128-135.
124. Messner, B., Knoflach, M., Seubert, A., Ritsch, A., Pfaller, K., Henderson, B., Shen, Y.H., Zeller, I., Willeit, J., Laufer, G., et al. (2009). Cadmium is a novel and independent risk factor for early atherosclerosis mechanisms and in vivo relevance. Arterioscler Thromb Vasc Biol 29, 1392-1398.
125. Knoflach, M., Messner, B., Shen, Y.H., Frotschnig, S., Liu, G., Pfaller, K., Wang, X., Matosevic, B., Willeit, J., Kiechl, S., et al. (2011). Non-toxic cadmium concentrations induce vascular inflammation and promote atherosclerosis. Circ J 75, 2491-2495.
126. Satarug, S., Nishijo, M., Lasker, J., Edwards, R., and Moore, M. (2006). Kidney dysfunction and hypertension: role for cadmium, p450 and heme oxygenases? The Tohoku journal of experimental medicine 208, 179-202.
127. Nakagawa, H., and Nishijo, M. (1996). Environmental cadmium exposure, hypertension and

cardiovascular risk. J Cardiovasc Risk 3, 11-17.
128. Tomera, J.F., Lilford, K., Kukulka, S.P., Friend, K.D., and Harakal, C. (1994). Divalent cations in hypertension with implications to heart disease: calcium, cadmium interactions. Methods Find Exp Clin Pharmacol 16, 97-107.
129. Gallagher, C., and Meliker, J. (2010). Blood and urine cadmium, blood pressure, and hypertension: a systematic review and meta-analysis. Environmental health perspectives 118, 1676-1684.
130. Tellez-Plaza, M., Navas-Acien, A., Crainiceanu, C., and Guallar, E. (2008). Cadmium exposure and hypertension in the 1999-2004 National Health and Nutrition Examination Survey (NHANES). Environmental health perspectives 116, 51-56.
131. Eum, K.D., Lee, M.S., and Paek, D. (2008). Cadmium in blood and hypertension. Science of the Total Environment 407, 147-153.
132. Pizent, A., Jurasovie, J., and Telisman, S. (2001). Blood pressure in relation to dietary calcium intake, alcohol consumption, blood lead, and blood cadmium in female nonsmokers. J Trace Elem Med Biol 15, 123-130.
133. Staessen, J.A., Kuznetsova, T., Roels, H.A., Emelianov, D., and Fagard, R. (2000). Exposure to cadmium and conventional and ambulatory blood pressures in a prospective population study. Public Health and Environmental Exposure to Cadmium Study Group. Am J Hypertens 13, 146-156.
134. Tellez-Plaza, M., Navas-Acien, A., Crainiceanu, C.M., and Guallar, E. (2008). Cadmium exposure and hypertension in the 1999-2004 National Health and Nutrition Examination Survey (NHANES). Environmental Health Perspectives 116, 51-56.
135. Staessen, J., Kuznetsova, T., Roels, H., Emelianov, D., and Fagard, R. (2000). Exposure to cadmium and conventional and ambulatory blood pressures in a prospective population study. Public Health and Environmental Exposure to Cadmium Study Group. American journal of hypertension 13, 146-156.
136. Prozialeck, W., Edwards, J., Nebert, D., Woods, J., Barchowsky, A., and Atchison, W. (2008). The vascular system as a target of metal toxicity. Toxicological sciences : an official journal of the Society of Toxicology 102, 207-218.
137. Alissa, E.M., and Ferns, G.A. (2011). Heavy metal poisoning and cardiovascular disease. J Toxicol 2011, 870125.
138. Houtman, J. (1993). Prolonged low-level cadmium intake and atherosclerosis. The Science of the total environment 138, 31-36.
139. Menke, A., Muntner, P., Silbergeld, E.K., Platz, E.A., and Guallar, E. (2009). Cadmium levels in urine and mortality among U.S. adults. Environ Health Perspect 117, 190-196.
140. Messner, B., Knoflach, M., Seubert, A., Ritsch, A., Pfaller, K., Henderson, B., Shen, Y., Zeller, I., Willeit, J., Laufer, G.n., et al. (2009). Cadmium is a novel and independent risk factor for early atherosclerosis mechanisms and in vivo relevance. Arteriosclerosis, thrombosis, and vascular biology 29, 1392-1398.
141. Houtman, J.P. (1993). Prolonged low-level cadmium intake and atherosclerosis. Sci Total Environ 138, 31-36.
142. Everett, C., and Frithsen, I. (2008). Association of urinary cadmium and myocardial infarction. Environmental research 106, 284-286.
143. Navas-Acien, A., Selvin, E., Sharrett, A.R., Calderon-Aranda, E., Silbergeld, E., and Guallar, E. (2004). Lead, cadmium, smoking, and increased risk of peripheral arterial disease. Circulation 109, 3196-3201.
144. Alissa, E., and Ferns, G. (2011). Heavy metal poisoning and cardiovascular disease. Journal of toxicology 2011, 870125.
145. Varoni, M., Palomba, D., Gianorso, S., and Anania, V. (2003). Cadmium as an environmental factor of hypertension in animals: new perspectives on mechanisms. Veterinary research communications 27 Suppl 1, 807-810.
146. Sarkar, S., Yadav, P., Trivedi, R., Bansal, A., and Bhatnagar, D. (1995). Cadmium-induced lipid peroxidation and the status of the antioxidant system in rat tissues. Journal of trace elements in medicine and biology : organ of the Society for Minerals and Trace Elements (GMS) 9, 144-149.
147. Kim, J., Lim, W., Ko, Y., Kwon, H., Kim, S., Kim, O., Park, G., and Choi, H. (2012). The effects of cadmium on VEGF-mediated angiogenesis in HUVECs. Journal of applied toxicology : JAT 32, 342-349.

148. Satarug, S., Nishijo, M., Lasker, J.M., Edwards, R.J., and Moore, M.R. (2006). Kidney dysfunction and hypertension: role for cadmium, p450 and heme oxygenases? Tohoku J Exp Med 208, 179-202.
149. Garcia Zozaya, J.L., and Padilla Viloria, M. (1997). [Alterations of calcium, magnesium, and zinc in essential hypertension:their relation to the renin-angiotensin-aldosterone system]. Invest Clin 38 Suppl 2, 27-40.
150. Carpenter, W.E., Lam, D., Toney, G.M., Weintraub, N.L., and Qin, Z. (2013). Zinc, copper, and blood pressure: Human population studies. Med Sci Monit 19, 1-8.
151. Shahbaz, A.U., Sun, Y., Bhattacharya, S.K., Ahokas, R.A., Gerling, I.C., McGee, J.E., and Weber, K.T. (2010). Fibrosis in hypertensive heart disease: molecular pathways and cardioprotective strategies. J Hypertens 28 Suppl 1, S25-32.
152. Bergomi, M., Rovesti, S., Vinceti, M., Vivoli, R., Caselgrandi, E., and Vivoli, G. (1997). Zinc and copper status and blood pressure. J Trace Elem Med Biol 11, 166-169.
153. Canatan, H., Bakan, I., Akbulut, M., Halifeoglu, I., Cikim, G., Baydas, G., and Kilic, N. (2004). Relationship among levels of leptin and zinc, copper, and zinc/copper ratio in plasma of patients with essential hypertension and healthy normotensive subjects. Biol Trace Elem Res 100, 117-123.
154. Harlan, W.R., Landis, J.R., Schmouder, R.L., Goldstein, N.G., and Harlan, L.C. (1985). Blood lead and blood pressure. Relationship in the adolescent and adult US population. JAMA 253, 530-534.
155. Tubek, S. (2007). Role of zinc in regulation of arterial blood pressure and in the etiopathogenesis of arterial hypertension. Biol Trace Elem Res 117, 39-51.
156. Zozaya, J.L. (2000). Nutritional factors in high blood pressure. J Hum Hypertens 14 Suppl 1, S100-104.
157. Houston, M. (2014). The role of nutrition and nutraceutical supplements in the treatment of hypertension. World J Cardiol 6, 38-66.
158. Litwin, M., Clark, K., Noack, L., Furze, J., Berndt, M., Albelda, S., Vadas, M., and Gamble, J. (1997). Novel cytokine-independent induction of endothelial adhesion molecules regulated by platelet/endothelial cell adhesion molecule (CD31). J Cell Biol 139, 219-228.
159. Ross, R., and Glomset, J.A. (1976). The pathogenesis of atherosclerosis (second of two parts). The New England journal of medicine 295, 420-425.
160. Meerarani, P., Reiterer, G., Toborek, M., and Hennig, B. (2003). Zinc modulates PPARgamma signaling and activation of porcine endothelial cells. J Nutr 133, 3058-3064.
161. Coudray, C., Charlon, V., de Leiris, J., and Favier, A. (1993). Effect of zinc deficiency on lipid peroxidation status and infarct size in rat hearts. Int J Cardiol 41, 109-113.
162. Powell, S.R., Aiuto, L., Hall, D., and Tortolani, A.J. (1995). Zinc supplementation enhances the effectiveness of St. Thomas' Hospital No. 2 cardioplegic solution in an in vitro model of hypothermic cardiac arrest. J Thorac Cardiovasc Surg 110, 1642-1648.
163. Tan, I.K., Chua, K.S., and Toh, A.K. (1992). Serum magnesium, copper, and zinc concentrations in acute myocardial infarction. J Clin Lab Anal 6, 324-328.
164. Chausmer, A.B. (1998). Zinc, insulin and diabetes. J Am Coll Nutr 17, 109-115.
165. Taylor, C.G. (2005). Zinc, the pancreas, and diabetes: insights from rodent studies and future directions. Biometals 18, 305-312.
166. Perkins, N.D. (2007). Integrating cell-signalling pathways with NF-kappaB and IKK function. Nat Rev Mol Cell Biol 8, 49-62.
167. Hayden, M.S., and Ghosh, S. (2004). Signaling to NF-kappaB. Genes Dev 18, 2195-2224.
168. Hayden, M.S., and Ghosh, S. (2008). Shared principles in NF-kappaB signaling. Cell 132, 344-362.
169. Claudio Mauro, e.a. The NF-kB Transcription Factor Pathway as a Therapeutic Target in Cancer: Methods for Detection of NF-kB Activity.(Humana Press, a part of Springer Science + Business Media, LLC 2009).
170. Foster, M., Petocz, P., and Samman, S. (2010). Effects of zinc on plasma lipoprotein cholesterol concentrations in humans: a meta-analysis of randomised controlled trials. Atherosclerosis 210, 344-352.
171. Begum, N.A., Kobayashi, M., Moriwaki, Y., Matsumoto, M., Toyoshima, K., and Seya, T. (2002). Mycobacterium bovis BCG cell wall and lipopolysaccharide induce a novel gene, BIGM103, encoding a 7-TM protein: identification of a new protein family having Zn-transporter and Zn-metalloprotease signatures. Genomics 80, 630-645.
172. Gerbod-Giannone, M.-C., Li, Y., Holleboom, A., Han, S., Hsu, L.-C., Tabas, I., and Tall, A. (2006). TNFalpha induces ABCA1 through NF-kappaB in macrophages and in phagocytes ingesting

apoptotic cells. Proceedings of the National Academy of Sciences of the United States of America 103, 3112-3117.
173. Van der Heiden, K., Cuhlmann, S., Luong le, A., Zakkar, M., and Evans, P.C. (2010). Role of nuclear factor kappaB in cardiovascular health and disease. Clin Sci (Lond) 118, 593-605.
174. Gordon, J.W., Shaw, J.A., and Kirshenbaum, L.A. (2011). Multiple facets of NF-kappaB in the heart: to be or not to NF-kappaB. Circ Res 108, 1122-1132.
175. Hosokawa, S., Haraguchi, G., Sasaki, A., Arai, H., Muto, S., Itai, A., Doi, S., Mizutani, S., and Isobe, M. (2013). Pathophysiological roles of nuclear factor kappaB (NF-kB) in pulmonary arterial hypertension: effects of synthetic selective NF-kB inhibitor IMD-0354. Cardiovasc Res 99, 35-43.
176. Lloyd, A.C. (2006). Distinct functions for ERKs? J Biol 5, 13.
177. Ramos, J.W. (2008). The regulation of extracellular signal-regulated kinase (ERK) in mammalian cells. Int J Biochem Cell Biol 40, 2707-2719.
178. Yang, C.S., Tzou, B.C., Liu, Y.P., Tsai, M.J., Shyue, S.K., and Tzeng, S.F. (2008). Inhibition of cadmium-induced oxidative injury in rat primary astrocytes by the addition of antioxidants and the reduction of intracellular calcium. J Cell Biochem 103, 825-834.
179. Chuang, S.M., Wang, I.C., and Yang, J.L. (2000). Roles of JNK, p38 and ERK mitogen-activated protein kinases in the growth inhibition and apoptosis induced by cadmium. Carcinogenesis 21, 1423-1432.
180. Cagnol, S., Van Obberghen-Schilling, E., and Chambard, J.C. (2006). Prolonged activation of ERK1,2 induces FADD-independent caspase 8 activation and cell death. Apoptosis 11, 337-346.
181. Lag, M., Refsnes, M., Lilleaas, E.M., Holme, J.A., Becher, R., and Schwarze, P.E. (2005). Role of mitogen activated protein kinases and protein kinase C in cadmium-induced apoptosis of primary epithelial lung cells. Toxicology 211, 253-264.
182. Yang, L.Y., Wu, K.H., Chiu, W.T., Wang, S.H., and Shih, C.M. (2009). The cadmium-induced death of mesangial cells results in nephrotoxicity. Autophagy 5, 571-572.
183. Martin, P., and Pognonec, P. (2010). ERK and cell death: cadmium toxicity, sustained ERK activation and cell death. The FEBS journal 277, 39-46.
184. Marshall, C.J. (1995). Specificity of receptor tyrosine kinase signaling: transient versus sustained extracellular signal-regulated kinase activation. Cell 80, 179-185.
185. Murphy, L.O., and Blenis, J. (2006). MAPK signal specificity: the right place at the right time. Trends Biochem Sci 31, 268-275.
186. Tamemoto, H., Kadowaki, T., Tobe, K., Ueki, K., Izumi, T., Chatani, Y., Kohno, M., Kasuga, M., Yazaki, Y., and Akanuma, Y. (1992). Biphasic activation of two mitogen-activated protein kinases during the cell cycle in mammalian cells. The Journal of biological chemistry 267, 20293-20297.
187. Emge, N., Uygur, M., Radivoj, M., T, W.K., Royer, T., and Jaric, S. (2014). Selective effects of arm proximal and distal muscles fatigue on force coordination in manipulation tasks. Journal of motor behavior 46, 259-265.
188. R, M., S, H., and W, K. (2012). Recent Surgical and Medical Advances in the Treatment of Dupuytren's Disease - A Systematic Review of the Literature. The open orthopaedics journal 6, 77-82.
189. P, M., R, M., S, H., M, G., and W, K. (2012). A systematic review of dynamometry and its role in hand trauma assessment. The open orthopaedics journal 6, 95-102.
190. Kim, S., Murakami, T., Izumi, Y., Yano, M., Miura, K., Yamanaka, S., and Iwao, H. (1997). Extracellular signal-regulated kinase and c-Jun NH2-terminal kinase activities are continuously and differentially increased in aorta of hypertensive rats. Biochem Biophys Res Commun 236, 199-204.
191. Touyz, R.M., Deschepper, C., Park, J.B., He, G., Chen, X., Neves, M.F., Virdis, A., and Schiffrin, E.L. (2002). Inhibition of mitogen-activated protein/extracellular signal-regulated kinase improves endothelial function and attenuates Ang II-induced contractility of mesenteric resistance arteries from spontaneously hypertensive rats. J Hypertens 20, 1127-1134.
192. Kim, J., Lee, Y.R., Lee, C.H., Choi, W.H., Lee, C.K., Kim, J., Bae, Y.M., Cho, S., and Kim, B. (2005). Mitogen-activated protein kinase contributes to elevated basal tone in aortic smooth muscle from hypertensive rats. Eur J Pharmacol 514, 209-215.
193. Cagnol, S., and Chambard, J.C. (2010). ERK and cell death: mechanisms of ERK-induced cell death--apoptosis, autophagy and senescence. FEBS J 277, 2-21.
194. Wang, S.H., Shih, Y.L., Ko, W.C., Wei, Y.H., and Shih, C.M. (2008). Cadmium-induced autophagy and apoptosis are mediated by a calcium signaling pathway. Cell Mol Life Sci 65, 3640-3652.

195. Kondoh, M., Araragi, S., Sato, K., Higashimoto, M., Takiguchi, M., and Sato, M. (2002). Cadmium induces apoptosis partly via caspase-9 activation in HL-60 cells. Toxicology 170, 111-117.
196. Martin, P., Poggi, M., Chambard, J., Boulukos, K., and Pognonec, P. (2006). Low dose cadmium poisoning results in sustained ERK phosphorylation and caspase activation. Biochemical and biophysical research communications 350, 803-807.
197. Renna, N.F., de Las Heras, N., and Miatello, R.M. (2013). Pathophysiology of vascular remodeling in hypertension. Int J Hypertens 2013, 808353.
198. Zhang, H., Chalothorn, D., Jackson, L.F., Lee, D.C., and Faber, J.E. (2004). Transactivation of epidermal growth factor receptor mediates catecholamine-induced growth of vascular smooth muscle. Circ Res 95, 989-997.
199. Kida, T., Chuma, H., Murata, T., Yamawaki, H., Matsumoto, S., Hori, M., and Ozaki, H. (2011). Chronic treatment with PDGF-BB and endothelin-1 synergistically induces vascular hyperplasia and loss of contractility in organ-cultured rat tail artery. Atherosclerosis 214, 288-294.
200. Iryo, Y., Matsuoka, M., Wispriyono, B., Sugiura, T., and Igisu, H. (2000). Involvement of the extracellular signal-regulated protein kinase (ERK) pathway in the induction of apoptosis by cadmium chloride in CCRF-CEM cells. Biochemical pharmacology 60, 1875-1882.
201. Kim, J., Kim, S.H., Johnson, V.J., and Sharma, R.P. (2005). Extracellular signal-regulated kinase-signaling-dependent G2/M arrest and cell death in murine macrophages by cadmium. Environmental toxicology and chemistry / SETAC 24, 3069-3077.
202. Jung, Y.S., Jeong, E.M., Park, E.K., Kim, Y.M., Sohn, S., Lee, S.H., Baik, E.J., and Moon, C.H. (2008). Cadmium induces apoptotic cell death through p38 MAPK in brain microvessel endothelial cells. Eur J Pharmacol 578, 11-18.
203. Miguel, B.G., Rodriguez, M.E., Aller, P., Martinez, A.M., and Mata, F. (2005). Regulation of cadmium-induced apoptosis by PKCdelta in U937 human promonocytic cells. Biochim Biophys Acta 1743, 215-222.
204. Biagioli, M., Pifferi, S., Ragghianti, M., Bucci, S., Rizzuto, R., and Pinton, P. (2008). Endoplasmic reticulum stress and alteration in calcium homeostasis are involved in cadmium-induced apoptosis. Cell Calcium 43, 184-195.
205. Seo, S.R., Chong, S.A., Lee, S.I., Sung, J.Y., Ahn, Y.S., Chung, K.C., and Seo, J.T. (2001). Zn2+-induced ERK activation mediated by reactive oxygen species causes cell death in differentiated PC12 cells. Journal of neurochemistry 78, 600-610.
206. Chan, D.W., Liu, V.W., Tsao, G.S., Yao, K.M., Furukawa, T., Chan, K.K., and Ngan, H.Y. (2008). Loss of MKP3 mediated by oxidative stress enhances tumorigenicity and chemoresistance of ovarian cancer cells. Carcinogenesis 29, 1742-1750.
207. Lopez, E., Figueroa, S., Oset-Gasque, M.J., and Gonzalez, M.P. (2003). Apoptosis and necrosis: two distinct events induced by cadmium in cortical neurons in culture. Br J Pharmacol 138, 901-911.
208. Thevenod, F. (2009). Cadmium and cellular signaling cascades: to be or not to be? Toxicol Appl Pharmacol 238, 221-239.
209. Th √ ©venod, F., and Friedmann, J. (1999). Cadmium-mediated oxidative stress in kidney proximal tubule cells induces degradation of Na+/K(+)-ATPase through proteasomal and endo-/lysosomal proteolytic pathways. FASEB journal : official publication of the Federation of American Societies for Experimental Biology 13, 1751-1761.
210. Jaffe, E.A., Nachman, R.L., Becker, C.G., and Minick, C.R. (1973). Culture of human endothelial cells derived from umbilical veins. Identification by morphologic and immunologic criteria. J Clin Invest 52, 2745-2756.
211. Genomes Project, C., Abecasis, G.ß., Altshuler, D., Auton, A., Brooks, L., Durbin, R., Gibbs, R., Hurles, M., and McVean, G. (2010). A map of human genome variation from population-scale sequencing. Nature 467, 1061-1073.
212. Genomics, L. KASP genotyping chemistry user guide and manual. In. (
213. Shen, G.Q., Abdullah, K.G., and Wang, Q.K. (2009). The TaqMan method for SNP genotyping. Methods Mol Biol 578, 293-306.
214. Technologies, L. TaqMan SNP genotyping asasys product bulletin In. (
215. Sigma.com. Mammalian total RNA miniprep kit. In. (
216. Pastinen, T., and Hudson, T.J. (2004). Cis-acting regulatory variation in the human genome. Science 306, 647-650.
217. Akkinepalli, H., Ereful, N., Liu, Y., Malabanan, K., Howells, R., Stamati, K., Powell, W., Leung, H., Greenland, A., Mackay, I., et al. (2012). Snapshots of gene expression in rice: limitations for

allelic expression imbalance determination. Genome 55, 400-406.
218. Santhosh, S.R., Parida, M.M., Dash, P.K., Pateriya, A., Pattnaik, B., Pradhan, H.K., Tripathi, N.K., Ambuj, S., Gupta, N., Saxena, P., et al. (2007). Development and evaluation of SYBR Green I-based one-step real-time RT-PCR assay for detection and quantitation of Japanese encephalitis virus. J Virol Methods 143, 73-80.
219. Miyaguchi, H., Kurosawa, N., and Toda, T. (2008). Real-time polymerase chain reaction assays for rapid detection and quantification of Noctiluca scintillans zoospore. Mar Biotechnol (NY) 10, 133-140.
220. Gubelmann, C., Gattiker, A., Massouras, A., Hens, K., David, F., Decouttere, F., Rougemont, J., and Deplancke, B. (2011). GETPrime: a gene- or transcript-specific primer database for quantitative real-time PCR. Database : the journal of biological databases and curation 2011, bar040.
221. Nelson, M., and McClelland, M. (1992). Use of DNA methyltransferase/endonuclease enzyme combinations for megabase mapping of chromosomes. Methods Enzymol 216, 279-303.
222. Brown, M., and Wittwer, C. (2000). Flow cytometry: principles and clinical applications in hematology. Clin Chem 46, 1221-1229.
223. Berridge, M.V., and Tan, A.S. (1993). Characterization of the cellular reduction of 3-(4,5-dimethylthiazol-2-yl)-2,5-diphenyltetrazolium bromide (MTT): subcellular localization, substrate dependence, and involvement of mitochondrial electron transport in MTT reduction. Arch Biochem Biophys 303, 474-482.
224. Stergachis, A.B., Haugen, E., Shafer, A., Fu, W., Vernot, B., Reynolds, A., Raubitschek, A., Ziegler, S., LeProust, E.M., Akey, J.M., et al. (2013). Exonic transcription factor binding directs codon choice and affects protein evolution. Science 342, 1367-1372.
225. Ritter, D.I., Dong, Z., Guo, S., and Chuang, J.H. (2012). Transcriptional enhancers in protein-coding exons of vertebrate developmental genes. PLoS One 7, e35202.
226. Cunningham, F., Amode, M.R., Barrell, D., Beal, K., Billis, K., Brent, S., Carvalho-Silva, D., Clapham, P., Coates, G., Fitzgerald, S., et al. (2015). Ensembl 2015. Nucleic Acids Res 43, D662-669.
227. Ashkenazy, H., Erez, E., Martz, E., Pupko, T., and Ben-Tal, N. (2010). ConSurf 2010: calculating evolutionary conservation in sequence and structure of proteins and nucleic acids. Nucleic Acids Res 38, W529-533.
228. Kim, D.E., Chivian, D., and Baker, D. (2004). Protein structure prediction and analysis using the Robetta server. Nucleic Acids Res 32, W526-531.
229. Krogh, A., Larsson, B., von Heijne, G., and Sonnhammer, E.L. (2001). Predicting transmembrane protein topology with a hidden Markov model: application to complete genomes. J Mol Biol 305, 567-580.
230. Rodriguez, S., Gaunt, T.R., and Day, I.N. (2009). Hardy-Weinberg equilibrium testing of biological ascertainment for Mendelian randomization studies. Am J Epidemiol 169, 505-514.
231. Sankaranarayanan, S., Kellner-Weibel, G., de la Llera-Moya, M., Phillips, M.C., Asztalos, B.F., Bittman, R., and Rothblat, G.H. (2011). A sensitive assay for ABCA1-mediated cholesterol efflux using BODIPY-cholesterol. J Lipid Res 52, 2332-2340.
232. Templeton, D.M., and Liu, Y. (2010). Multiple roles of cadmium in cell death and survival. Chem Biol Interact 188, 267-275.
233. Ng, E., Lind, P.M., Lindgren, C., Ingelsson, E., Mahajan, A., Morris, A., and Lind, L. (2015). Genome-wide association study of toxic metals and trace elements reveals novel associations. Hum Mol Genet.
234. Crescenzi, A., Papini, E., Pacella, C.M., Rinaldi, R., Panunzi, C., Petrucci, L., Fabbrini, R., Bizzarri, G.C., Anelli, V., Nardi, F., et al. (1996). Morphological changes in a hyperfunctioning thyroid adenoma after percutaneous ethanol injection: histological, enzymatic and sub-microscopical alterations. J Endocrinol Invest 19, 371-376.
235. He, L., Wang, B., Hay, E.B., and Nebert, D.W. (2009). Discovery of ZIP transporters that participate in cadmium damage to testis and kidney. Toxicol Appl Pharmacol 238, 250-257.
236. Koh, E.S., Kim, S.J., Yoon, H.E., Chung, J.H., Chung, S., Park, C.W., Chang, Y.S., and Shin, S.J. (2014). Association of blood manganese level with diabetes and renal dysfunction: a cross-sectional study of the Korean general population. BMC Endocr Disord 14, 24.
237. Chung, S., Chung, J.H., Kim, S.J., Koh, E.S., Yoon, H.E., Park, C.W., Chang, Y.S., and Shin, S.J. (2014). Blood lead and cadmium levels and renal function in Korean adults. Clin Exp Nephrol 18, 726-734.
238. Kim, M.H., and Choi, M.K. (2013). Seven dietary minerals (Ca, P, Mg, Fe, Zn, Cu, and Mn) and their

relationship with blood pressure and blood lipids in healthy adults with self-selected diet. Biol Trace Elem Res 153, 69-75.
239. Wu, S., Deng, F., Huang, J., Wang, H., Shima, M., Wang, X., Qin, Y., Zheng, C., Wei, H., Hao, Y., et al. (2013). Blood pressure changes and chemical constituents of particulate air pollution: results from the healthy volunteer natural relocation (HVNR) study. Environ Health Perspect 121, 66-72.
240. Hung, J.J., Cheng, T.J., Lai, Y.K., and Chang, M.D. (1998). Differential activation of p38 mitogen-activated protein kinase and extracellular signal-regulated protein kinases confers cadmium-induced HSP70 expression in 9L rat brain tumor cells. J Biol Chem 273, 31924-31931.
241. Galan, A., Garcia-Bermejo, M.L., Troyano, A., Vilaboa, N.E., de Blas, E., Kazanietz, M.G., and Aller, P. (2000). Stimulation of p38 mitogen-activated protein kinase is an early regulatory event for the cadmium-induced apoptosis in human promonocytic cells. J Biol Chem 275, 11418-11424.
242. Tamemoto, H., Kadowaki, T., Tobe, K., Ueki, K., Izumi, T., Chatani, Y., Kohno, M., Kasuga, M., Yazaki, Y., and Akanuma, Y. (1992). Biphasic activation of two mitogen-activated protein kinases during the cell cycle in mammalian cells. J Biol Chem 267, 20293-20297.
243. Krens, S.F., Corredor-Adamez, M., He, S., Snaar-Jagalska, B.E., and Spaink, H.P. (2008). ERK1 and ERK2 MAPK are key regulators of distinct gene sets in zebrafish embryogenesis. BMC Genomics 9, 196.
244. Lefloch, R., Pouyssegur, J., and Lenormand, P. (2008). Single and combined silencing of ERK1 and ERK2 reveals their positive contribution to growth signaling depending on their expression levels. Mol Cell Biol 28, 511-527.
245. Vantaggiato, C., Formentini, I., Bondanza, A., Bonini, C., Naldini, L., and Brambilla, R. (2006). ERK1 and ERK2 mitogen-activated protein kinases affect Ras-dependent cell signaling differentially. J Biol 5, 14.
246. Hoffmann, A., Levchenko, A., Scott, M.L., and Baltimore, D. (2002). The IkappaB-NF-kappaB signaling module: temporal control and selective gene activation. Science 298, 1241-1245.
247. Nelson, D.E., Ihekwaba, A.E., Elliott, M., Johnson, J.R., Gibney, C.A., Foreman, B.E., Nelson, G., See, V., Horton, C.A., Spiller, D.G., et al. (2004). Oscillations in NF-kappaB signaling control the dynamics of gene expression. Science 306, 704-708.
248. Owen, D.R., Lindsay, A.C., Choudhury, R.P., and Fayad, Z.A. (2011). Imaging of atherosclerosis. Annu Rev Med 62, 25-40.
249. Rosenson, R.S., Brewer, H.B., Jr., Chapman, M.J., Fazio, S., Hussain, M.M., Kontush, A., Krauss, R.M., Otvos, J.D., Remaley, A.T., and Schaefer, E.J. (2011). HDL measures, particle heterogeneity, proposed nomenclature, and relation to atherosclerotic cardiovascular events. Clin Chem 57, 392-410.
250. Rosenson, R.S., Brewer, H.B., Jr., Davidson, W.S., Fayad, Z.A., Fuster, V., Goldstein, J., Hellerstein, M., Jiang, X.C., Phillips, M.C., Rader, D.J., et al. (2012). Cholesterol efflux and atheroprotection: advancing the concept of reverse cholesterol transport. Circulation 125, 1905-1919.
251. Bodzioch, M., Orso, E., Klucken, J., Langmann, T., Bottcher, A., Diederich, W., Drobnik, W., Barlage, S., Buchler, C., Porsch-Ozcurumez, M., et al. (1999). The gene encoding ATP-binding cassette transporter 1 is mutated in Tangier disease. Nat Genet 22, 347-351.
252. Brooks-Wilson, A., Marcil, M., Clee, S.M., Zhang, L.H., Roomp, K., van Dam, M., Yu, L., Brewer, C., Collins, J.A., Molhuizen, H.O., et al. (1999). Mutations in ABC1 in Tangier disease and familial high-density lipoprotein deficiency. Nat Genet 22, 336-345.
253. Chinetti, G., Lestavel, S., Bocher, V., Remaley, A.T., Neve, B., Torra, I.P., Teissier, E., Minnich, A., Jaye, M., Duverger, N., et al. (2001). PPAR-alpha and PPAR-gamma activators induce cholesterol removal from human macrophage foam cells through stimulation of the ABCA1 pathway. Nat Med 7, 53-58.
254. Parizek, J., and Zahor, Z. (1956). Effect of cadmium salts on testicular tissue. Nature 177, 1036.
255. WHO/IPCS. (1992). Cadmium. Environmental Health Criteria Document 134. In. (Geneva), pp 1-280.
256. Lauwerys, R., Bernard, A., Buchet, J.P., Roels, H., Bruaux, P., Claeys, F., Ducoffre, G., De Plaen, P., Staessen, J., Amery, A., et al. (1991). Does environmental exposure to cadmium represent a health risk? Conclusions from the Cadmibel study. Acta Clin Belg 46, 219-225.
257. Nordberg, G.F. (1976). Effects and dose-response relationships of toxic metals. A report from an international meeting. Scand J Work Environ Health 2, 37-43.
258. Hotz, P., Buchet, J.P., Bernard, A., Lison, D., and Lauwerys, R. (1999). Renal effects of low-level environmental cadmium exposure: 5-year follow-up of a subcohort from the Cadmibel study.

Lancet 354, 1508-1513.
259. Cherian, M.G. (1985). Rat kidney epithelial cell culture for metal toxicity studies. In Vitro Cell Dev Biol 21, 505-508.
260. DelRaso, N.J., Foy, B.D., Gearhart, J.M., and Frazier, J.M. (2003). Cadmium uptake kinetics in rat hepatocytes: correction for albumin binding. Toxicol Sci 72, 19-30.
261. Prozialeck, W.C., Edwards, J.R., Nebert, D.W., Woods, J.M., Barchowsky, A., and Atchison, W.D. (2008). The vascular system as a target of metal toxicity. Toxicol Sci 102, 207-218.
262. Varoni, M.V., Palomba, D., Gianorso, S., and Anania, V. (2003). Cadmium as an environmental factor of hypertension in animals: new perspectives on mechanisms. Vet Res Commun 27 Suppl 1, 807-810.
263. Sarkar, S., Yadav, P., Trivedi, R., Bansal, A.K., and Bhatnagar, D. (1995). Cadmium-induced lipid peroxidation and the status of the antioxidant system in rat tissues. J Trace Elem Med Biol 9, 144-149.
264. Woods, J.M., Leone, M., Klosowska, K., Lamar, P.C., Shaknovsky, T.J., and Prozialeck, W.C. (2008). Direct antiangiogenic actions of cadmium on human vascular endothelial cells. Toxicol In Vitro 22, 643-651.
265. Messner, B., Knoflach, M., Seubert, A., Ritsch, A., Pfaller, K., Henderson, B., Shen, Y.H., Zeller, I., Willeit, J., Laufer, G., et al. (2009). Cadmium is a novel and independent risk factor for early atherosclerosis mechanisms and in vivo relevance. Arterioscler Thromb Vasc Biol 29, 1392-1398.
266. Sunyaev, S., Ramensky, V., and Bork, P. (2000). Towards a structural basis of human non-synonymous single nucleotide polymorphisms. Trends Genet 16, 198-200.
267. Diallinas, G. (2014). Understanding transporter specificity and the discrete appearance of channel-like gating domains in transporters. Front Pharmacol 5, 207.
268. Petrey, D., and Honig, B. (2005). Protein structure prediction: inroads to biology. Mol Cell 20, 811-819.
269. Dalton, T.P., He, L., Wang, B., Miller, M.L., Jin, L., Stringer, K.F., Chang, X., Baxter, C.S., and Nebert, D.W. (2005). Identification of mouse SLC39A8 as the transporter responsible for cadmium-induced toxicity in the testis. Proceedings of the National Academy of Sciences of the United States of America 102, 3401-3406.
270. Everett, C.J., and Frithsen, I.L. (2008). Association of urinary cadmium and myocardial infarction. Environ Res 106, 284-286.

Appendices

A1. Primer sequences

	Primer name	5'→3'
1	KASP rs13107325_ALT-fam	GAAGGTGACCAAGTTCATGCTGGCATTTT GGTGGGCAACAATTTCA
2	KASP rs13107325_ALC-vic	GAAGGTCGGAGTCAACGGATTGCATTTTG GTGGGCAACAATTTCG
3	KASP rs13107325_C2	CATGCCTCCAGCAAGTGCAAATATAATAT
4	genomic DNA forward primer F1	TCC TGC ACC TTG TCT CTC CT
5	Genomic DNA forward primer F2	GAGACTTTGTGATCCTACTCAAT
6	genomic DNA reverse primer R	AGC AGA AGG CCA CCC TTA GT
7	*SLC39A8* cDNA forward primer F1	GAG GAG TTT CCC CAC GAG TT
8	*SLC39A8* cDNA forward primer F2	TCC TGC ACC TTG TCT CTC CT
9	*SLC39A8* cDNA reverse primer R2	GGT GAA ATC GGT TTT TCT TCC
10	*SLC39A8* cDNA reverse primer R3	AAC ATG CCT CCA GCA AGT G
11	Cloning Hind III forward	ATGCAAAGCTTCTCGCCATGGCCCCGGG TCGCG
12	Cloning EcoR I reverse	ATGCAGAATTCTTACTCCAATTCGATTTCT CCTGCA
13	Mutagenic forward primer	GCAACAATTTCACTCCAAATATT
14	Mutagenic reverse primer	AATATTTGGAGTGAAATTGTTGC
15	SLC39A8 plasmid insert primer 1	CCCAAATAACCAGCTCCAAA
16	SLC39A8 plasmid insert primer 2	AGCTGCACTTCAACCAGTGT
17	SLC39A8 plasmid insert primer 2	GGCTGGCTATTGGGACTCTT
18	SLC39A8 plasmid insert primer 2	TGGTGTGACATGCTATGCAA

19	SLC39A8 plasmid insert reverse primer	GGCTGGCTATTGGGACTCTT
20	*SLC39A8* qRT-PCR primers	Forward: ATGTTGAGAAGGCAGTTGC Reverse: ATGACCATTCTGACCATATGTC
21	*SR-BI* qRT-PCR primers	Forward: GAACTTCTGGGCAAATGTGG Reverse: TAGCTTCATGGATCGGCAG
22	*PPAR-α* qRT-PCR primers	Forward: CATTTGCTGTGGAGATCGT Reverse: CTGAGCACATGTACAATACCC
23	*PPAR-Y* qRT-PCR primers	Forward: GGCGAGGGCGATCTTGACAGG Reverse: TGCGGATGGCCACCTCTTTGC
24	*NF-κB* qRT-PCR primers	Forward: TACAGGTCCAGGGTATAGC Reverse: AGATTTAGTAGTTCCAGGATGG
25	*ABCA1* qRT-PCR primers	Forward: AAAGACACCAGCATGAAGGA Reverse: AAGCTTCAAGTTTGAGCTGG

A 2. Solution recipes (all components listed as final concentration in mM)

A 2.1 Subjects and samples

PSS solution - NaCl 110 mM, $CaCl_2$ 0.15 mM, KCl 5 mM, MgCl2 2 mM, HEPES 10 mM, $NaHCO_3$ 10 mM, KH_2PO_4 0.5 mM, glucose 10 mM, EDTA 0.49 mM

A 2.2 DNA study

The reagent mix for post PCR restriction enzyme digestion reaction - 10µl DNA (from PCR reaction), 2µl 10 x buffer, 4u *Bcg*I enzyme (2u/µl), 6µl nuclease-free H_2O in a total reaction volume of 20µl.

DNA lysis buffer - 10Mm Tris pH 8.0, 10Mm EDTA, 100MmNaCl, 0.5% SDS.

PCR recipe for genomic DNA and cDNA amplification - 1xPCR buffer, 2.5mM $MgCl_2$, 0.2mM dNTP, 10µM primer mix, 1u Taq polymerase (Sigma, D4545), 12.5ng/50ng genomic DNA or 50ng cDNA in a total volume of 25µl.

A 2.3 RNA study

Reverse transcription (RT) reaction recipe - 1xbuffer, 3mM $MgCl_2$, 1mM dNTP, 20u of RNase inhibitor (Promega, N251A), 0.5/1µg of total RNA, and 200u of M-MLV reverse transcriptase (Promega, M1708) in a total volume of 25µl.

A 2.4 Protein study

5 x loading buffer – 0.313 M Tris-HCl (pH 6.8 at 25°C), 10% SD, 0.05% bromophenol blue, 50% glycerol

RIPA Lysis buffer for protein extraction- 50mM Tris, HCl pH7.4, 150mM NaCl, 0.5% sodium deoxycholate, 1% NP-40, 0.1%SDS

Protease inhibitor (PI) - 1mM PMSF, 1µg/ml leupeptin, 1µg/ml Aprotinin, 1µg/ml pepstatin.

Homogenization buffer- 10mM Tris HCl pH7.2, 1mM EDTA, 250mM sucrose, 1 x P.I.)

Chemiluminescence ECL - luminol, p-coumaric acid, Tris 8.5 and 30% H_2O_2

A 2.5 Cell culture

HUASMC supplements (final concentration) -

15% fetal bovine serum (FBS, Appleton Woods, FB021), 1.67mM L-glutamine (Sigma, G7513, 200mM) and 0.83% penicillin-streptomycin (Sigma, P0781) (10,000 units penicillin and 10 mg streptomycin per mL), epidermal growth factor human (Sigma, E9644) 0.5ng/ml, human fibroblast growth factor (SLS, F5542-25µg) 2ng/ml, insulin

from bovine pancreas (SLS, I6634-100mg) 5ng/ml.

HUVEC supplements (500 x concentration) -

15% fetal bovine serum (FBS, Appleton Woods), 1.67mM L-glutamine (Sigma, G7513, 200mM) and 0.83% penicillin-streptomycin (Sigma, P0781) (10,000 units penicillin and 10 mg streptomycin per mL), human beta-endothelial cell growth factor (Sigma, E1388-25) 1.25mg/ml, endothelial cell growth supplement from bovine neural tissue (Sigma, E2759) 2.25mg/ml, thymidine (Sigma, 89270-1g) 1.25mg/ml, heparin from porcine intestinal mucosa (H3393) 5,000 units/ml. 1ml of the 500 x supplements was used a 500ml bottle of M199 medium.

Freezing medium components -

70% FBS, 10% DMSO and 20% respective culture medium

A 2.6 Cloning

The PCR reaction for site-directed mutagenesis and generation of pcDNA3.1(+)-ZIP8-threonine plasmid - 1x reaction buffer, 50ng plasmid DNA, 125ng primer mix, 1µl dNTP mix, 2.5u QuickChange Lightning enzyme, and nuclease-free H_2O to a final volume of 50µl.

A3 Sequence of pcDNA3.1-SLC39A8 expression plasmid inserts

pcDNA3.1(+)-SLC39A8-Ala391 (C allele) plasmid sequence

ATGGCCCCGGGTCGCGCGGTGGCCGGGCTCCTGTTGCTGGCGGCCGCCGGCCT
CGGAGGAGTGGCGGAGGGGCCAGGGCTAGCCTTCAGCGAGGATGTGCTGAGCG
TGTTCGGCGCGAATCTGAGCCTGTCGGCGGCGCAGCTCCAGCACTTGCTGGAGC
AGATGGGAGCCGCCTCCCGCGTGGGCGTCCCGGAGCCTGGCCAGCTGCACTTC
AACCAGTGTTTAACTGCTGAAGAGATCTTTTCCCTTCATGGCTTTTCAAATGCTAC

CCAAATAACCAGCTCCAAATTCTCTGTCATCTGTCCAGCAGTCTTACAGCAATTGA

ACTTTCACCCATGTGAGGATCGGCCCAAGCACAAAACAAGACCAAGTCATTCAGA

AGTTTGGGGATATGGATTCCTGTCAGTGACGATTATTAATCTGGCATCTCTCCTCG

GATTGATTTTGACTCCACTGATAAAGAAATCTTATTTCCCAAAGATTTTGACCTTTT

TTGTGGGGCTGGCTATTGGGACTCTTTTTTCAAATGCAATTTTCCAACTTATTCCA

GAGGCATTTGGATTTGATCCCAAAGTCGACAGTTATGTTGAGAAGGCAGTTGCTG

TGTTTGGTGGATTTTACCTACTTTTCTTTTTTGAAAGAATGCTAAAGATGTTATTAA

AGACATATGGTCAGAATGGTCATACCCACTTTGGAAATGATAACTTTGGTCCTCAA

GAAAAAACTCATCAACCTAAAGCATTACCTGCCATCAATGGTGTGACATGCTATGC

AAATCCTGCTGTCACAGAAGCTAATGGACATATCCATTTTGATAATGTCAGTGTGG

TATCTCTACAGGATGGAAAAAAAGAGCCAAGTTCATGTACCTGTTTGAAGGGGCC

CAAACTGTCAGAAATAGGGACGATTGCCTGGATGATAACGCTCTGCGATGCCCTC

CACAATTTCATCGATGGCCTGGCGATTGGGGCTTCCTGCACCTTGTCTCTCCTTC

AGGGACTCAGTACTTCCATAGCAATCCTATGTGAGGAGTTTCCCCACGAGTTAGG

AGACTTTGTGATCCTACTCAATGCAGGGATGAGCACTCGACAAGCCTTGCTATTC

AACTTCCTTTCTGCATGTTCCTGCTATGTTGGGCTAGCTTTTGGCATTTTGGTGGG

CAACAATTTCGCTCCAAATATTATATTTGCACTTGCTGGAGGCATGTTCCTCTATAT

TTCTCTGGCAGATATGTTTCCAGAGATGAATGATATGCTGAGAGAAAAGGTAACT

GGAAGAAAAACCGATTTCACCTTCTTCATGATTCAGAATGCTGGAATGTTAACTGG

ATTCACAGCCATTCTACTCATTACCTTGTATGCAGGAGAAATCGAATTGGAGTAA

pcDNA3.1(+)-SLC39A8-Thr391 (T allele) plasmid sequence

ATGGCCCCGGGTCGCGCGGTGGCCGGGCTCCTGTTGCTGGCGGCCGCCGGCCT

CGGAGGAGTGGCGGAGGGGCCAGGGCTAGCCTTCAGCGAGGATGTGCTGAGCG

TGTTCGGCGCGAATCTGAGCCTGTCGGCGGCGCAGCTCCAGCACTTGCTGGAGC

AGATGGGAGCCGCCTCCCGCGTGGGCGTCCCGGAGCCTGGCCAGCTGCACTTC

AACCAGTGTTTAACTGCTGAAGAGATCTTTTCCCTTCATGGCTTTTCAAATGCTAC

CCAAATAACCAGCTCCAAATTCTCTGTCATCTGTCCAGCAGTCTTACAGCAATTGA

ACTTTCACCCATGTGAGGATCGGCCCAAGCACAAAACAAGACCAAGTCATTCAGA

AGTTTGGGGATATGGATTCCTGTCAGTGACGATTATTAATCTGGCATCTCTCCTCG

GATTGATTTTGACTCCACTGATAAAGAAATCTTATTTCCCAAAGATTTTGACCTTTT

TTGTGGGGCTGGCTATTGGGACTCTTTTTTCAAATGCAATTTTCCAACTTATTCCA

GAGGCATTTGGATTTGATCCCAAAGTCGACAGTTATGTTGAGAAGGCAGTTGCTG

TGTTTGGTGGATTTTACCTACTTTTCTTTTTTGAAAGAATGCTAAAGATGTTATTAA

AGACATATGGTCAGAATGGTCATACCCACTTTGGAAATGATAACTTTGGTCCTCAA

GAAAAAACTCATCAACCTAAAGCATTACCTGCCATCAATGGTGTGACATGCTATGC

AAATCCTGCTGTCACAGAAGCTAATGGACATATCCATTTTGATAATGTCAGTGTGG

TATCTCTACAGGATGGAAAAAAAGAGCCAAGTTCATGTACCTGTTTGAAGGGGCC

CAAACTGTCAGAAATAGGGACGATTGCCTGGATGATAACGCTCTGCGATGCCCTC

CACAATTTCATCGATGGCCTGGCGATTGGGGCTTCCTGCACCTTGTCTCTCCTTC

AGGGACTCAGTACTTCCATAGCAATCCTATGTGAGGAGTTTCCCCACGAGTTAGG

AGACTTTGTGATCCTACTCAATGCAGGGATGAGCACTCGACAAGCCTTGCTATTC

AACTTCCTTTCTGCATGTTCCTGCTATGTTGGGCTAGCTTTTGGCATTTTGGTGGG

CAACAATTTCACTCCAAATATTATATTTGCACTTGCTGGAGGCATGTTCCTCTATAT

TTCTCTGGCAGATATGTTTCCAGAGATGAATGATATGCTGAGAGAAAAGGTAACTG

GAAGAAAAACCGATTTCACCTTCTTCATGATTCAGAATGCTGGAATGTTAACTGGA

TTCACAGCCATTCTACTCATTACCTTGTATGCAGGAGAAATCGAATTGGAGTAA